OXIDATION OF MERCURY DURING SELECTIVE CATALYTIC REDUCTION OF NITRIC OXIDE

by

GIANG TONG

PETER M. WALSH, COMMITTEE CHAIR
HENG BAN
CHIH-HSIUNG CHENG
THOMAS K. GALE
MELINDA M. LALOR

A DISSERTATION

Submitted to the graduate faculty of The University of Alabama at Birmingham,
in partial fulfillment of the requirements for the degree of
Doctor of Philosophy in Interdisciplinary Engineering

BIRMINGHAM, ALABAMA

2009

OXIDATION OF MERCURY DURING SELECTIVE CATALYTIC REDUCTION OF NITRIC OXIDE

GIANG TONG

INTERDISCIPLINARY ENGINEERING

ABSTRACT

A promising method for mercury removal from the gaseous products of coal combustion is the catalytic oxidation of elemental mercury to water-soluble mercuric chloride during selective catalytic reduction of NO_x by ammonia, followed by removal of the oxidized mercury during wet flue gas desulfurization.

Measurements of the mercury species distribution and sulfate formation at the outlet of a 310 mm long square cell monolithic V_2O_5-WO_3/TiO_2 commercial SCR catalyst showed the following trends: (1) Mercury oxidation was highly sensitive to HCl at the low levels characteristic of Powder River Basin subbituminous coals (0-5 ppmv). (2) Mercury oxidation was inhibited by NH_3, and promoted by NO in the absence of NH_3. The inhibitory effect of NH_3 increased with decreasing HCl, increased on approach to stoichiometric NH_3/NO, and increased markedly in the presence of excess NH_3. (3) CO had a strong inhibitory effect on mercury oxidation at low levels of HCl, which decreased with increasing HCl levels. Variation in the CO content of flue gas when burning low chlorine coals is thus a possible source of variability and uncertainty in the extent of mercury oxidation in SCR. This is regarded as one of the most significant findings of the work and addressed a specific research need identified by Presto et al. (2006) and Presto and Granite (2006).

Implementation of the Tennessee Valley Authority's thermal mercury reduction system for the determination of total mercury resulted in a great improvement in data

quality and a marked decrease in the time required to identify steady-state conditions, resulting in a higher probability of success in each test run attempted.

Measurements of sulfate formation made in conjunction with the mercury oxidation measurements showed little change in SO_2 oxidation to SO_3 with increasing HCl volume fraction in the absence of NH_3. However, the addition of NH_3 inhibited the oxidation of SO_2 to SO_3, regardless of HCl content. CO had little effect on the oxidation of SO_2 to SO_3.

A one-dimensional mass transfer and chemical reaction model was developed for three of the important processes in SCR: NO reduction by NH_3, mercury oxidation by HCl, and SO_2 oxidation by O_2.

Keywords: Mercury oxidation, SCR, Flue gas, Carbon monoxide, Sulfate

DEDICATION

I would like to dedicate this body of work to my loving family, Kirstin, Magdalena Lu, and Lauryn Anh Tong. This accomplishment would not have been possible without your loving support.

ACKNOWLEDGMENTS

I would like to thank Dr. Peter M. Walsh for his support and guidance through this work and George A. Blankenship of Southern Research Institute for his guidance and expertise in SCR and operation of the complex experimental setup at the SRI Catalyst Test Facility. I would also like to thank the other members of my dissertation committee, Dr. Heng Ban, Dr. Gary Cheng, Dr. Thomas K. Gale, and Dr. Melinda M. Lalor, for their guidance.

This work was supported by the U.S. Department of Energy, National Energy Technology Laboratory, under Contract No. DE-FG26-04NT42195 entitled, "Oxidation of Mercury in Products of Coal Combustion." The author is grateful to Cormetech, Inc. for providing the commercial catalyst sample used in this work and to the Tennessee Valley Authority for permission to use its converter technology for reduction of oxidized mercury to elemental form for analysis.

TABLE OF CONTENTS

Page

LIST OF TABLES

LIST OF FIGURES

Figure *Page*

LIST OF ABBREVIATIONS

APH	air preheater
APCD	air pollution control device
CAIR	Clean Air Interstate Rule
CAMR	Clean Air Mercury Rule
CAU	Clark Atlanta University
CEM	continuous emission monitor
CFBA	circulating fluidized bed adsorber
CRF	Combustion Research Facility (Southern Company and Southern Research Institute)
CTF	Catalyst Test Facility (Southern Research Institute)
CVAA	cold-vapor atomic absorption
$DeNO_x$	NO_x reduction
DOE	U.S. Department of Energy
EERC	Energy & Environmental Research Center
EIA	U.S. Energy Information Administration
EPA	U.S. Environmental Protection Agency
ESP	electrostatic precipitator
FF	fabric filter
FGD	flue gas desulfurization

FTIR	Fourier transform infrared spectroscopy
GAC	granulated activated carbon
GTI	Gas Technology Institute, Des Plaines, IL
ICR	U.S. EPA Mercury Information Collection Request
IPA	isopropyl alcohol
MACT	Maximum Achievable Control Technology
NETL	U.S. Department of Energy, National Energy Technology Laboratory
SOH	Solid Ontario Hydro
PRB	Powder River Basin
RfD	exposure reference dose
SCR	selective catalytic reduction
SNCR	selective non-catalytic reduction
SRI	Southern Research Institute, Birmingham, AL
TST	transition state theory
TVA	Tennessee Valley Authority
UAB	University of Alabama at Birmingham
UBC	unburned carbon
UNEP	United Nations Environmental Programme
Uni-Hg	unified mercury mechanism
VOC	volatile organic compound

CHAPTER 1

INTRODUCTION

1.1 Coal

Coal has two major advantages over other fossil fuels for the generation of electricity: it is the least expensive of all the fossil fuels and it is readily available. Coal is an economical fuel for electric power production, second only to hydroelectric generation. Eighty-eight percent of the coal mined in the United States is used to generate electricity, accounting for approximately half of the electric power produced in the U.S. Recoverable coal reserves in the U.S. stand at 275 billion tons, having an estimated life time of over 200 years at the current rate of consumption, as determined by the U.S. Energy Information Administration (EIA) (Freme, 2008). Therefore, coal is expected to remain the predominant fuel for the production of electricity in the U.S. for many years.

1.1.1 *Coal Quality*

The quality of coal as a fuel is measured by several criteria: coal rank, calorific value (kJ/kg) of the coal, and the levels of impurities in the coal. The major ranks of coal from lowest to highest are lignite, subbituminous, bituminous, and anthracite. The higher ranks of coal have higher fixed carbon contents and higher calorific values. The majority of coal in the U.S. recoverable reserves is bituminous (52%), followed by subbituminous

(37%), lignite (9%), and anthracite (2%). Bituminous coal, subbituminous coal, and lignite are the most common fuels for the generation of electricity; anthracite, on the other hand, is too expensive and is mainly used to make coke for the production of steel. Bituminous coal is mined predominantly in the Appalachian and Interior regions of the U.S., whereas subbituminous coal is mined primarily in the Western U.S. and Alaska. The majority of lignite mined in the U.S. comes from Texas, Montana, and North Dakota, while anthracite is found mostly in a small region of Northeastern Pennsylvania. In addition to rank and calorific value, the properties of greatest importance for coal are the concentrations of impurities, such as sulfur, nitrogen, chlorine, ash, and mercury. A major contaminant that lowers coal quality is sulfur. Sulfur in coal can occur as organic sulfur or as pyrite (FeS_2), and, sometimes, as mineral sulfates. Coal quality can sometimes be improved relatively easily by removing pyrite, but the process can be costly due to the loss of coal along with the pyrite. Organic sulfur is more difficult to remove from coal than pyrite, and no commercial process is currently in use for removal of organic sulfur.

1.1.2 *Air Pollutants from Coal Combustion*

A disadvantage of burning coal for power generation is the formation of air pollutants that, if emitted, could degrade air and water quality, resulting in damage to vegetation and harmful health effects in humans and animals. The burning of coal produces particulate matter (PM-10 and PM-2.5), sulfur oxides (SO_2 and SO_3), nitrogen oxides (NO and NO_2), and mercury (Hg), which would be emitted to the atmosphere if not removed from the combustion products.

Particulate matter refers to suspended solid or liquid particles, produced from a variety of mobile and stationary sources, including diesel engines, wood stoves, and power plants. The composition of particulate matter varies widely, according to its origin. Human exposure to particulate matter may affect the respiratory system and breathing, damage lung tissue, and cause cancer and premature death (U.S. EPA, 2007a). The portion of the population especially sensitive to the effects of particulate matter includes the elderly, children, and people with chronic lung disease, influenza, or asthma (U.S. EPA, 2007a). In addition, acidic particulate matter can damage materials of construction and reduces visibility in many parts of the U.S. (U.S. EPA, 2007a).

Sulfur dioxide and sulfur trioxide gases (SO_x) are formed when fuels containing sulfur, such as coal and oil, are burned, and during smelting of metal ores and other industrial processes. Exposure to high concentrations of SO_2 can affect breathing, cause respiratory illness and changes to pulmonary defenses, and aggravate existing cardiovascular disease (U.S. EPA, 2007a). Therefore, asthmatics, individuals with cardiovascular disease or chronic lung disease, such as bronchitis and emphysema, as well as children and the elderly are most sensitive to effects of SO_2. SO_2 emissions can also damage the foliage of trees and agricultural crops. SO_2 can also be converted in the atmosphere to fine particulate sulfate that scatters and absorbs light, reduces visual range, and alters the apparent color of landscapes, resulting in a regional haze that covers many big cities and scenic rural areas. U.S. EPA's health-based national air quality standard for SO_2 is 0.03 ppm (annual average) and 0.14 ppm (24 hour average), and the secondary national ambient air quality standard designed to prevent environmental deterioration is 0.50 ppm (3 hour average) (U.S. EPA, 2007a).

The nitrogen oxides, NO and NO_2, are formed from nitrogen in the fuel and nitrogen in the air when fuel is burned in air at high temperatures, such as in internal combustion engines and electric utility and industrial boilers. Nitrogen dioxide is a strong oxidizing agent that reacts in the air to form corrosive nitric acid, as well as toxic organic nitrates. Long-term exposure to high ambient concentrations of NO_2 may cause acute respiratory illness in children (U.S. EPA, 2007a). U.S. EPA's health-based national air quality standard for NO_2 is 0.053 ppm (annual average).

Nitrogen dioxide and volatile organic compounds (VOCs) react in the atmosphere in the presence of sunlight to form ground-level ozone and smog. Prevailing levels of photo-oxidant and particulate pollution in spring and early summer, even though they may be within international air quality standards, have been shown to have measurable short-term effects on children with mild-to-moderate asthma (Just et al., 2002). Therefore, the World Health Organization has recommended that a short-term one hour standard of 0.10 - 0.17 ppm be established to protect public health and that this standard not be exceeded more than once a month. The State of California has already adopted a short term NO_2 standard of 0.25 ppm, averaged over one hour.

Together, SO_2 and NO_X are the major precursors to acid rain and ambient fine particle aerosol, associated with the acidification of lakes and streams, accelerated corrosion of buildings and monuments, and reduced visibility. The burning of coal also produces a small amount of nitrous oxide (N_2O), which is a known greenhouse gas and reactant with ozone in the stratosphere.

1.2 Mercury in Coal

Yet another air pollutant produced from burning coal is mercury. The mercury concentration in coal-derived flue gas is roughly 1 part per billion by volume (Granite et al., 1998). The total global mercury emissions from all sources, natural and anthropogenic, are from approximately 4,400 to 7,500 metric tons per year (Pacyna and Pacyna, 2002), with Asia accounting for 53% of the total global emissions, while the U.S. is responsible for only 9% (Pacyna and Munthe, 2004). Because mercury can be transported in the atmosphere over vast distances, a global reduction in mercury use and emissions is required to minimize mercury exposure at any particular location. Increased awareness of the harmful health and environmental effects of mercury exposure has resulted in a dramatic decrease in the use of mercury in industrialized nations. However, in less developed regions or nations of the world where mercury regulations and restrictions, such as the Mercury-Containing and Rechargeable Battery Management Act of 1996 (Battery Act), are not as comprehensive or not well enforced, the use of mercury has not decreased. In fact, the lower cost of mercury due to the decrease in demand from industrialized nations has resulted in its increased use in less developed nations. In the last decade, anthropogenic emissions of mercury have decreased in North America (Seigneur et al., 2001) and Europe (Pacyna et al., 2001), but have increased in India (UNESCAP, 2000) and China (Weidou and Sze, 1998; Ho et al., 1998) by about 27% and 55%, respectively. Mercury emissions per ton of coal from China's electric utilities are roughly three times higher than those from U.S. utilities (Belkin et al., 2005). China's high mercury emission, combined with the largest coal production and consumption rates in the world, make China the world's largest emitter of mercury to the atmosphere

(Kolker et al., 2006). Studies suggest that a lack of emission controls, such as electrostatic precipitators and wet flue gas desulfurization, on coal-fired utility boilers, rather than a higher average mercury concentration in local coal, is primarily responsible for China's large emissions of mercury (Kolker et al., 2006). While coal-fired utility boilers are the largest remaining anthropogenic sources of mercury emissions in the U.S., they contribute only an estimated 1% to the annual mercury emissions around the world (UNEP Chemicals, 2002). In spite of its relatively small contribution to the world mercury cycle, the U.S. has spearheaded an effort under the United Nations Environment Programme (UNEP) to establish partnerships that will help developing nations around the world to reduce their mercury use and emissions.

1.3 Mercury Speciation in Coal Derived Flue Gas

Mercury is emitted from coal-fired utility boilers in three different forms, elemental mercury [Hg(0)], oxidized mercury [Hg(II)], and mercury, either elementa or oxidized, that is adsorbed on particles [Hg(ads)] (Pavlish et al., 2003). The fractions of total mercury appearing as Hg(0), Hg(II), and Hg(ads) vary, depending on the coal composition, combustion conditions, and flue gas quench rate. Each mercury form has distinctive physical and chemical properties that give it unique emission, transport, and deposition characteristics (Galbreath et al., 2004).

Hg(0) is the most abundant and persistent form of mercury, having an estimated residence time in the atmosphere of up to a year (Schroeder and Munthe, 1998) . Therefore, Hg(0) can be transported over continental distances. Hg(0) is highly volatile, having a vapor pressure at 25 ^{o}C of 0.002 mm Hg. Hg(0) is chemically relatively inert

because of its closed-shell electronic structure $[Xe]4f^{14}5d^{10}6s^2$ and it has an oxidation potential for Hg(0) = Hg(II) + $2e^-$ of 0.854 V. Additionally, Hg(0) has a very low water solubility (0.06 g/L at 25 ^oC), making it very difficult to capture with conventional air pollution control devices (Galbreath et al., 2004).

Hg(II), however, is less volatile, more water soluble, and more chemically reactive than Hg(0) (Galbreath et al., 2004). Hg(II) and Hg(ads), when emitted, are more likely to be deposited locally or regionally. In contrast to Hg(0), Hg(II) and Hg(ads) are more effectively captured in conventional pollution control systems such as wet scrubbers and fabric filters (Galbreath et al., 2004).

Mercury in the atmosphere is deposited to the land and water through rain, snow, and dry deposition. Eventually, the mercury is washed into streams, lakes, and rivers where it is converted to methylmercury (CH_3Hg^+ or $MeHg^+$) by bacteria in soils and sediments. $MeHg^+$ is taken in by small aquatic plants and animals and enters the food chain. The concentration of $MeHg^+$ increases as it moves up the food chain through the process of bioaccumulation. Large fish such as shark, swordfish, tilefish, and king mackerel that prey on other fish, have the highest concentrations of $MeHg^+$ in their tissues. The concentrations of $MeHg^+$ in these fish can bioaccumulate to over one million times greater than in the surrounding water (U.S. EPA, 2004), which can result in deleterious health impact from consumption of the contaminated fish.

1.4 Health Impact of Mercury

Mercury and most of its compounds are toxic, but methylmercury poses the biggest health threat. The concern about $MeHg^+$ arises because it is a teratogen and

neurotoxin. The extent of these toxic and teratogenic properties depends on methylmercury's action on the human nervous system and internal organs, especially the liver and kidneys. People and animals are exposed to $MeHg^+$ by eating contaminated fish and shellfish. The National Research Council (NRC) estimates the public exposure to $MeHg^+$ from fish consumption to fall between 1 and 6 μg of mercury/day (U.S. EPA, 2001). The U.S. EPA's exposure reference dose (RfD) for $MeHg^+$ is 0.1 μg mercury/kg body weight/day. Women of childbearing age are regarded as the population of greatest concern because the developing fetus is the most vulnerable to the toxic effects of $MeHg^+$ (U.S. EPA, 2004). Two large epidemiological studies conducted in the Faroe Islands and New Zealand have shown that children who are exposed to $MeHg^+$ before birth may be at increased risk of poor brain and nervous system development, which may result in poor performance on neurobehavioral tasks, such as cognitive thinking, memory, attention, fine motor function, language skills, and visual-spatial abilities (U.S. EPA, 2007b). Symptoms of acute $MeHg^+$ poisoning may include tingling sensations around the hands, feet, and mouth, lack of coordination of movements, and impaired speech, hearing, walking, and peripheral vision (U.S. EPA, 2007b).

Although elemental or metallic mercury is commonly used as a filler material in dental amalgam for restoring teeth, the Centers for Disease Control and Prevention (CDC) presently reports neither adverse health effects from exposure to Hg(0) in dental amalgam, nor any health benefits from the removal of the amalgam fillings (U.S. EPA, 2007b). However, when Hg(0) is inhaled as a vapor and is absorbed through the lungs, the exposure can be harmful. Exposure occurs commonly through the breakage of devices containing the liquid metal, such as thermometers, barometers, and thermostats

and other electrical switches. In warm and poorly ventilated spaces, the exposed liquid Hg(0) can evaporate and become an invisible, odorless, toxic vapor. Symptoms of exposure to Hg(0) include tremors, insomnia, neuromuscular changes, headaches, disturbances in sensations, changes in nerve responses, and performance deficits on tests of cognitive function (U.S. EPA, 2007b). At higher levels of exposure there may be kidney damage, respiratory failure, and death (U.S. EPA, 2007b).

Mercury ingested in elemental, organic, or inorganic form is converted to Hg(II), which is only slowly eliminated from the kidneys and remains fixed in the brain indefinitely (Aposhian and Aposhian, 2000). High exposures to inorganic mercury may result in damage to the gastrointestinal tract, the nervous system, and the kidneys. Symptoms of high exposures to inorganic mercury include skin rashes and dermatitis, mood swings, memory loss, mental disturbances, and muscle weakness (U.S. EPA, 2007b).

Due to its harmful health impacts, mercury has been designated as one of the most persistent bioaccumulative substances of immediate concern in North America (Sherwell, 2000). Of the 188 hazardous air pollutants targeted for study by the 1990 Clean Air Act Amendments, only mercury was singled out for intense study. The United States Environmental Protection Agency submitted a comprehensive report to Congress on mercury seven years later (U.S. EPA, 1997). In August 2000, the National Research Council determined that the U.S. EPA's exposure reference dose (RfD) of 0.1 µg mercury/kg body weight/day was justified to protect against harmful neurological effects during fetal development and early childhood. Subsequently, the U.S. EPA announced in December 2000, that it would start regulating mercury emission from most coal and oil-

fired utility boilers to reduce the amount of mercury emitted into the environment. As a result, the U.S. is the first nation to begin regulating mercury emissions from coal-fired electric utility boilers.

1.5 Mercury Air Emission Regulations

The U.S. EPA Mercury Report (U.S. EPA, 1997) stated that approximately 87% of the estimated 144 megagrams of total mercury emitted annually into the atmosphere around the world is from combustion point sources, such as boilers and incinerators. The U.S. EPA also estimated that four specific source categories account for approximately 80% of the total anthropogenic mercury emissions around the world: coal-fired utility boilers, municipal waste combustion, commercial/industrial boilers, and medical waste incinerators.

In an attempt to significantly reduce mercury emissions from coal-fired utility boilers, President George W. Bush announced the Clear Skies Initiative in February 2002, which targets reductions in NO_x, SO_2, and mercury emissions of 70% by 2018. In addition, the U.S. EPA issued the final Clean Air Mercury Rule (CAMR) on March 15, 2005, which builds on the Clean Air Interstate Rule (CAIR) (U.S. EPA, 2004). Both the CAMR and the CAIR are part of a set of inter-related rules collectively known as the Clean Air Rules of 2004, which together address ozone and fine particle pollution, non-road diesel emissions, and power plant emissions of SO_2, NO_x, and mercury. When fully implemented, these rules will reduce electric utility emissions of mercury in the U.S. from 50 to 15 tons per year, a reduction of 70%. The CAMR established benchmarks limiting mercury emissions from new and existing power plants and created a market-

based cap-and-trade program that will reduce nationwide utility emissions of mercury in two distinct phases. In the first phase, due to begin in 2010, emissions will be capped at 38 tons by taking advantage of co-benefit reductions, that is, mercury reductions achieved while reducing SO_2 and NO_x under CAIR. In the second phase, due to begin in 2018, utilities will be subject to a second cap, reducing mercury emissions to 15 tons per year upon full implementation.

However, as of February of 2008, the CAMR has been vacated by the Circuit Court of Appeals for the District of Columbia. Several states have formulated their own rules for emission of mercury from coal-fired utility boilers, which are stricter than the CAMR and do not allow trading of mercury credits. Those states' rules should not be affected. If the ruling stands and is not appealed, the ultimate course of action for the U.S. EPA will probably be a Maximum Achievable Control Technology (MACT) rule for mercury. Since mercury capture technology has progressed, the resulting MACT may be stricter than the one that would have been put in place in 2005.

1.6 Approaches to Mercury Air Emission Control

Removal of mercury from products of combustion in coal-fired utility boilers presents a significant challenge (Granite et al., 2000). Data from the U.S. EPA's mercury Information Collection Request (ICR) (U.S. EPA, 1998) program suggest that mercury emissions are controlled by two factors: (1) feed coal rank, and (2) post-combustion control configuration (Yudovich and Ketris, 2005; Kolker et al., 2006). The amount of mercury removal achieved in coal-fired utility boilers with existing equipment varies widely, from near 0% to over 90%, depending on the coal, boiler operating parameters,

and air pollution control devices (APCDs). On average, about 40% of the mercury entering a coal-fired utility boiler is captured in ash and scrubber residues and 60% is emitted to the atmosphere (Pavlish et al., 2003). Typical APCDs can remove Hg(II) vapors and Hg(ads) relatively easily from flue gas (Presto and Granite, 2006). Hg(ads) is captured, along with fly ash and unburnerd carbon particles, in electrostatic precipitators (ESP) and/or baghouses. Hg(II) vapors, particularly mercuric chloride ($HgCl_2$), are soluble in water and, therefore, removed with high efficiency by wet flue gas desulfurization (wet FGD) equipment (Carey, 1999). Hg(0) vapor, however, is more difficult to capture because it has a significant vapor pressure and is insoluble in water and, therefore, able to pass through precipitators and scrubbers to the smokestack. Mercury oxidation from the elemental form to the more easily removed oxidized form has been observed in selective catalytic reduction (SCR) of NO_x ($DeNO_x$) using ammonia (NH_3), but the amount of mercury oxidized in SCR also varies from case to case. In fact, there remain many uncertainties in the speciation, chemistry, and overall fate of mercury from coal-fired utility boilers (Sherwell, 2000). Currently, there is no single best technology that can be broadly applied to offer high levels of control for different utility systems burning various types of coal.

1.6.1 *Flue Gas Time-Temperature History and Mercury Speciation*

Downstream from the boiler furnace, most coal-fired utility boilers are equipped with heat exchangers, consisting of superheaters, reheaters, an economizer, and an air heater, followed by gas cleaning systems; typically an ESP for particulate removal, before the flue gas is cooled further by wet flue gas desulfurization. A SCR unit for NO_x

removal may be incorporated into the gas cleaning system at any of three locations in a power plant: (1) upstream of the air preheater (APH) and cold-side ESP (referred to as hot-side, high dust SCR), (2) upstream of the APH and downstream of a hot-side ESP (hot-side, low dust SCR), or (3) downstream of the APH and ESP (cold-side, low dust SCR). In commercial practice, most SCR reactors are installed on the hot-side to avoid the need to reheat the flue gas to reaction temperature (343 to 399 ^{o}C), thereby minimizing loss of thermal efficiency. As a result, the time-temperature history of post-combustion flue gas is determined by the configuration of heat exchangers in the convection section and unit operations in the gas cleaning system.

In the high temperature (~1500 ^{o}C) combustion zone of a coal-fired utility boiler, all forms of mercury in coal decompose to form Hg(0) (Kolker et al., 2006). The distribution of Cl-species (HCl, Cl-atoms, and Cl_2) in post-combustion flue gas, responsible for mercury oxidation, is determined by chemical reactions in the superheater, reheater, and economizer (Niksa and Fujiwara, 2005a). Mercury oxidation, however, is initiated primarily across the air heater, where the flue gas is quickly quenched at several hundred degrees per second from approximately 550 to 175 ^{o}C (Niksa and Fujiwara, 2005a). The time-temperature window favorable for mercury oxidation is narrow (Laudal et al., 1996), as confirmed by the Chemical Equilibrium Analysis of the ICR data (U.S. EPA, 1998) conducted by Senior and Afonso (2001) .

Pavlish et al. (2003) reviewed ICR data and found that at higher temperatures typical of a hot-side ESP, between 250 and 400 ^{o}C, mercury remains predominantly as Hg(0), even at high chlorine levels, and that virtually no Hg(ads) is formed. As the flue gas is further cooled to temperatures in the range of 127 to 227 ^{o}C, Hg(0) is converted to

Hg(II) and Hg(ads) by a complex series of reactions. At the temperatures typical of a cold-side ESP, between 130 and 170 ^{o}C, Pavlish et al. (2003) found that Hg(0) was converted to Hg(II) in the presence of high chlorine levels and was typically 75% Hg(ads). As a result, mercury enters the flue gas cleaning device(s) as a mixture of Hg(0), Hg(II), and Hg(ads).

1.6.2 *Mercury Control Technologies*

According to Niksa and Fujiwara (2005), the coal-burning utility industry has launched a massive initiative to develop control strategies to comply with impending regulations on mercury emissions from power plants. Approaches for reducing mercury emissions include: selective coal mining, coal cleaning, combustion modification, sorbent injection, catalysts, and scrubbers, among others. Currently, three approaches for control of mercury emissions from coal-burning power plants are most promising: (1) coal cleaning prior to burning, (2) injection of a sorbent, such as activated carbon or zeolite, into the flue gas, followed by collection in an electrostatic precipitator (ESP) or baghouse, and (3) conversion of Hg(0), the predominant form at high temperature, to the oxidized, water-soluble form, mercuric chloride [$HgCl_2$, Hg(II)] and removal in a wet FGD unit.

The first approach, coal cleaning through pyrite removal, is one of the most simple and cost effective procedures to reduce mercury emissions. Coal cleaning is currently used on most eastern bituminous coals for sulfur and ash removal, and results in some reduction in mercury. However, for extremely pyrite-rich coals, standard cleaning procedures may not always achieve the desired results (Yudovich and Ketris, 2005).

Shpirt (2002) estimated that coal cleaning processes could reduce mercury concentration by 31 to 33%. New cleaning methods have achieved higher levels of mercury removal, but are currently in various stages of development.

The second approach, sorbent injection, can be added to most existing power plants, and therefore, is a very popular research topic for a broad-based approach to mercury control. Sorbent injection may be done upstream or downstream of an ESP (Brown et al., 1999). However, sorbent injection downstream of an ESP will require installation of a fabric filter (FF) to separate the sorbent from flue gas. The injection of activated carbon upstream of an ESP can achieve greater than 60% mercury capture and even greater than 90% if injected upstream of a FF (Bustard et al., 2002). Sorbent injection upstream of an ESP is a relatively simple process, but the extent of mercury capture is less than optimum, due to the high temperature of the flue gas and the presence of other components, such as SO_2 and NO_2, in the flue gas (Miller et al., 2003). Presence of these acid gases has been shown to degrade the performance of some chemically-treated activated carbons and other sorbents such as noble-metal-impregnated alumina (Butz et al., 2000). Another disadvantage of injecting activated carbon upstream of an ESP is that the increased carbon content from the sorbent is likely to make the fly ash unusable as an additive in cement. The activated carbon could be injected downstream from the ESP and collected on a FF to avoid increasing the carbon content of the fly ash collected in the ESP, but at the cost of installing and maintaining this additional equipment.

Generally, activated carbon injection conditions include: (1) upstream of an ESP, carbon/mercury weight ratio 100:1 at 157 – 146 ^{o}C and (2) downstream of an ESP and

upstream of a FF, carbon/mercury weight ratio (9.4 – 12):1 at 110 – 120 ^{o}C (Yudovich and Ketris, 2005). However, carbon is a general sorbent and will adsorb many flue gas components to some extent, some of which may compete with mercury for binding sites (Granite et al., 2008). Therefore, a carbon/mercury ratio greater than the ones recommended by Yudovich and Ketris (2005) may be required to achieve a high level of mercury removal. Activated carbons can be expensive, costing around $500 - $3000/ton (Granite et al., 1998). The search for alternative sorbents, such as zeolite, that would not adversely affect the value of fly ash is an active area of research (Sjostrom et al., 2001), but cost-effective application of the technology for different coals and particulate control devices must be ensured.

The circulating fluidized bed adsorber (CFBA) is considered a promising gas-sorbent contacting reactor for simultaneous mercury capture and flue gas desulfurization (Yudovich and Ketris, 2005). The vertical CFBA is installed upstream of an ESP for SO_2 capture. Advantages of CFBA include: (1) increased solids residence time due to the recirculation of sorbent and fly ash in the fluidized bed, (2) conservation of expensive sorbent, and (3) allowance for simultaneous cooling of the flue gas for enhanced mercury capture either by sorbent or fly ash (Kilgore et al., 2002).

The third approach to mercury emissions control, conversion of Hg(0) to the oxidized, water-soluble form followed by collection in a FGD unit, is attractive because it may require fewer modifications to equipment and operations in plants already equipped with SCR and FGD. Direct monitoring of flue gas shows that 50 to 70% of Hg(II) is captured by a wet FGD, and up to 98% Hg(II) capture can be achieved by a dry FGD or spray dryer adsorber (SDA) (Yudovich and Ketris, 2005). Such high mercury capture

efficiency, however, was only observed for chlorine-containing U.S. bituminous coals (Kilgore et al., 2002). A modified dry FGD that incorporates a CFBA is also considered promising for efficient simultaneous flue gas desulfurization and mercury capture.

The most economical control approaches will most likely involve using existing particulate control devices and FGD scrubbers in conjunction with additives, sorbents, catalytic pretreatment reactors, or other supplemental measures to enhance mercury recoveries (Niksa and Fujiwara, 2005). However, in order for utilities to plan equipment improvements and new construction to meet emissions requirements, quantitative data on these promising mercury control approaches are needed to evaluate alternative designs.

1.6.3 *Cost of Mercury Control*

At present, it is unclear what will be the most cost-effective method for achieving the levels of mercury removal required by Federal regulations. However, the cost of removing mercury from flue gas using existing technology is estimated to be very high. The U.S. EPA estimates the cost for 90% control based on activated carbon injection to be in the range of U.S. $5000 - $28,000/lb of mercury removed (Brown et al., 1999), whereas the U.S. Department of Energy (DOE) estimated a higher cost of U.S. $25,000 - $70,000/lb of mercury removed using the same technology (Brown et al., 1999). Estimates of increased power generation costs due to additional mercury emissions control range from U.S. 0.1 cents - 0.8 cents/kW-h, with higher costs projected for plants smaller than 200 MW (Pavlish et al., 2003). Utility boilers burning bituminous coals that are equipped with wet FGD for SO_2 control are expected to experience the lowest costs. The higher chlorine content in these coals and their combustion products should promote

formation of Hg(II) that can be efficiently removed (80 - 95%) by wet FGD (Pavlish et al., 2003). Utility boilers having the highest costs for removal are likely to be those burning low-rank subbituminous coals or lignites having low chlorine content, which produce primarily Hg(0) that must first be oxidized before it can be removed by wet FGD or ESPs. In general, utility boilers burning coals that emit primarily Hg(0) will face a more difficult challenge in finding cost-effective methods for achieving high mercury control.

1.6.4 *Selective Catalytic Reduction*

Selective catalytic reduction has become the commercial technology of choice worldwide to meet current NO_x emissions standards for coal-fired utility boilers. A large number of SCR systems are under construction or planned for installation in the U.S. Cichanowicz and Muzio (2001) reported that by the year 2004, more than 100 GW of coal-fired capacity in the U.S. were expected to be equipped with SCR NO_x control technology to mitigate seasonal ozone production, as mandated by Title I of the 1990 Clean Air Act Amendments. Since SCR and wet FGD are increasingly being used to control NO_x and SO_2 emissions, respectively, their combination has the potential to provide effective mercury control. Maximizing the amount of mercury oxidized by SCR can improve the mercury capture performance by wet FGD systems downstream. Therefore, mercury oxidation by SCR catalysts upstream of wet FGD systems should create an opportunity for simultaneous and cost-effective control of mercury, NO_x, and SO_2 emissions from coal-fired utility boilers.

1.7 Goal and Objectives

The overall goal of this work was to provide experimental data on mercury reactions in SCR with which to test models that are needed to design and optimize the performance of SCR for NO_x, SO_3, and mercury control in plants equipped with SCR and a cold-side ESP (downstream from an air preheater), followed by wet FGD. A commercial catalyst generously provided by Cormetech, Inc. was chosen for a detailed study of mercury oxidation in the presence of simulated flue gas containing most of the major and minor constituents of real flue gas: Hg, N_2, O_2, CO_2, CO, NO, NH_3, SO_2, SO_3, HCl, and H_2O. The performance of the catalyst was measured in the Catalyst Test Facility (CTF) at Southern Research Institute (SRI). The variables of greatest interest were the concentrations of HCl and CO, and the ratio of NH_3 to NO. The effect of temperature was not examined in the present study.

The objectives of the study were motivated by areas of uncertainty regarding mercury reactions in SCR identified as important by Presto and Granite (2006). Specifically, the effects of gaseous components such as HCl, CO, NO, and NH_3 on mercury oxidation across a SCR catalyst:

- *Objective 1: Determine the effects of NO, HCl, and NH_3 to NO feed ratio on the catalytic oxidation of mercury.*
- *Objective 2: Determine whether carbon monoxide is an inhibitor or promoter of mercury oxidation.*
- *Objective 3: Measurements of the acceleration or inhibition of sulfate formation in an SCR catalyst as functions of HCl, NH_3 to NO feed ratio, and CO.*

- *Objective 4: Assemble a chemical kinetic mechanism and evaluate the rate coefficients needed to describe the heterogeneous reactions of Hg, CO, NO, NH_3, SO_2, SO_3, and HCl across an SCR catalyst with sufficient accuracy to be useful for design purposes.*

CHAPTER 2

LITERATURE REVIEW AND BACKGROUND INFORMATION

2.1 Evolution of Mercury in Products of Coal Combustion

The thermodynamics and chemical kinetics controlling the evolution of gas-phase mercury species in the products of coal combustion in power plants were analyzed by Senior et al. (2000b). As shown by these authors, mercury is released during combustion of coal as Hg(0) vapor and, as the flue gas is cooled in the convection heat transfer section downstream from the furnace exit, remains almost entirely in the elemental state, with a small fraction (~1%) as HgO vapor, until the temperature reaches approximately 700 ^{o}C. In the vicinity of this temperature, depending upon the chlorine content of the coal and combustion products, conversion of elemental mercury to $HgCl_2$ vapor begins. The distribution of mercury species between Hg(0) and $HgCl_2$ shifts toward $HgCl_2$ as the temperature continues to decrease until, at approximately 530 ^{o}C, again depending upon the chlorine content of the coal, the distribution of mercury species in flue gas becomes frozen. Were chemical equilibrium maintained as temperature continued to decrease, all mercury would be converted to $HgCl_2$ at approximately 450 ^{o}C, again depending on the chlorine-species concentration, but, below approximately 530 ^{o}C, where the reaction rate becomes slow, conversion of Hg(0) to $HgCl_2$ is controlled by chemical kinetics.

On further cooling, both Hg(0) and Hg(II) vapors can enter the particulate phase by adsorption onto fly ash (Hassett, 1999) and unburned char particles. The most stable species in coal-derived flue gas, and the corresponding temperature ranges, according to calculations by Dajnak et al. (2003) are:

$$Hg(0)\ (gas)\ (T > 527\ ^{o}C) \rightarrow HgCl_2\ (gas)\ (T = 527 \text{ to } 127\ ^{o}C) \rightarrow$$
$$HgSO_4\ (solid)\ (T < 127\ ^{o}C) \qquad (R1)$$

According to these calculations, all mercury would exist as $HgCl_2$ just upstream of a particulate control system, where temperatures should not exceed 450 to 527 ^{o}C, were it in chemical equilibrium (Senior et al., 2000a, 2000b; Dajnak et al., 2003; Wang et al., 2003; Yudovich and Ketris, 2005). The data obtained by U.S. EPA's mercury ICR (U.S. EPA, 1998) indicated that in plants burning eastern bituminous coals, 60 to 80% of the mercury in flue gas is in the oxidized state and therefore soluble in water, compared to only 10 to 20% of the mercury in flue gas from combustion of Powder River Basin coals (Schimmoller, 2001). The rate and extent of mercury oxidation are limited by a number of factors, including combustion characteristics, coal composition (such as chlorine content), concentrations of other species (such as NO_x and SO_x) in the flue gas, and the time-temperature history (Presto and Granite, 2006).

Because of the large number of variables, including coal properties, equipment, and operating conditions, explanations for differences in mercury capture performance are not easily derived from the ICR data. As a result of their analysis, Chu et al. (2001) emphasized the importance of coal chlorine content, while Weilert and Randall (2001) focused on the effects of coal rank and the type of FGD system. Afonso and Senior (2001) found no statistically significant correlation of mercury removal with coal

chlorine, sulfur, ash content, or flue gas temperature, except in the case of dry FGD, where a significant correlation of mercury removal with coal chlorine was observed.

Oxidation of Hg(0) can occur by either homogeneous or heterogeneous reaction paths. Heterogeneous chemistry oxidation, facilitated by a catalytic surfacec (such as SCR catalyst, unburned carbon, or fly ash), is faster than homogeneous oxidation over the range of temperatures where $HgCl_2$ formation is favored. However, conversion of Hg(0) to Hg(II) in post-combustion flue gas is still kinetically limited below approximately 530 ^oC, regardless of the governing mechanism. Though at temperatures below approximately 450 ^oC, at equilibrium, the majority of the mercury would exist as $HgCl_2$ (Senior et al., 2000b; Dajnak et al., 2003; Wang et al., 2003), even in the presence of catalytic surface, thermodynamic chemical equilibrium is apparently only rarely reached during the residence time available in the optimum temperature range. As a result, the fraction of Hg(II) in flue gas downstream from the air preheater varies from nearly 0 to 100%, depending on the factors mentioned above (Presto and Granite, 2006). A recent survey of catalysts for mercury oxidation in flue gas by Presto and Granite (2006) revealed that neither the homogeneous nor the heterogeneous mechanism for mercury oxidation is completely understood, and that improvement in the quantitative description of the kinetics and mechanism of mercury oxidation is critical to control of mercury emissions from coal-fired electric utility boilers.

2.2 Homogeneous Mercury Chemistry

The factors affecting homogeneous reactions of mercury in post-combustion flue gas, or simulated flue gas, under conditions relevant to those encountered in the gas

cleaning systems of coal-fired utility boilers have been extensively investigated. A suggested pathway for mercury oxidation involves the gas-phase or homogeneous reaction of Hg(0) with atomic chlorine (Cl). Therefore, understanding the kinetics of chlorine speciation (Cl, chlorine gas (Cl_2), and HCl) in post-combustion flue gas is important to understanding mercury oxidation (Senior et al., 2000a, 2000b; Pavlish et al., 2003).

An early investigation by Hall et al. (1991) studied the effects of HCl, Cl_2, NO_x, and O_2 on mercury speciation. That work, and subsequent experimental investigations, including those by Sliger et al. (1992, 2000), Ghorishi (1998), and Widmer et al. (2000), concluded that the concentration of HCl in the flue gas mixture significantly affected mercury conversion from Hg(0) to Hg(II). However, Hg(0) is not believed to be directly oxidized by HCl, but instead requires a chlorinating agent such as Cl or Cl_2, produced in trace quantities from the HCl. Due to a low energy barrier, the Hg(0) + Cl reaction occurs at a rate near the collision limit, even at room temperature, and is therefore much faster than the Hg(0) + HCl reaction, which has a higher energy barrier that retards the reaction at typical flue gas temperatures (Hranisavljevic and Fontijin, 1997).

Sliger et al. (1992, 2000) suggested that the rate-determining step in homogeneous mercury oxidation is the reaction between Hg(0) and Cl atoms, where Hg(0) reacts with Cl atoms during flue gas quenching to produce an intermediate product, HgCl, by the following reaction:

$$Hg(0) + Cl \rightarrow HgCl \qquad (R2)$$

HgCl is then further oxidized by HCl, Cl_2, or chlorine radicals to form $HgCl_2$. Senior et al. (2000a) confirmed that the major pathway to $HgCl_2$ is via the reaction of Hg(0) with

atomic Cl. Mamani-Paco and Helble (2000) observed nearly complete oxidation of Hg(0) at 500 ^{o}C in the presence of 500 ppmv Cl_2. Thus, the key parameters in predicting homogeneous mercury oxidation are the initial HCl, Cl, and Cl_2 concentrations in the flue gas at the onset of mercury oxidation, the gas quench rate, the rate of dissociation of HCl, and the rate at which Cl atoms combine to form Cl_2 (Senior et al., 2000a, 2000b).

Experiments and kinetic calculations by Mamani-Paco and Helble (2000), Senior et al. (2000b), and Niksa et al. (2001) show that chlorine speciation is greatly affected by the rapid gas quench rates. Calculatons by Senior et al. (2000a) showed that high concentrations of atomic Cl present at peak flame temperatures are converted primarily to HCl and trace amounts of molecular Cl_2 as the gas cools, according to the following elementary reactions:

Interconversion reactions of Cl and HCl:

$$HCl + OH \leftrightarrow H_2O + Cl \quad \text{(R3)}$$

$$HCl + O \leftrightarrow OH + Cl \quad \text{(R4)}$$

$$HCl + M \leftrightarrow H + Cl + M \quad \text{(R5)}$$

$$HCl + O_2 \leftrightarrow HO_2 + Cl \quad \text{(R6)}$$

Interconversion reactions of Cl and Cl_2:

$$Cl_2 + M \leftrightarrow Cl + Cl + M \quad \text{(R7)}$$

$$Cl_2 + O \leftrightarrow ClO + Cl \quad \text{(R8)}$$

$$Cl_2 + H \leftrightarrow HCl + Cl \quad \text{(R9)}$$

The evaluation by Niksa et al. (2001) of data from four laboratory studies resulted in a mixed conclusion about the effect of NO on homogeneous mercury oxidation, as NO was found to either inhibit or promote mercury oxidation, depending on its concentration.

The laboratory data also showed an increase in the extent of mercury oxidation at higher flue gas quench rates in the presence of NO.

Kramlich and Castiglone (2004) investigated the effect of H_2 and CO introduction to the quench region of post-combustion flue gas on Cl production and its subsequent oxidation of elemental mercury. Chemical kinetic models suggested that H_2 and CO should both individually promote the atomic Cl production needed to drive mercury oxidation, via the following reactions:

$$H_2 + OH \rightarrow H_2O + H \quad \text{(R10)}$$

$$H + O_2 \rightarrow OH + O \quad \text{(R11)}$$

$$O + H_2 \rightarrow OH + H \quad \text{(R12)}$$

$$CO + OH \rightarrow CO_2 + H \quad \text{(R13)}$$

$$H + O_2 \rightarrow OH + O \quad \text{(R14)}$$

$$HCl + OH \rightarrow Cl + H_2O \quad \text{(R15)}$$

The experimental results reported by these authors showed that 50 ppmv of H_2 slightly promoted mercury oxidation at low temperatures (< 400 ^oC), significantly promoted oxidation around 600 ^oC, and significantly inhibited oxidation at high temperature (> 900 ^oC). The introduction of 100 ppmv CO in the absence of H_2 resulted in either no promotion, or a small inhibition of mercury oxidation. The introduction of 100 ppmv CO with 20 ppmv H_2 resulted in a behavior similar to that of H_2 alone, indicating CO does not appear to significantly participate in the homogeneous oxidation of elemental mercury.

Sliger et al. (1992) reported that homogeneous mercury oxidation is governed primarily by: (1) HCl concentration, (2) quench rate, and (3) background gas

composition. The experimental results of Galbreath et al., (2000) confirm that the extent of mercury oxidation increases with HCl concentration and coal-Cl content, and that Hg(0) reacts with chlorine radicals between 400 and 700 ^{o}C (Sliger et al., 2000). Widmer et al. (2000) and Ghorishi (1998) also investigated the effect of temperature and found that Hg(0) oxidation increased with increasing flue gas temperature over the range from 515 to 754 ^{o}C. Mamani-Paco and Helble (2000) observed no reaction between Hg(0) and Cl_2 below 500 ^{o}C and concluded that reports of homogeneous mercury oxidation at near ambient temperatures are likely due to catalytic surface effects.

Ghorishi et al. (1998) found that gas-phase oxidation of Hg(0) was inhibited in the presence of SO_2 and water vapor. Lighty et al. (2006) showed that Hg(0) oxidation in the presence of 300 ppmv HCl was reduced from 70% to 0 when the SO_2 concentration was increased from 0 to 300 ppmv. Experimental work by Fry et al. (2006) also showed inhibition of mercury oxidation by SO_2 in the presence of a high quench rate temperature profile. It was suggested that SO_2 and water vapor may inhibit homogeneous oxidation of Hg(0) by scavenging the chlorine-containing oxidizing agent, through the following reaction:

$$Cl_2\ (g) + SO_2\ (g) + H_2O\ (g) \leftrightarrow 2HCl\ (g) + SO_3\ (g) \qquad \text{(R16)}$$

2.2.1 *Homogeneous Chemical Kinetic Model Development*

The development of mathematical models to estimate mercury speciation, in parallel with the development of control technologies, is necessary to formulate cost-effective mercury control strategies. Both homogeneous and heterogeneous reactions must be considered. Some homogeneous reaction mechanisms include up to 107 steps

involving 30 species (Xu et al., 2003), using reaction rate constants derived from experimental data and from theoretical estimates. Recent work includes rate constants calculated using Transition State Theory (TST) and quantum chemistry (Xu et al., 2003).

Edwards et al. (2001) developed a model for mercury chlorination, consisting of 60 elementry reactions, including a pathway involving HgO, and 21 species. The performance of this model was assessed by comparing it with results from laboratory-scale experiments by Ghorishi et al. (1998) and Widmer et al. (2000). At temperatures below 630 ^{o}C, the model drastically under-predicted the measured mercury conversion trends. Explanations offered for the discrepancies between the model predictions and the experimental data were the need for additional mercury chlorination and oxidation pathways or surface-induced catalytic effects (Edwards et al., 2001).

Niksa et al. (2001) developed and evaluated a homogeneous mechanism containing eight reactions, based on the framework proposed by Widmer et al. (2000), describing the direct oxidation of Hg(0) to HgCl and $HgCl_2$ by four chlorine species (Cl, Cl_2, HCl, and HOCl):

$$Hg(0) + Cl + M \leftrightarrow HgCl + M \quad \text{(R17)}$$

$$Hg(0) + Cl_2 \leftrightarrow HgCl + Cl \quad \text{(R18)}$$

$$Hg(0) + HCl \leftrightarrow HgCl + H \quad \text{(R19)}$$

$$Hg(0) + HOCl \leftrightarrow HgCl + OH \quad \text{(R20)}$$

$$HgCl + Cl_2 \leftrightarrow HgCl_2 + Cl \quad \text{(R21)}$$

$$HgCl + Cl + M \leftrightarrow HgCl_2 + M \quad \text{(R22)}$$

$$HgCl + HCl \leftrightarrow HgCl_2 + H \quad \text{(R23)}$$

$$HgCl + HOCl \leftrightarrow HgCl_2 + OH \quad \text{(R24)}$$

These reactions were coupled to submechanisms describing the reactions of C, H, N, O, S, and Cl species, adopted from published work. The complete mechanism consisted of 160 elementary reactions. The model was able to accurately explain several sets of experimental measurements in synthetic, particle-free flue gases and quantitatively described the oxidation of Hg(0) via partial oxidation to HgCl, then complete oxidation to $HgCl_2$ for a broad range of temperatures and HCl concentrations. The homogeneous mechanism alone, however, was not able to accurately predict the measured extent of mercury oxidation in coal-derived flue gases, in tests using five different coals in a laboratory-scale flame. The model under-predicted the extent of mercury oxidation for a high Cl content coal and over-predicted oxidation for the other coals tested. These discrepancies were rectified by the addition of a heterogeneous reaction subset, to reflect mercury oxidation by chlorinated surface sites on unburned carbon (UBC) in place of gas-phase Cl atoms (Niksa and Fujiwara, 2005a).

An alternative version of the 8-step mechanism was developed by Qiu et al. (2003). Krishnakumar and Helble (2007) compared calculations using the models of Niksa et al. (2001) and Qiu et al. (2003) with experimental measurements by Sliger et al. (2000), Sterling et al. (2004), and Fry et al. (2006). The mechanism of Qiu et al. (2003) was in agreement with the broadest set of experimental data, while the mechanism of Niksa et al. (2001) was in best agreement with a single set of data gathered under extremely rapid quench rate conditions.

Xu et al. (2003) have run simulations of mercury reactions using CHEMKIN (Reaction Design, San Diego, CA) and other computer-based tools. A comparison of the simulation results with experimental data from other authors showed a divergence from

the experimental data in many cases (Xu et al., 2003). The discrepancies may have been due to the absence of accurate rate constants in the proposed mechanisms, the need for reactions involving intermediate products, such as HgO, or the presence of catalytic effects in the experiments (Xu et al., 2003). Further work needs to be directed toward improving the accuracy of rate constants for Hg-Cl reactions by transition state theory, and/or by experiments (Xu et al., 2003).

Wilcox (2004) calculated rate constants for elementary reactions of mercury and chlorine species using theoretical methods from quantum chemistry and transition state theory (Wilcox et al., 2003, 2004; Wilcox and Blowers, 2004). Wilcox (2004) provided theoretical estimates of rate constants for seven of the eight gas-phase reactions discussed above (R17 to R19 and R21 to 24). Lighty et al. (2006) compared calculations using this mechanism with experimental measurements by Fry et al. (2005) and calculations using the 8-step mechanism of Qiu et al. (2003). Although the seven elementary reactions do not consider the initial step in mercury oxidation mediated by HOCl, as described by reaction R20, they account for the majority of the kinetic pathways for mercury oxidation by chlorine. Though the HOCl reactions are potentially as important as those of Cl_2 and HCl, they are less important than those of Cl (Lighty et al., 2006). The mercury reaction sequence was coupled to the sub-models describing Cl, NO_x, and SO_x chemistry, adopted from the literature and incorporated in the models developed by Helble and coworkers (Niksa et al., 2001; Qiu et al., 2003). The model containing the rate coefficients derived from theory by Wilcox (2004) overpredicted the sensitivity of mercury oxidation to HCl concentration at low HCl levels (< 100 ppmv) and underpredicted sensitivity to HCl at higher levels (100 to 700 ppmv) (Lighty et al., 2006), but the agreement with

measurements was surprisingly good, considering that the rate coefficients were derived from first principles.

Carbon monoxide is commonly present at low levels (less than approximately 100 ppmv) in furnace exit gas from coal-fired boilers. Higher levels of CO can be present in the flue gas if there is incomplete combustion due to insufficient air or poor mixing of the coal and air. Carbon monoxide is expected to be the most active reducing agent present in significant concentration in flue gas. Therefore, CO might be expected to have an influence on the distribution of mercury species, especially if HgO is an intermediate in any of the reactions involving mercury.

Rather than predicting reduction of Hg(II) by CO, Niksa et al. (2002) predicted an increase from 28 to 54 % in the extent of mercury oxidation on increasing the CO concentration in flue gas from 1 to 100 ppmv, based upon their homogenous and heterogeneous reaction mechanism, discussed in Section 2.3.3. A homogeneous kinetic model developed by Breen and Gabrielson (2003) predicted that an increase in CO from 0 to 50 ppmv resulted in a 50% increase in Cl concentration in the flue gas.

Calculations to examine the effect of CO on homogeneous oxidation of mercury were performed by Balaji Krishnakumar in Joseph J. Helble's group at Dartmouth College (B. Krishnakumar and J. J. Helble, Personal communication, 2008)*. The calculations were performed using the current version of the semi-empirical 8-step mechanism for homogeneous reactions of mercury and chlorine species developed by Niksa et al. (2001) and Qiu et al. (2003) (Krishnakumar and Helble, 2007). The calculations were performed for a simulated flue gas from an Ohio bituminous coal

* Dr. Krishnakumar is now with Niksa Energy Associates, Belmont, CA.

(130 ppmv HCl) using both a constant quench rate and a full-scale industrial boiler post-flame temperature profile.

In the constant quench rate analysis, the flue gas was first cooled from 1177 to 367 ^{o}C in 1.5 seconds, then held at the final temperature for 2 seconds, simulating the gas temperature and residence time in SCR. The CO level was varied from 1.5 to 1500 ppmv. Homogeneous mercury oxidation was predicted to begin below 477 ^{o}C and continue during the 2 seconds of residence time under SCR conditions. The model predicted that approximately 11% of the mercury would be oxidized, increasing to 12% at 1500 ppmv CO. A similar calculation was performed for a full-scale industrial boiler temperature profile from the furnace exit to the stack, with the flue gas held at 377 ^{o}C for 2 seconds, as in SCR. In this case, an increase in CO concentration from 1.5 to 1500 ppmv also had little effect on the extent of mercury oxidation. A third case, in which the calculation was begun at 377 ^{o}C and held at that temperature for 2 seconds, showed a 3% increase in the extent of mercury oxidation over the range of CO from 1.5 to 1500 ppmv. Based on these simulations of the homogeneous system by Krishnakumar and Helble, CO is not expected to have a significant effect on the gas-phase oxidation of mercury over the entire post-combustion temperature range in coal-fired electric utility boilers, from the furnace exit to the stack (1177 to 77 ^{o}C), consistent with the experimental measurements reported by Kramlich and Castiglone (2004).

Investigation of pilot-scale coal combustion data by Niksa and Fujiwara (2005a) showed that coal-Cl content is not the determining factor for the extent of mercury oxidation, indicating that either the homogeneous mechanism reviewed was incomplete or heterogeneous mercury oxidation was involved.

2.3 Heterogeneous Mercury Chemistry

Thermodynamic chemical equilibrium calculations predict that conversion of Hg(0) to $HgCl_2$ begins at approximately 700 ^oC, increases as temperature decreases, and is complete at approximately 450 ^oC (Senior et al., 2000b). Since typical flue gas temperatures range from 127 to 327 ^oC at the outlet of the air heater (the last section of heat exchange equipment) (Sliger et al., 2000), mercury should exist entirely as Hg(II) downstream from the air heater. However, the oxidation of mercury in the convection section of coal-fired utility boilers is kinetically limited (Laudal et al., 1996). In addition to the low concentrations of mercury and its oxidizing agents in coal-fired combustion products, favorable reactions for mercury oxidation have narrow temperature and time windows in the presence of quenching (Laudal et al., 1996). Homogeneous models alone, consistently under-predict the extent of oxidation of mercury from coal-fired utility boilers (Laudal et al., 1996; Niksa and Fujiwara, 2005). In order to account for the full extent of mercury oxidation to the presumed final product ($HgCl_2$), solid-catalyzed heterogeneous reactions of mercury are evidently important.

When discussing the heterogeneous oxidation of mercury in flue gas from coal combustion, it is necessary to consider how both the properties of the solid surfaces, as well as the composition of flue gas, together affect the oxidation and capture of mercury. A number of studies have been performed to evaluate the mercury oxidation and adsorption properties of actual and simulated fly ash, activated carbons (including halogen or sulfur-impregnated carbons), various mineral compounds, and noble metals (Presto and Granite, 2006). Laudal et al. (1996), Galbreath and Zygarlicke (2000), Fujiwara et al. (2002), Norton et al. (2003), Dunham et al. (2003), and many others have

focused their research on the effects of fly ash on mercury oxidation. The unburned carbon and iron oxides components of fly ash were both found to promote mercury oxidation (Ghorishi, 1998). Catalysts such as SCR catalysts for NO_x control as well as Ce, V, and Co-based catalysts have also been shown to accelerate the oxidation of mercury.

2.3.1 *Heterogeneous Mercury Oxidation Mechanisms*

Many different mechanisms by which heterogeneous catalysts participate in mercury oxidation have been proposed. Pan et al. (1994) showed that a metal oxide catalyst could promote the generation of Cl_2 gas from HCl, via the Deacon reaction:

$$2HCl\ (g) + 1/2O_2\ (g) \leftrightarrow Cl_2\ (g) + H_2O\ (g) \qquad (R25)$$

resulting in an increase in the extent of mercury oxidation to the intermediate product, HgCl, by the gas phase reaction between Hg(0) and Cl_2. HgCl is then further oxidized by HCl, Cl_2, or chlorine radicals to form $HgCl_2$. However, in the absence of such a catalyst, the flue gas concentration of Cl_2 is too low to account for the full extent of oxidation of mercury observed in coal-fired boilers (Senior et al., 2000b).

The gas-phase species thought to react with catalytic surface, forming the adsorbed species primarily responsible for mercury oxidation is HCl. Galbreath and Zygarlicke (2000), Laudal et al. (2000), Sliger et al. (2000), and Senior et al. (2006) have all shown a correlation between HCl concentration and the extent of mercury oxidation in the presence of catalysts. In addition, Gale (2002) and Ghorishi et al. (2005) have shown that the extent of mercury oxidation is reduced in the presence of HCl sorbents, such as

CaO. Niksa et al. (2001) showed that coals having high chlorine concentrations generated an abundance of oxidized mercury species, independent of the residence time.

Several different mechanisms involving adsorbed species are possible. The Langmuir-Hinshelwood mechanism describes reaction between two species adsorbed on a solid surface (Pilling and Seakins, 1995):

$$A\ (g) \leftrightarrow A\ (ads) \qquad (R26)$$

$$B\ (g) \leftrightarrow B\ (ads) \qquad (R27)$$

$$A\ (ads) + B\ (ads) \rightarrow AB\ (ads) \qquad (R28)$$

$$AB\ (ads) \rightarrow AB\ (g) \qquad (R29)$$

In this mechanism, Hg(0) and a chlorine species (most likely, HCl) are the two reactants, and the rate of reaction is determined by the concentrations (or partial pressures, p_i) of the reactants in the gas phase, the adsorption equilibrium constants for the two reactants (K_i), and the rate constant for the surface reaction (k_{surf}). The Langmuir-Hinshelwood mechanism is a plausible mechanism for catalysis of Hg(0) oxidation, provided the catalyst can adsorb both Hg(0) and HCl.

The Eley-Rideal mechanism describes the interaction between an adsorbed species and a gas-phase species, according to the following reactions:

$$A\ (g) \leftrightarrow A\ (ads) \qquad (R30)$$

$$A\ (ads) + B(g) \rightarrow AB(g) \qquad (R31)$$

Niksa and Fujiwara (2005b) suggested that HCl is adsorbed on the catalyst surface and that Hg(0) is not (or is only weakly adsorbed). However, because Hg(0) is known to be adsorbed on various sorbents (such as activated carbon) and surfaces, an Eley-Rideal

mechanism for reaction between adsorbed Hg(0) and gas-phase HCl is also possible (Senior et al., 2000b).

The Mars-Maessen mechanism describes the interaction between an adsorbed species [Hg(0)] and a lattice oxidant (either O or Cl) that is replenished from the gas-phase, as described by the following reactions (with lattice oxygen) (Mars and Maessen, 1968):

$$A(g) \leftrightarrow A(ads) \quad \text{(R32)}$$

$$A(ads) + M_xO_y \rightarrow AO(ads) + M_xO_{y-1} \quad \text{(R33)}$$

$$M_xO_{y-1} + 1/2O_2 \rightarrow M_xO_y \quad \text{(R34)}$$

$$AO(ads) \rightarrow AO(g) \quad \text{(R34a)}$$

The Mars-Maessen mechanism explains the enhancement of Hg(0) sorption on halogen-promoted sorbents and fly ashes, and is consistent with the observation of Hg(0) oxidation in the absence of gas-phase oxygen and chlorine (Granite et al., 2000).

Niksa et al. (2005) developed the following heterogeneous mechanism to describe the oxidation of Hg(0) to HgCl on unburned carbon:

$$StSA\ (S) + HCl \rightarrow StCl\ (S) + H \quad \text{(R35)}$$

$$StCl\ (S) + Cl \rightarrow Cl_2 + StSA\ (S) \quad \text{(R36)}$$

$$StCl\ (S) + Hg(0) \rightarrow StSA\ (S) + HgCl \quad \text{(R37)}$$

There are two types of carbon sites in the mechanism: StSA (S) denotes an unoccupied surface site and StCl (S) denotes a chlorinated surface site. Unoccupied sites may be chlorinated by adsorption of HCl, with release of H atoms according to reaction R35. Chlorinated sites are freed either by recombination with Cl atoms, to generate Cl_2 gas (R36), or by partial oxidation of Hg(0) to HgCl on a chlorinated site (R37).

Currently, the elementary surface reactions responsible for the catalytic oxidation of Hg(0) in the presence of fly ash, unburned carbon, and SCR catalysts have not been identified. As a result, the ability to accurately predict the extent of Hg(0) oxidation by various catalysts is limited. Presto and Granite (2006) identified four major areas for further research in order to improve our understanding of the catalytic oxidation of Hg(0), as listed below:

1. Is Hg(0) chemically or physically adsorbed on sorbent and catalyst surfaces?
2. What are the intermediate products, if any?
3. What is the final Hg(II) species?
4. What are the effects of other gaseous components (such as CO, NO_x, and SO_2) on the reaction mechanism?

2.3.2. *Overview of Mercury Capture on Fly Ash and Unburned Carbon*

Fly ash has the dual role of catalyzing the oxidation of mercury as well as capturing mercury. Fly ash is characterized by its surface area, carbon content (loss on ignition), and major elements (Si, Al, Fe, Ca, Mg, K, Na). Both fly ash surface area and composition seem to play an important role in mercury oxidation. Dunham et al. (2003) showed that the oxidation of mercury is directly proportional to the content of magnetite in fly ash. However, the carbon content of fly ash seems to be an even more important factor (Laudal et al., 1996). High levels of unburned carbon in fly ash have been observed to promote mercury oxidation, confirming the role and importance of heterogeneous chemistry.

Norton et al. (2003) examined the effects of different types of fly ash on mercury oxidation. They also found the presence of fly ash to be critical for mercury oxidation, but the composition of the ash was not so important. Gas composition was found to be more important than ash composition, especially the presence of NO_2 and HCl, both of which promoted mercury oxidation.

Nitrogen oxides (NO_x) are also considered potential Hg(0) reactants in flue gas that may promote the formation of Hg(II) (Yudovich and Ketris, 2005). The NO_x distribution in flue gas is generally approximately ≤ 5% NO_2 and ≥ 95% NO. Kinetic limitations and the relatively short flue gas residence time in a duct or stack limit the occurrence of homogeneous reactions involving Hg(0) and NO or NO_2. Some tests indicate, however, that NO_2 reacts heterogeneously with Hg(0) on fly ash and sorbent surfaces to form Hg(II) in heated (< 200 ^oC), simulated coal combustion products (Galbreath et al., 2004). This effect was noted for NO_2 concentrations as low as 20 ppmv.

Ghorishi et al. (1999) have demonstrated that NO is a potent Hg(0) reactant in the presence of fly ash components. These authors showed that the chemisorption of NO on fly ash surface created active sites for Hg(0) adsorption, enhancing mercury oxidation. Niksa and Fujiwara (2005a) observed that variations in both NO and O_2 are usually associated with changes in the levels of unburned carbon in the fly ash, which can impact mercury oxidation.

In full-scale boilers, mercury removal by fly ash alone, without sorbent injection, has been reported to range from near 0 to 90% for some western U.S. coals and up to about 60% for certain U.S. and British bituminous coals (Ghorishi, 1998), depending on the temperature, the level of unburned carbon in the ash, and the catalytic effects of

inorganic ash constituents. The mercury adsorption capacity of the inorganic fraction of fly ash is typically low, although certain fly ashes having low carbon content may still exhibit significant mercury capture (Laudal et al., 1996; Xu et al., 2003). The capture of mercury on fly ash is progressively increased as the flue gas temperature is reduced below 400 ^{o}C and is increased by extending the effective contact time between flue gas and the fly ash (Butz et al., 2000). Mercury capture is often enhanced by high levels of unburned carbon in the fly ash (Butz et al., 2000). Results of mercury analyses performed on different fractions of fly ash separated by screening or triboelectrostatic techniques have shown that mercury enrichment often correlates directly with carbon content (Laudal et al., 1996).

The combustion of bituminous coals leaves unburned carbon in fly ash that has been shown to increase mercury adsorption. Experimental work by Li and Hwang (1997) also found mercury to be concentrated in the carbon-rich fraction of fly ash. Preliminary experimental work by Wu et al. (2000) found that adsorption of Hg(II) was 2 to 50 times greater than adsorption of Hg(0) under the same conditions, and was correlated with char surface area. Unburned carbon in the fly ash and flue-gas chlorine content are therefore important factors determining mercury oxidation and capture in coal-fired boiler flue gas.

In general, mercury capture by fly ash is most effective in combustion of bituminous coals (Yudovich and Ketris, 2005). Subbituminous coals and lignites produce fly ash low in unburned carbon, and having low sorption capacity. In addition, these coals are generally low in chlorine content. Gale (2005) obtained mercury speciation and capture data for three different bituminous coals, a Powder River Basin subbituminous coal, and blends of these coals. Most of the data were taken across a baghouse, and the

focus was on moderate- to low-chlorine and sulfur coals. The data suggested that unburned carbon is the dominant parameter affecting mercury sorption as long as some HCl (e.g. 1 ppmv HCl or greater) is present, which is normally the case with any coal. The findings are consistent with other studies showing that the capture of mercury by unburned carbon may be enhanced in the presence of acid gases (HCl and SO_2) (Yudovich and Ketris, 2005).

Laumb et al. (2004) observed that SO_2 competes with HCl for carbon sites on activated carbon and fly ash sorbents. High concentrations of SO_2 have been observed to inhibit mercury oxidation in simulated flue gas (Laudal et al., 2000), possibly by the same competitive adsorption process. In contrast, Norton et al. (2003) have observed SO_2 to enhance mercury oxidation on fly ash, while Ghorishi et al. (2005) and Zhao et al. (2006) did not observe any effect of SO_2 on mercury oxidation on fly ash.

Galbreath and Zygarlicke (1996, 2000) suggested that SO_2 can inhibit mercury oxidation on fly ash via two mechanisms. The first mechanism is a direct reduction of Hg(II) oxide by SO_2 through the following reaction:

$$HgO\ (s,g) + SO_2\ (g) \rightarrow Hg(0)\ (g) + SO_3\ (g) \qquad \text{(R38)}$$

The second mechanism is an indirect inhibition of mercury oxidation by SO_2 interference with the supply of a chlorinating agent, Cl_2 (g), for mercury oxidation, through the previously discussed reaction R16. Ghorishi et al. (2005) observed that a decrease in SO_2/HCl ratio in the presence of water vapor resulted in an increase in the extent of mercury oxidation, due to a reduction in Cl_2 scavenging by SO_2, via a reaction similar to reaction R16:

$$Cl_2\ (g) + SO_2\ (g) + 2H_2O\ (g) = 2HCl\ (g) + H_2SO_4\ (g) \qquad \text{(R39)}$$

In other experiments at the SRI Combustion Research Facility (CRF), Gale et al. (2008) investigated the mechanisms driving mercury oxidation and capture in the back pass of utility boilers. The roles of flue-gas chlorine concentration and the concentrations of carbon and calcium in ash were studied. These three parameters were considered to be the dominant parameters governing mercury speciation and removal from coal-derived flue gas. The study also showed a synergistic relationship between unburned carbon and calcium that enhanced mercury capture by fly ash, but changes in chlorine concentration (~5 ppmv to ~60 ppmv HCl) had a minimal impact on mercury removal. Senior et al. (2000a) found that extensive mercury capture can sometimes occur in high-calcium fly ashes from western U.S. subbituminous coals, possibly by newly-formed calcium silicates. In addition, other components of high-calcium fly ashes have been found to capture Hg(0), but the mechanisms are currently unclear (Senior et al., 2000a).

2.3.3 *Heterogeneous Chemical Kinetic Model Development*

Niksa et al. (2005a) developed a combined homogeneous-heterogeneous reaction model to predict mercury oxidation in coal-derived flue gas for different types of coals. These authors used a 168-step homogeneous mechanism, including the 8-step mechanism for mercury oxidation by gas-phase chlorine species (R17 through R24), combined with the heterogeneous reaction subset for mercury oxidation on unburned carbon (R35 through R37). The combined mechanism was able to predict the marked increase in extent of mercury oxidation across a layer containing unburned carbon in a lab-scale gas cleaning system, consistent with the behavior observed in baghouse filter cakes (Niksa and Fujiwara, 2005a).

Niksa et al. (2002) also developed a comprehensive unified mercury mechanism (Uni-Hg) for simultaneous mercury oxidation and sorption on unburned carbon. Mercury is oxidized via adsorption of Hg(0) on chlorinated carbon sites, as originally proposed (R30). In Uni-Hg, Niksa and coworkers added finite-rate desorption kinetics. Desorption becomes rate-limiting at low temperatures, increasing the surface coverage. A reverse adsorption step for $HgCl_2$, forming adsorbed-HgCl, was included to account for the different sorption rates of Hg(0) and Hg(II). An abridged version of Uni-Hg, without homogeneous chemistry and finite-rate transport, accurately interpreted the reported concentration histories of Hg(0) and Hg(II) during adsorption on unburned carbon alone and on granulated activated carbon (GAC).

Gale et al. (2008) developed mechanisms for the enhancement of mercury capture by carbon and calcium in fly ash for various coal-fired scenarios, including coal blending and sorbent injection. These authors investigated and described the specific mechanisms associated with mercury oxidation and capture across a baghouse and ESP for various sorbent injection and coal blending conditions. An empirical model, derived using response surface concepts, was developed to correlate mercury removal with calcium and carbon concentrations in the flue gas. The experimental results were illustrated in contour plots of mercury removal (at both the inlet and exit from the ESP) as functions of carbon and calcium concentrations (at the ESP inlet). The contour plots were based on a least-squares multiple regression analysis used to determine rate constants for the quadratic model (Gale et al., 2008), which accurately described the experimental data.

The removal of mercury by fly ash in full-scale boilers depends on the temperature, the level of unburned carbon in the ash, the properties of unburned carbon,

and the catalytic effects of inorganic ash constituents. Calcium helps to enhance mercury removal by stabilizing the oxidized mercury formed on carbon surfaces (Gale et al., 2008).

2.4 Air Pollution Control Devices

The most common combination of APCDs on coal-fired power plants in the U.S. is an ESP for removal of particulate matter located downstream from the air pre-heater (cold-side ESP), followed by a wet FGD system, for capture of SO_2 (Chu et al., 2001; Weilert and Randall, 2001). The next-most common configuration is a cold-side ESP followed by a spray dryer absorber (dry FGD) and fabric filter. According to the ICR data (U.S. EPA, 1998), overall mercury removal by the latter system, when firing bituminous coals, was greater than 88%, but removal was typically less than half of that value in units firing subbituminous coals and lignites, though there were cases in which mercury capture was higher (Weilert and Randall, 2001). Mercury removal efficiencies in systems equipped with a cold-side ESP and wet FGD were below 85% in all cases, including units firing bituminous coals, subbituminous coals, and lignites. The need for new coal-fired power plants throughout the U.S. increases the importance of understanding the causes of poor performance of existing FGD systems with respect to mercury removal. The choice of FGD process for these new units may be influenced by their relative ability to remove mercury, should that approach be taken to meeting the existing and anticipated regulations on mercury emissions from coal-fired electric utility boilers.

2.5 Mercury Oxidation during Selective Catalytic Reduction of NO_x

Commercial SCR catalysts are required to have several characteristics, including high NO_x removal activity, high durability and stability, low pressure drop, low ammonia slip, good resistance to poisoning and erosion, and low SO_2 oxidation activity (Svachula, 1993). A common commercial catalyst formulation contains titanium dioxide (TiO_2), tungsten trioxide (WO_3), and vanadium pentoxide (V_2O_5), acting as support, promoter, and active component, respectively. Catalysts are shaped in the form of honeycomb monoliths or plates to provide high abrasion resistance and large geometric surface areas, comparable to those of packed beds of catalyst pellets (Beretta et al., 1997).

Oxidation of mercury has been observed in SCR systems for NO_x control, but less so in the presence of low chlorine, as when firing Powder River Basin coals. The ICR data from plants equipped with SCR or selective non-catalytic reduction (SNCR) for NO_X control were inconclusive. Experience in Europe indicates that SCR catalysts are effective mercury oxidation catalysts under some conditions (Chu et al., 2001). In fact, European investigators have reported complete oxidation of Hg(0) to $HgCl_2$ on the surface of SCR catalyst in the presence of HCl in laboratory tests (Hocquel et al., 2001). However, mercury oxidation across the catalyst was dependent upon coal type, especially the CaO content of the ash, and catalyst formulation. Experimental data show that V_2O_5 is primarily responsible for the oxidation of mercury by SCR catalyst, while other metal oxides such as CaO, MoO_3, or WO_3 cause the reduction of Hg(II) to Hg(0) (Hocquel, 2004). Data collected from coal-fired utility boilers in the Netherlands, burning bituminous coal, showed that 90% mercury removal can be achieved in plant equipped with SCR, ESP, and wet FGD, when the ESP are maintained at the lower temperatures

characteristic of those units, which fire coals having lower sulfur than is typical of U.S. bituminous coals (Meij et al., 2001). Benson et al. (2005) observed that alkali and alkaline earth species from power plants burning subbituminous and lignite coals could reduce the effectiveness of SCR catalysts for mercury oxidation by depositing on the catalyst and reacting with the acidic sites on the catalyst surface. In the same study it was also observed that the entrances to pores and pores of the SCR catalyst could be blocked by ash, thereby severely reducing both Hg(0) oxidation and NO_x reduction performance. The oxidation of SO_2 to SO_3 by SCR catalysts may also affect mercury oxidation in SCR systems (Kai et al., 2006).

Changes in mercury speciation in SCR are coal-specific and appear to be related to the chlorine, sulfur, and calcium contents of the coal, as well as operating temperature and ammonia-to-NO_x ratio. In spite of these limitations, with proper control of conditions, the installation of SCR for reduction of NO_x could significantly increase oxidation and improve mercury removal from coal-fired utility boilers in the U.S., but further research is needed to better understand mercury reactions across SCR catalysts (Pavlish et al., 2003).

2.6 Mercury Oxidation by a Low Temperature Selective Catalytic and Adsorptive Reactor

Pinto and Smirniotis (2006) investigated the feasibility of a Low Temperature Selective Catalytic and Adsorptive Reactor (LTSCAR) for the simultaneous removal of NO_x and mercury from the flue gas of coal-fired power plants. The study found that it was possible to efficiently reduce NO_x to N_2 using carbon monoxide instead of ammonia or urea as the reductant over a titania-supported MnO_2 catalyst at low temperature

(175 ^{o}C). In addition, chelating sorbents were developed and shown to have very high capacities for Hg(II) (at least 58 mg/g sorbent at 160 ^{o}C). The capture of Hg(0) on the chelating sorbent was also shown to be possible through the inclusion of a mercury oxidation step, either in situ or separately on the titania-supported MnO_2 catalyst. Porous silica substrates were proposed to support an engineered sorbent layer that would oxidize elemental mercury and strongly and selectively bind the oxidized mercury. These preliminary findings suggest that the proposed LTSCAR approach for the simultaneous reduction of NO_x by CO and the oxidation and capture of mercury by sorbents has significant potential economic and environmental advantages.

2.7 Effect of Ammonia and Acid Gases (HCl, NO_x, and SO_x) on Mercury Oxidation in SCR Systems

Mercury oxidation across a SCR catalyst involves many complex interactions between mercury and other flue gas constituents. Fuel quality is extremely important, because it determines the flue gas concentrations of acid gases (HCl, NO_x, and SO_x) (Niksa and Fujiwara, 2005b). Preliminary pilot tests have shown that SCR affects mercury oxidation very differently in boilers burning Powder River Basin coal versus eastern bituminous coal (Laudal, 2000). Results from bench-scale testing showed that HCl provides the critical chlorine source required to oxidize Hg(0) to Hg(II) under SCR operating conditions (Srivastava et al., 2003). Pilot and field tests also showed that high concentrations of HCl in flue gas promoted mercury oxidation, while NH_3 injected for NO_x reduction inhibited mercury oxidation in SCR systems (Niksa and Fujiwara, 2005b; Senior, 2006).

Richardson et al. (2001) measured the change in the fraction of mercury oxidized across a full-scale SCR system in a plant firing Powder River Basin coal. The study found the fraction of mercury in the Hg(II) state upstream of the SCR to be 10 to 18%. However, downstream of the SCR, with the unit operating normally in the presence of ammonia, the fraction of oxidized mercury decreased to 4 to 7%. When ammonia addition to the SCR unit was shut off, the fraction of oxidized mercury increased to 50%, suggesting that ammonia made a strong contribution to the inhibition of mercury oxidation. Measurements of mercury oxidation by Machalek et al. (2003) in a slipstream SCR reactor as a function of NH_3/NO ratio also provided valuable insight into the inhibition of mercury oxidation by ammonia. The effect has been modeled and discussed by Niksa and Fujiwara (2005b) and Senior (2006). Further examination of the effect of ammonia is warranted, to determine whether conditions in an SCR catalyst can be adjusted to optimize three aspects of its performance: high NO_x reduction, low ammonia slip, and high mercury oxidation.

Niksa and Fujiwara (2005b) proposed that the oxidation of mercury by HCl across a SCR catalyst proceeds by a reaction similar to NO reduction by NH_3. HCl and NH_3 compete for sites on the catalyst, but NH_3 is the dominant adsorbed species when both are present. Near the entrance to the SCR catalyst, NH_3 is adsorbed on the catalyst surface and reduces NO_x. As the supply of NH_3 is exhausted towards the exit of the catalyst, HCl becomes the dominant adsorbed species, and mercury oxidation occurs. This mechanism explains the observed decrease in the extent of mercury oxidation with increasing NH_3/NO feed ratio (Machalek et al., 2003; Senior, 2004), but the assumption that HCl, not Hg(0), is the adsorbed species is at odds with the observed uptake of Hg(0) by

catalysts and desorption of Hg(0) from catalyst on increasing the NH_3 concentration in the feed (Hocquel, 2004; Eswaran and Stenger, 2005).

Senior (2006) proposed a model for mercury oxidation in SCR also based on an Eley-Rideal mechanism, but between adsorbed Hg(0) and gas-phase HCl, in which Hg(0) competes with NH_3 for active sites on the catalyst surface. This model also explained the extents of mercury oxidation observed in both lab-scale and pilot-scale experiments, and accounted for the effects of temperature, space velocity, HCl concentration, and catalyst geometry.

Hocquel (2004) proposed a model in which NH_3, HCl, and Hg(0) all compete for active sites on the catalyst surface. Mercury oxidation then occurs via a Langmuir-Hinshelwood reaction between adsorbed Hg(0) and HCl adsorbed at an adjacent site. The model was able to explain the decrease in the extent of mercury oxidation and the desorption of Hg(0) from the catalyst surface with increasing NH_3 concentration.

Ammonia and water vapor in SCR systems are known to react with the SO_3 produced through the oxidation of SO_2 in the flue gas to form ammonium bisulfate (NH_4HSO_4) or ammonium sulfate [$(NH_4)_2SO_4$]. The NH_4HSO_4 or $(NH_4)_2SO_4$ formed may deposit on cold surfaces in equipment, especially the air heater, downstream of the SCR reactor, causing corrosion problems and reduced performance (Svachula, 1993). Since the rate of deposition is controlled by the equilibrium between ammonium sulfates and $NH_3 + SO_3 + H_2O$, industry specifications for SCR reactors generally include upper limits on NH_3 slip and the increase in concentration of SO_3 across the reactor. The admissible increase in SO_3 across an SCR reactor is typically on the order of 10 ppmv (Svachula, 1993) or 1% of the SO_2 in the flue gas.

Olson et al. (1999) identified a Hg(0) – NO_2 – C – MnO_2 reaction product as gaseous mercuric nitrate monohydrate, $Hg(NO_3)2{\cdot}H_2O$, using gas chromatography–mass spectrometry. They hypothesized that $Hg(NO_3)_2{\cdot}H_2O$, in addition to Hg(0) and mercuric chloride ($HgCl_2$,), is a major mercury species existing in coal combustion flue gas and the atmosphere (Galbreath et al., 2004).

In contrast, the addition of sulfur oxides, SO_2 and SO_3, has been shown to inhibit mercury oxidation across a SCR catalyst to some degree (Zhuang et al., 2007). These authors' experimental data suggest that SO_3 competes with HCl for catalyst sites, and that the sulfated sites are less efficient at oxidizing mercury than chlorinated sites. The same group also showed that the addition of HCl, SO_2, and SO_3, mobilized previously adsorbed mercury from the catalyst, resulting in a spike in mercury concentration at the outlet of the SCR catalyst (Zhuang et al., 2007).

2.8 Effect of Carbon Monoxide on Mercury Oxidation in SCR Systems

In the presence of a catalyst, SO_2, NO, and CO in the gas phase can react with surface chlorine to form sulfuryl chloride, nitrosyl chloride, and carbonyl chloride respectively, thereby stripping the catalyst surface of chlorine and reducing the rate of mercury oxidation. Presto and Granite (2006) suggested that further investigation is needed to confirm the effects of these gas-phase species on surface species. Senior et al. (2000a) pointed to the need for additional kinetic information on reactions such as those of chlorine species with Hg(0) and reactions of CO with refractory oxides for NO_x reduction and Hg(0) oxidation, to expand and improve predictive models.

Experimental measurements of mercury oxidation in the presence of CO, varying the CO content with other conditions fixed at those typical of flue gas, would provide useful data with which to validate kinetic models. An incremental improvement in mercury oxidation and capture might be achieved by requiring that CO in flue gas be maintained within a particular range, though such a condition might be difficult to meet in practice.

CHAPTER 3

RESEARCH METHODOLOGY

The present work is the experimental and modeling component of a program of SCR catalyst development and evaluation of catalyst performance conducted by the University of Alabama at Birmingham (UAB), Southern Research Institute (SRI), Clark Atlanta University (CAU), Gas Technology Institute (GTI), and Southern Company Services with support from U.S. DOE. The purpose of the experiments was to obtain data on mercury, NO, and SO_2 reactions in SCR with which to develop and validate models describing catalyst performance. SRI provided its Catalyst Test Facility and its expertise in measurements and analysis of mercury chemistry. CAU and GTI are exploring new SCR catalyst formulations. Southern Company Services provides guidance and advice from the electric utility perspective. The goal is to identify conditions that maximize the conversion of mercury from the elemental state to water-soluble mercuric chloride during SCR of NO_x by NH_3, while maintaining good NO_x reduction performance and minimizing oxidation of SO_2 to SO_3.

3.1 Experimental Apparatus

Southern Research Institute is at the forefront of research on the measurement of mercury in coal combustion products, the transformation of mercury in exhaust treatment

systems, and the removal of mercury from flue gas using sorbents. The present measurements of catalyst performance were performed in the Catalyst Test Facility at SRI.

3.1.1 *Catalyst Test Facility*

The CTF at SRI has been described by Gale et al. (2006) and, briefly, by Tong et al. (2007). The tube furnace, flue-gas continuous emission monitors (CEMs), Fourier transform-infrared spectrometer (FTIR), and gas-flow control systems are pictured in Figure 1. The vertical 3-inch diameter by 3-foot long tube furnace (Lindberg/Blue Model Tube Furnace) containing the micro-reactor has nine separately controllable zones in which temperatures can be set at any level from ambient to a maximum of 1200 ^{o}C. The quartz reactor housing the catalyst is shown in Figure 2. All of the present measurements were obtained at a constant temperature of 378 ^{o}C (+11, -25 ^{o}C), the midpoint of the SCR catalyst manufacturer's suggested operating temperature range for coal-fired applications (316 to 427 ^{o}C). The reactor temperature was measured using a K-type thermocouple inserted directly into the catalyst monolith. The heated sections of the micro-reactor were all made of quartz glass to minimize wall effects. The micro-reactor was designed to contact simulated flue gas with catalysts of various sizes and shapes. The sample of monolithic honeycomb catalyst chosen for the present measurements was wrapped with quartz wool, then pressed into the micro-reactor to prevent gas flow around the outside of the catalyst. Both elemental and total mercury were measured at the outlet from the micro-reactor. Figure 3 shows a schematic diagram of the apparatus used for the measurements of the reduction of NO_x by NH_3 and oxidation of Hg(0) and SO_2.

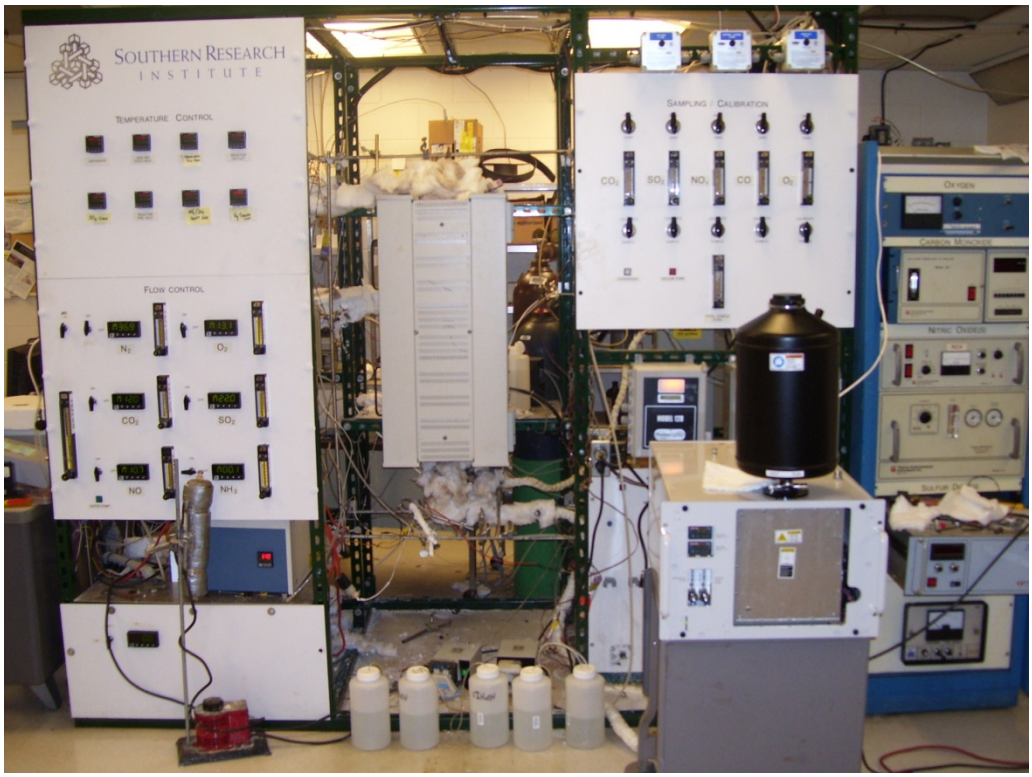

Figure 1. Catalyst Test Facility at Southern Research Institute. The quartz cell housing the catalyst sample is in the vertical tube furnace just to the left of center in the photograph. Continuous gas analyzers are on the far right and the Fourier transform-infrared spectrometer is in the foreground on the right.

Simulated particulate-free flue gas mixed from compressed-gas cylinders was used in the CTF for all the catalyst measurements. All of the major flue-gas species were present, including CO, CO_2, H_2O, O_2, N_2, HCl, NO, SO_2, SO_3, NH_3, and Hg(0), in concentrations mimicking flue gases in real power plants. NO was used exclusively in this work to simulate the NO_x concentrations in the flue gas, since NO represents the majority ($\geq$ 95%) of NO_x in the flue gas of coal-fired boiler systems. Brooks Instrument (Hatfield, PA) 5850E series and OMEGA Engineering, Inc. (Stamford, CT) DMA-

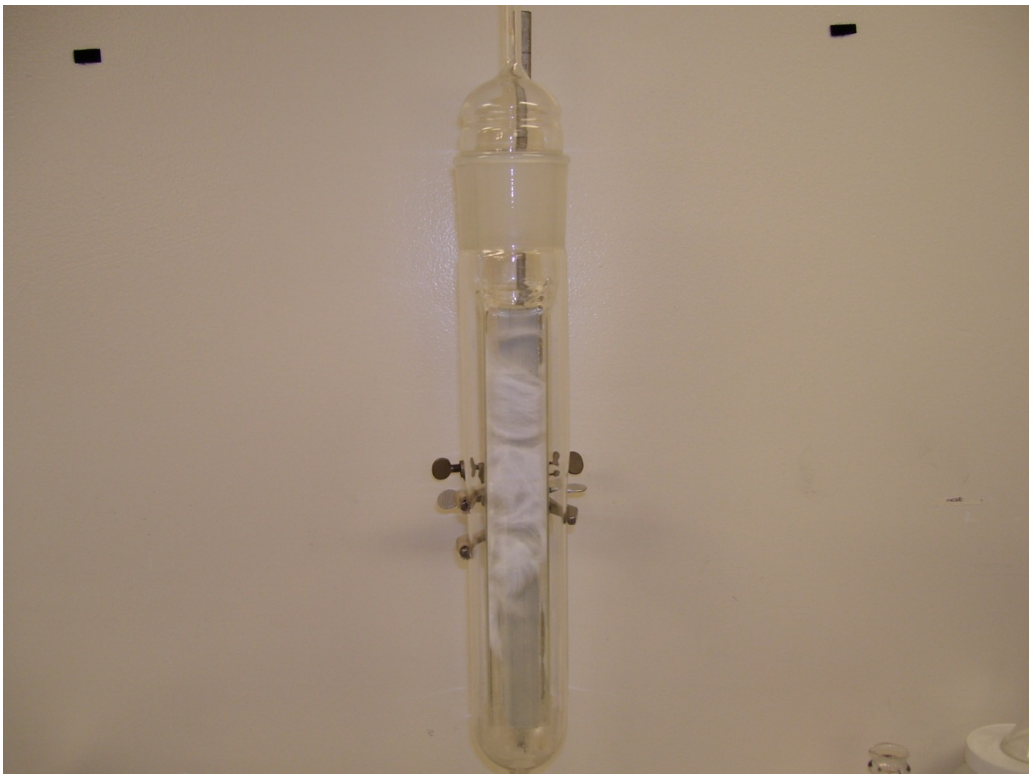

Figure 2. Catalyst Test Facility's quartz reactor with catalyst.

7104E, 7108E, 7102E, and 7101E mass flow controllers were used to control the flow rates of the individual components. Gas flow rates were monitored using a HP-34970A Data acquisition/switch unit. All measurements were made at a constant space velocity of 10,000 h^{-1} (21^{o}C, 1 atm, wet). Specific moisture content was generated through precise control of water evaporation by feeding water through a Cole-Palmer (Vernon Hills, IL) Model Masterflex C/L metering micro-pump. Mercury (10,000 ng/m^3 at 21^{o}C, 1 atm) was introduced to the system using a PS Analytical LTD (Deerfield Beach, FL) Model 10.534 CavKit Mercury Calibration System, which consisted of a reservoir containing an

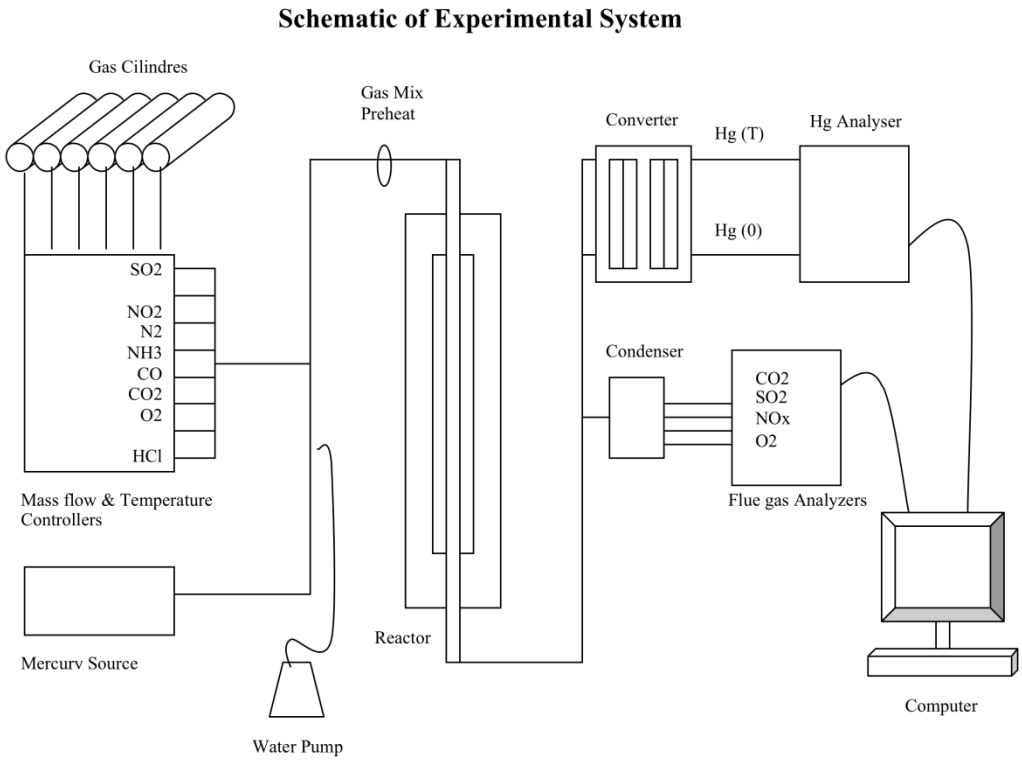

Figure 3. Schematic diagram of the Catalyst Test Facility's experimental apparatus.

inert substrate impregnated with elemental mercury maintained at a constant temperature. The mercury reservoir supplied a saturated stream of Hg(0), which was diluted by nitrogen carrier gas before mixing with the other gases. All gas contact surfaces at and downstream from the mercury generator were made from Teflon™ or glass to minimize adsorption of mercury. Also, all connecting lines downstream from the mercury vapor generator were heated to approximately 120 ºC using heating tape, to prevent vapor condensation or adsorption. The simulated flue-gas stream was premixed and preheated in a quartz tube before entering the micro-reactor. The compositions of the inlet and outlet gas streams were determined using Thermo Electron Corp. (Waltham, MA)

continuous emission monitors (CEMs) and by an MKS Instruments (Andover, MA) Model MultiGas 2030 Fourier transform-infrared spectrometer (FTIR) for most species. A heated sample transport line maintained at approximately 232 ^{o}C was used to transport a sample gas stream from the reactor outlet to the FTIR.

A fresh commercial-type monolithic honeycomb V_2O_5-WO_3/TiO_2 SCR catalyst, generously provided by Cormetech, Inc. (Durham, NC), was used for all of the measurements in this study. A photograph of the catalyst sample is shown in Figure 4. The V_2O_5 loading of the commercial catalyst is low (< 2% w/w), and is homogeneously distributed across the thickness of the monolith in order to ensure constant activity in the presence of abrasion by particles in the gas stream. The TiO_2 support does not exhibit activity for mercury oxidation (Zhuang et al., 2000). The monolithic honeycomb geometry is most suitable for low and no dust SCR applications, operating in a temperature range of 171 – 427 °C, depending on details of composition and design. The geometry also ensures a high active surface area per unit volume. The catalyst properties and synthetic flue gas composition during the measurements are summarized in Table 1. The gas composition is representative of an untreated flue gas from combustion of medium-sulfur (~1.3 wt %) bituminous coal.

A thermal mercury reduction system developed by the Tennessee Valley Authority (TVA) (Van Pelt and Meischen, 1999; Meischen et al., 2004) replaced the original SRI/ADA-ES modified wet chemistry gas-conditioning impingers, and was used to convert mercury into the elemental form for detection, using a combined gold trap and Tekran (Knoxville, TN) Model 2573A Mercury Vapour Analyzer, by Cold Vapor Atomic Fluorescence Spectrometry. A heated sample transport line maintained at approximately

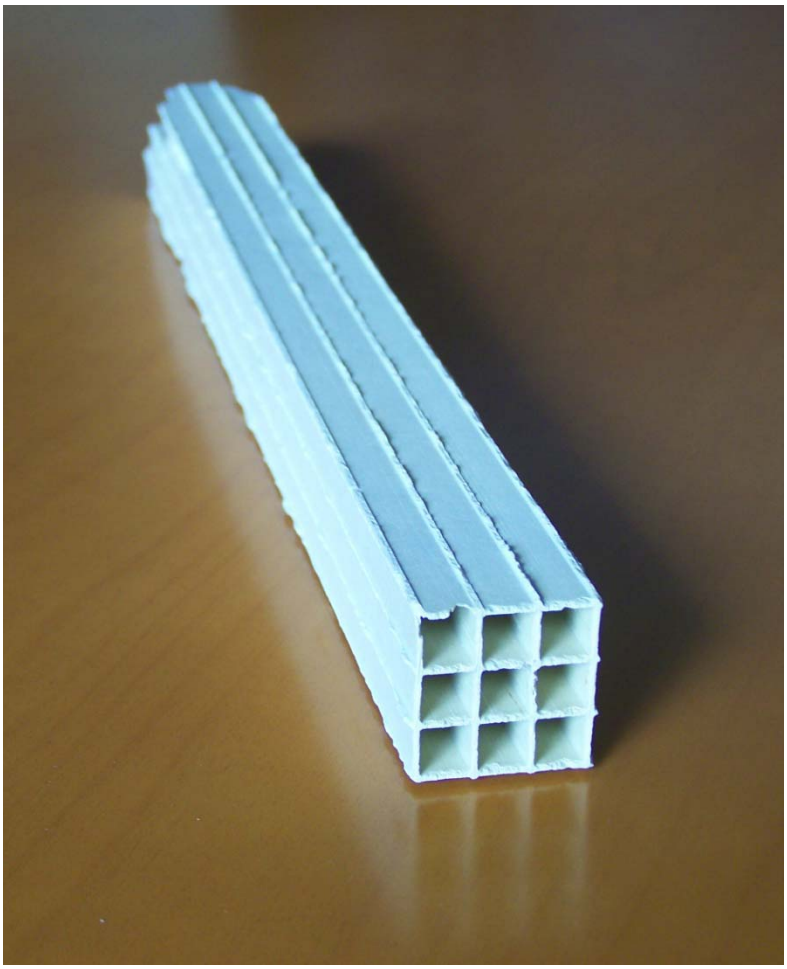

Figure 4. Test specimen of selective catalytic reduction (SCR) catalyst.

232 ^{o}C was used to transport a sample stream from the reactor outlet to the thermal mercury reduction system. The Tekran instrument was configured to provide an integrated mercury value every 150 seconds. Mercury analysis data from the Tekran instrument were downloaded to capture software via a RS232 serial port, and the data were exported to a MicroSoft Excel spreadsheet for analysis and graphing. All mercury

Table 1. SCR Catalyst Properties and Experimental Conditions.

Property or Condition	**Value**
Catalyst supplier	Cormetech, Inc.
Catalyst composition	V_2O_5-WO_3/TiO_2
Catalyst geometry	Honeycomb monolith
Catalyst cross-section	square 25 x 25 mm
Catalyst channel open area	square 7 x 7 mm
Catalyst wall thickness	1 mm
Catalyst length	310 mm
Catalyst void volume	136.7 cm^3
Catalyst geometric surface/volume ratio	0.571 mm^{-1}
Total surface/volume ratio	3.23 mm^{-1}
Catalyst temperature	378 ^oC (+11, -25 ^oC)
Space velocity at 21^oC, 1 atm	10,000 hr^{-1}
Residence time in catalyst at 378 ^oC	0.53 s
Flue gas flow rate at 21^oC, 1 atm	7 std. L/min
Synthetic flue gas composition (dry basis, other than H_2O):	
O_2	4 - 7 vol%
CO_2	14 - 16 vol%
H_2O	7 - 10 vol%
HCl	0 - 100 ppmv
SO_2	800 - 900 ppmv
NO	0 - 350 ppmv
NH_3	0 - 345 ppmv
CO	0 - 2000 ppmv
Hg(0) at 20^oC, 1 atm	10,000 ng/m^3
N_2	balance

concentrations reported in the present study are expressed at 20 ^{o}C, 1 atm pressure, and dry.

3.1.2 *Mercury Continuous Emission Monitors*

Until recently, analyzing for mercury in coal-derived flue gas was extremely difficult. Traditionally, the amount of mercury emitted to the atmosphere was estimated as the difference between the mercury in the coal fed to a utility boiler and the sum of the mercury in ash collected in the ESP hoppers and the mercury in sludge from the scrubber (Yudovich and Ketris, 2005). The use of vapor phase mercury continuous emission monitors (CEMs) was not implemented until 1996, when the U.S. EPA added total mercury to the proposed set of national emission standards for hazardous waste combustors. Mercury CEMs provide near real-time mercury measurements from coal-fired boilers for control and compliance monitoring. Any "cap and trade" provisions will likely require the use of a mercury CEM to analyze and track mercury emissions.

Measurements of mercury in coal-derived flue gas are still challenging, due to the low mercury concentrations, typically below 10 ng/normal m^3, and the presence of fine particulate and acid gases, including HCl, SO_2, and NO_x. Most mercury CEMs use UV photometry for mercury measurements, detecting only Hg(0), not Hg(II) or Hg(ads) (Meischen et al., 2004). Therefore, to measure Hg(II), all of the mercury in the flue gas must be converted to its elemental form by pretreatment. The difference between the measured Hg(0) before reduction of Hg(II) to Hg(0) and the total mercury measured after reduction is the concentration of Hg(II) in the flue gas sample. A wet-chemical gas

pretreatment system such as that specified in the Ontario Hydro method can be used to reduce Hg(II) to its elemental form for analysis by a vapor-phase mercury CEM.

3.1.3 *Ontario Hydro Method*

The Ontario Hydro Method (ASTM D6784-02, 2002) was developed by Keith Curtis and other researchers at Ontario Hydro Technologies in late 1994. This method was extensively tested at the Energy & Environmental Research Center (EERC) and has been established as the accepted wet-chemical method for measuring Hg(0) and Hg(II) concentrations in the flue gas of coal-fired boilers. The technique was selected by U.S. EPA as its recommended method for sampling and analysis of combustion products for mercury in the ICR tests (U.S. EPA, 1996). The Ontario Hydro method is an expensive technique, requiring skilled personnel to obtain reliable measurements. It was found that the ICR results were dependent on the lab personnel's attention to detail in the preparation of the sample trains and sample recovery (U.S. EPA, 1996).

The Ontario Hydro method measures three forms of mercury: (1) Hg(ads), separated by filtration, (2) gaseous Hg(II), collected in potassium chloride impingers, and (3) gaseous Hg(0) that has been oxidized and collected in nitric acid/peroxide and acidified permanganate solutions. Potassium permanganate is also added to the KCl impingers when measuring flue gas containing high levels of SO_2, to avoid possible reduction of Hg(II) to Hg(0) by absorbed SO_2. Sample impinger solutions should be stabilized and analyzed as soon as possible at a qualified, experienced laboratory. The preparation and maintenance of the sampling system introduce both complexity and uncertainty into the process, requiring that experienced personnel always be available

(Meischen et al., 2004). Precautions must be taken to prevent sampling artifacts, as indicated by selected ICR stack data (Pavlish et al., 2000). Ontario Hydro measurements are especially subject to sampling artifacts when made under challenging conditions, for example, from flue gas containing high-carbon ash and acid gases (Norton, 2000; Gale, 2005). A modified Solid Ontario Hydro method that substitutes solid reagent cartridges for the liquid-filled impingers is under development.

Laudal (1999) found that the greatest source of error in the Ontario Hydro method was not in the sampling but in the preparation of the impinger solutions for analysis, following sampling. The preparation steps include: (1) tearing down the impinger train, (2) transferring the solutions to flasks or bottles, and (3) digesting the solutions so that they can be analyzed using a portable cold-vapor atomic absorption (CVAA) analyzer. The overall measurement error was found to be reduced if the sample preparation and analysis were conducted immediately, in the field, by qualified technicians instead of shipping the samples off-site for preparation and analysis.

Southern Research Institute formerly used a modified wet chemistry method developed in conjunction with ADA Environmental Solutions (Littleton, CO) for gas pretreatment upstream from a vapor-phase mercury monitor (Merritt et al., 2005). To measure mercury species using the wet chemistry method, a sample of flue gas is withdrawn from the main stream to the sampling train. In the system at SRI's CTF, the sample is taken directly from the last section of the quartz micro-reactor and split into two equal streams. The two gas streams flow through two separate sets of 30 mL midget impingers (Chemglass, Vineland, NJ). One stream is bubbled through an impinger containing a solution of stannous chloride, to reduce oxidized mercury species to

elemental mercury. That stream is then bubbled through a second impinger containing a solution of 5% sodium hydroxide, to remove acid gases. Analysis of this stream gives the total mercury concentration in the flue gas. The second stream is first bubbled through an impinger containing a solution of potassium chloride, to remove oxidized mercury species, and is then treated in a second impinger containing a solution of 5% sodium hydroxide to remove acid gases. Analysis of this stream gives the elemental mercury concentration in the flue gas. The samples are cooled and moisture is removed by a set of chillers. The treated gas streams are then sent, alternately, to the Tekran 2537A Mercury Vapour Analyzer via a Tekran Sample Valve Control Unit for measurement of Hg(0). Oxidized mercury species are the difference between the total and elemental mercury concentrations in the two gas streams.

3.1.4 *Tennessee Valley Authority's Dry Mercury Conversion System*

Van Pelt and Meischen (1999) and Meischen et al. (2004) at TVA developed a dry, thermal dissociation mercury reduction system (Dry Conversion System) to reduce Hg(II) to its elemental form for analysis using atomic fluorescence or UV spectroscopy. Gas-phase thermal reduction is a well-established method, by which Hg(II) reduction is accomplished with high efficiency in a thermal converter at 750 ^{o}C (Meischen et al., 2004). However, on cooling downstream from the thermal reduction chamber, Hg(0) may be re-oxidized by reaction with components of the flue gas. To prevent re-oxidation before analysis, hydrogen is introduced to the sample at a rate of 2:1 by volume to oxygen in a cell, where it reacts with O_2 to form water. Water vapor formed by this reaction, plus that already present in the sample, inhibits interaction of Hg(0) with acid

gases, such as HCl, to prevent re-oxidation of mercury (Van Pelt and Meischen, 1999). Field tests of the TVA system conducted at a 700-MW steam turbine plant equipped with SCR and a scrubber gave total mercury measurements that were within 20% of those obtained using the Ontario Hydro method. A TVA Dry Conversion System assembled at SRI using a reaction cell and design guidelines generously provided by TVA, is illustrated in Figure 5. A portable Teledyne Analytical Instruments (City of Industry, CA) Model 320P-D O_2 analyzer with a micro fuel cell sensor was used to periodically check the O_2 concentration in the flue gas sample after addition of H_2, to ensure that enough hydrogen was being added for sufficient O_2 removal and for mercury reduction to be maintained. Maintaining unreacted O_2 at ≤ 0.5 vol % was sufficient to prevent re-oxidation of Hg(0). The O_2 analyzer is insensitive to flow rate and detects O_2 concentration within ± 0.1% from 0 to 100% O_2. The TVA system was used for all mercury speciation measurements during this study.

3.1.5 *Sulfate Measurements*

Sulfate (SO_3, SO_4^{2-}, and H_2SO_4) measurements are required to diagnose and solve a variety of operating and emissions problems in coal-fired utility boilers, such as a visible stack plume, cold-end corrosion, and poor precipitator performance. Currently, there are two basic manual sulfate-sampling techniques: an impinger method, based on sulfate adsorption in solution, and a controlled condensation method, based on sulfuric acid collection below its dew point. In the controlled condensation method, SO_3, in the presence of water vapor, selectively condenses as H_2SO_4 while the flue gas, containing SO_2 and water vapor, passes through the condenser. The major advantage of the

Figure 5. The Tennessee Valley Authority thermal dissociation mercury reduction system.

controlled condensation method is that it provides reliable and reproducible SO_3 values with minimal interference from high SO_2 concentrations. Another advantage of the controlled condensation method is that it also collects and measures ammonium sulfate and bisulfate formed by reaction of SO_3 and water vapor with ammonia. Therefore, all the measurements using the controlled condensation method in this investigation are reported as sulfate, rather than as sulfuric acid.

In the present investigation, all sulfate measurements were obtained using a modified controlled condensation method. The flue gas sample (~14.2 L) is taken directly from the exit of the reactor into a tube loosely packed with glass wool maintained at

79.5 ^{o}C by a heated water jacket, where sulfuric acid condenses and ammonium sulfate and bisulfate are trapped. The condenser is extracted with 10 mL of deionized water, followed by two 10 mL washes with isopropyl alcohol (IPA) that has been pH adjusted (100 μL of 70% perchloic acid/4 L of IPA). The extraction solution and washes are combined and diluted to 50 mL with IPA. A drop of thorin indicator is added to the sample and a titration is conducted on a magnetic stir plate using a 0.01 N barium perchlorate standard solution to precipitate barium sulfate from the sample, as described in EPA Method 6.

3.2 Catalyst Preconditioning and Obtaining Steady State Conditions

3.2.1 *Procedure for Inert Reactor Experiments*

An initial experiment with an inert reactor (no catalyst) was conducted to test the inertness of the reactor and accuracy of the analytical methods. The quartz reactor was filled with an appropriate amount of washed sea sand (Thermo Fisher Scientific Inc., Waltham, MA) to reproduce the space velocity across the test catalyst sample, installed in the flow system in the tube furnace, and allowed to reach a steady-state temperature of 365 ^{o}C (for measurements in the absence of CO) and 353 ^{o}C (for measurements in the presence of 102 ppmv CO) in the presence of a N_2 gas stream. Synthetic flue gas constituents were introduced to the gas stream, allowed to reached and maintained steady-state conditions, and the data set was recorded. After sufficient data on the extent of homogeneous NO reduction and mercury oxidation were collected, the inert reactor

was removed and replaced with the reactor containing catalyst, for the catalytic reactor studies.

3.2.2 *Procedure for NO Reduction Experiments*

A series of experiments was conducted to examine the dependence of catalytic NO reduction on synthetic flue gas composition. Approximately 7 std. L/min of synthetic flue gas were sent through the reactor, and the gas composition was maintained at the desired experimental conditions, as given in Table 1. The reactor containing the catalyst sample was allowed to reach a steady-state temperature of 378 ^{o}C (+11, -25 ^{o}C) in the presence of a N_2 gas stream. Concentrations of the input synthetic flue gas constituents were determined by mass flow calculations, regulated by mass flow controllers, and verified by CEM and FTIR measurements at the outlet of the reactor. The NO concentration as measured by the FTIR at the reactor outlet was allowed to reach a steady-state value of approximately 300 ppmv, and recorded as the inlet NO concentration to the catalyst. Following the inlet NO concentration measurement, NH_3 was introduced to the gas mixture at a flow rates equivalent to inlet NH_3/NO feed ratios over the range from 0.2 to 1.15. The NO concentration as measured by the FTIR at the reactor outlet was again allowed to reach a steady-state value, which was then recorded as the outlet NO concentration. Throughout the experiments, N_2 was used as the base gas and its flow rate was adjusted to maintain a constant space velocity of 10,000 hr^{-1}. The catalytic reduction of NO is defined as the difference between the NO mole fractions at the inlet and outlet of the reactor, as a percentage of the NO mole fraction at the inlet,

$$[(\text{NO inlet} - \text{NO outlet}) / \text{NO inlet}] \times 100\%.$$

Based on the rules for propagation of errors (Lindberg, 2000) through the calculation of the percentage mercury oxidation, the standard deviation in the result was calculated using the following equation:

$$StDev = |\%\ NO\ Reduction| * \{ \{[(NO\ Inlet\ StDev)^2 + (NO\ Outlet\ StDev)^2]^{1/2} / (NO\ Inlet - NO\ Outlet)^2\} + (NO\ Inlet\ StDev/NO\ Inlet)^2 \}^{1/2}$$

3.2.3 *Procedure for Mercury Oxidation Experiments*

A series of experiments was conducted to examine the dependence of catalytic mercury oxidation on synthetic flue gas composition. Similar to the start-up procedure for the NO reduction experiments, the reactor containing the catalyst sample was allowed to reach a steady-state temperature of 378 ^{o}C (+11, -25 ^{o}C) in the presence of a N_2 gas stream, and concentrations of the input synthetic flue gas constituents were determined by mass flow calculations, regulated by mass flow controllers, and verified by CEM and FTIR measurements at the outlet of the reactor. The condition of the catalyst was checked before each set of measurements by verifying that the reduction in NO by the catalyst was at least 90% at an NH_3/NO ratio of 0.95. A saturated stream of Hg(0), diluted by nitrogen carrier gas, was introduced to the synthetic flue gas, the mixture preheated, then fed to the reactor. Approximately 7 std. L/min of gas was sent through the reactor, and the gas composition, including Hg(0), was maintained close to the desired experimental conditions, as given in Table 1. The concentration of HCl, however, was kept at a reduced value and the system was run overnight at a temperature of 378 ^{o}C (+11, -25 ^{o}C) in a preconditioning mode to load or charge the catalyst with mercury. The following day, the synthetic flue gas concentration of HCl was increased to the desired value, NH_3

was introduced to achieve the desired NH_3/NO ratio, and the day's experiments were conducted. Throughout the experiments, N_2 was used as the base gas and its flow rate was adjusted to maintain a constant space velocity of 10,000 hr^{-1}. As previously stated, all of the mercury concentrations reported in the present study are expressed at 20 ^oC, 1 atm pressure, and dry.

An example of an experimental data set for a typical start up in preconditioning mode, to load or charge the catalyst with mercury, is shown in Figure 6. The measurements were made under the conditions given in Table 1 and in the absence of HCl, NO, NH_3, and CO. The Figure shows a catalyst loading phase, a short steady-state phase, a non-steady-state phase due the exhaustion of the CO_2 supply that reduced the flow rate and disrupted the mass flow controllers, and re-establishment of steady-state upon re-initiation of the CO_2 flow.

The percentage of mercury oxidation was calculated using the following equation, in which HgT is the total (elemental + oxidized) mercury concentration and Hg0 is the elemental mercury concentration measured:

$$\% \text{ Mercury Oxidation} = [(\text{Avg HgT} - \text{Avg Hg0}) / \text{Avg HgT}] \times 100\%$$

Based on the rules for propagation of errors (Lindberg, 2000) through the calculation of the percentage mercury oxidation, the standard deviation in the result was calculated using the following equation:

$$\text{StDev} = |\% \text{ Mercury Oxidation}| * \{\{[(\text{HgT StDev})^2 + (\text{Hg0 StDev})^2]^{1/2} / (\text{Avg HgT} - \text{Avg Hg0})^2\} + (\text{HgT StDev/Avg HgT})^2\}^{1/2}$$

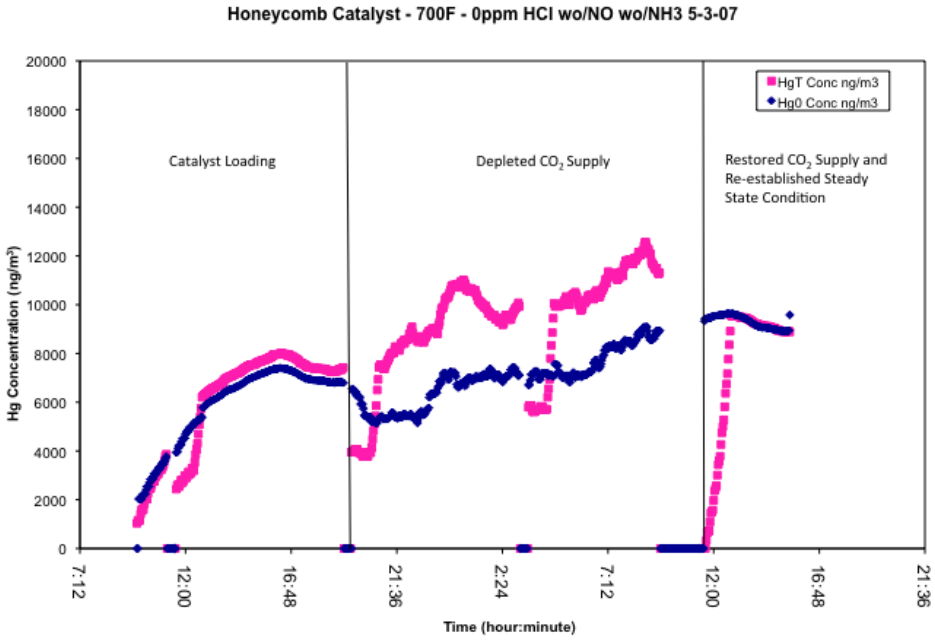

Figure 6. Mercury concentration measurements (HgT = Total Hg, Hg0 = Elemental Hg) during catalyst loading, upset condition, and arrival at steady state conditions.

CHAPTER 4

RESULTS AND DISCUSSION

4.1 Modified Wet Chemistry Method vs Tennessee Valley Authority Dry Conversion System

When using the SRI/ADA-ES modified wet chemistry method, leaks and clogs in the impinger train were major problems when sampling for extended lengths of time. Clogs in the sample line due to build up of sodium hydroxide crystal from the impinger solution at the outlet of the reactor resulted in excessive back pressure that could cause leaks from the system. Leaks in the system resulted in the mercury concentration being less than expected, and achieving and maintaining steady state for a sufficient length of time was difficult. High variability in mercury concentration from day to day was not uncommon. A second problem was condensation on the inner walls of the inlet and down-comer tubes in the bubblers (Merritt et al., 2005). The loss of mercury from the sample during accumulation in the condensate, and later release of the droplets of condensate containing dissolved mercury caused noise and spikes in the concentration record, greatly increasing the difficulty in accurately determining the average steady-state concentrations of mercury. An example of the noisy signal observed when using the modified wet chemistry method is illustrated in Figure 7.

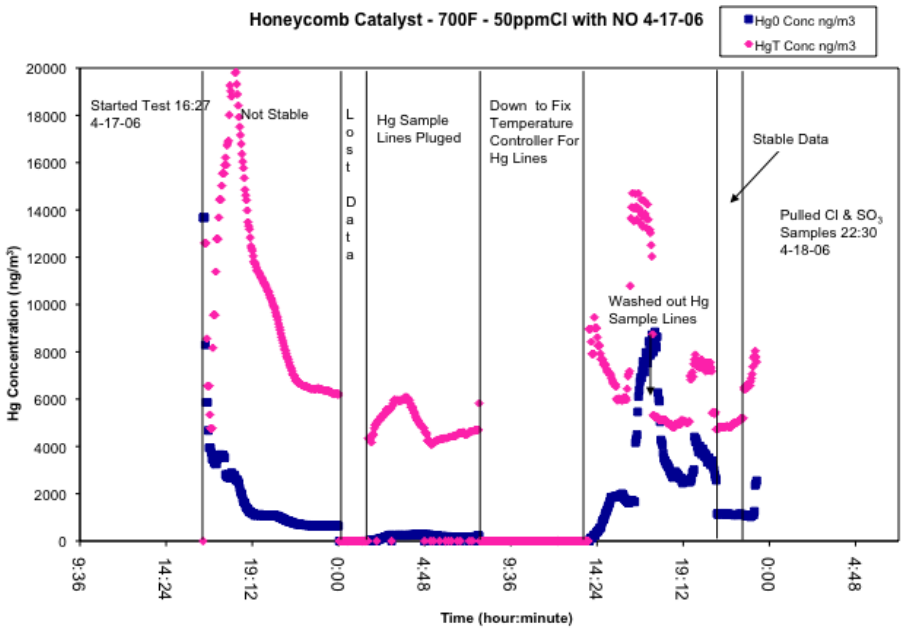

Figure 7. Mercury concentration measurements (HgT = Total Hg, Hg0 = Elemental Hg) using the SRI/ADA-ES wet chemistry method.

The TVA Dry Conversion System (Van Pelt and Meischen, 1999; Meischen et al., 2004) accomplishes mercury reduction entirely in the gas phase, avoiding the problem of accumulation and release of mercury via condensate. The use of this system eliminated the noise that had complicated the identification of steady-state conditions and determination of the extents of mercury oxidation in previous work under the present project. An example of the total and elemental mercury signals obtained using the TVA Dry Conversion System is illustrated in Figure 8. Implementation of the TVA Dry Conversion System resulted in a marked improvement in the quality of total mercury measurements and a significant reduction in the time required to determine the distribution of mercury species between elemental and oxidized states under a given

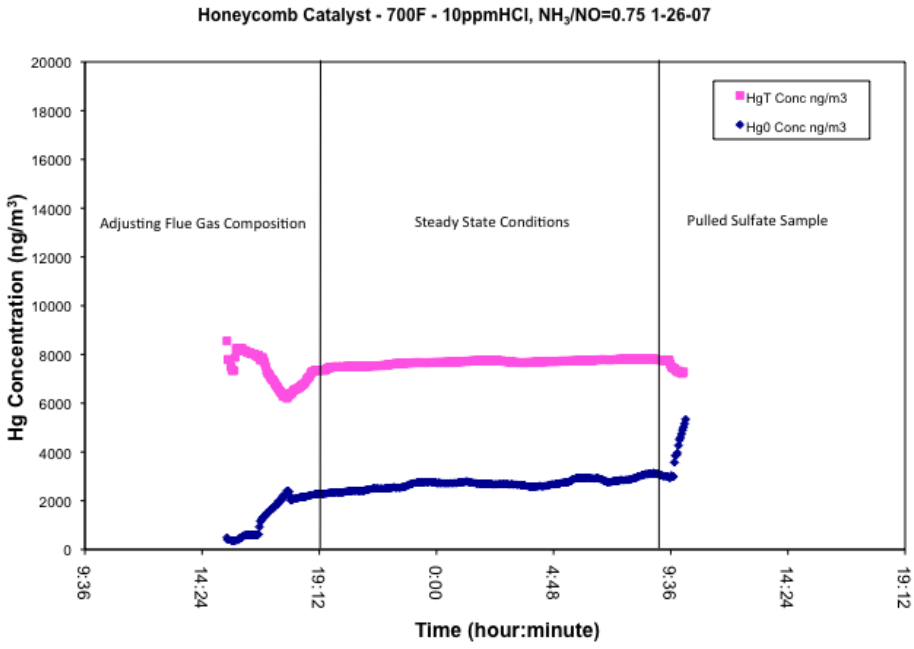

Figure 8. Mercury concentration measurements (HgT = Total Hg, Hg0 = Elemental Hg) using the TVA Dry Conversion System.

set of experimental conditions. All of the total mercury measurements presented in the following sections were obtained using this new system. The full set of experimental data is given in Appendix B.

4.2 Inert Reactor Experimental Results

Initial experiments with an inert reactor (no catalyst) were conducted to test the inertness of the reactor and demonstrate the absence of homogeneous reactions for mercury oxidation. The quartz reactor was filled with an appropriate amount of inert washed sea sand to simulate the space velocity across the test catalyst sample, inserted into the gas stream, and heated to 365 ^{o}C (for measurements in the absence of CO) and

353 ^{o}C (for measurements in the presence of CO). The first set of measurements was made in the presence of 1 ppmv HCl and $NH_3/NO = 0.95$, in the absence of CO, and the second set of measurements was made in the presence of 2.2 ppmv HCl, $NH_3/NO = 0.91$, and 102 ppmv CO, with other conditions as specified in Table 1. The experimental data set is summarized in Table 2 and the extent of mercury oxidation for the first case is illustrated in Figure 9. Here and in the tables and figures to follow, the fraction of mercury oxidized is defined as the difference between total Hg and elemental Hg, as a percentage of total Hg:

[(Total Hg – Elemental Hg) / Total Hg] x 100%.

As shown in the figure, the lack of significant drift in the total and elemental mercury concentrations across the reactor indicates that the reactor itself is no longer adsorbing elemental mercury. During this particular experiment, the average total mercury concentration (8604 ± 214 ng/m^3) is virtually identical to the average concentration of elemental mercury (8646 ± 281 ng/m^3), indicating no measureable oxidation of mercury (-0.5 ± 2.1%), in the absence of CO.

In the presence of 102 ppmv CO, the average total mercury concentration (9843 ± 55 ng/m^3) is actually less than the average concentration of elemental mercury (11,090 ± 72 ng/m^3), resulting in a -12.7 ± 0.8% in the extent of mercury oxidation. Both results indicate that there were no homogeneous or heterogeneous reactions in the sand-filled reactor promoting mercury oxidation. However, as will be shown later, there was little oxidation of mercury even in the SCR catalyst under both of these conditions, because HCl was low and the NH_3/NO ratio relatively high, and because CO was observed to suppress mercury oxidation. As it turned out, the conditions chosen for evaluation of

Table 2. Experimental Data Set for Mercury Oxidation in an Inert Reactor.

HCl (ppmv)	NH_3/NO (mol/mol)	CO (ppmv)	Total Hg (ng/m^3)*	Total Hg StdDev (ng/m^3)*	Hg(0) (ng/m^3)*	Hg(0) StdDev (ng/m^3)*	Hg Oxidation (%)	Hg Oxidation StdDev (%)
1	0.95	0	8604	214	8646	281	-0.5	2.1
2.2	0.92	102	9843	55	11090	72	-12.7	0.8

* Mercury concentrations at 20 ^oC, 1 atm pressure, and dry.

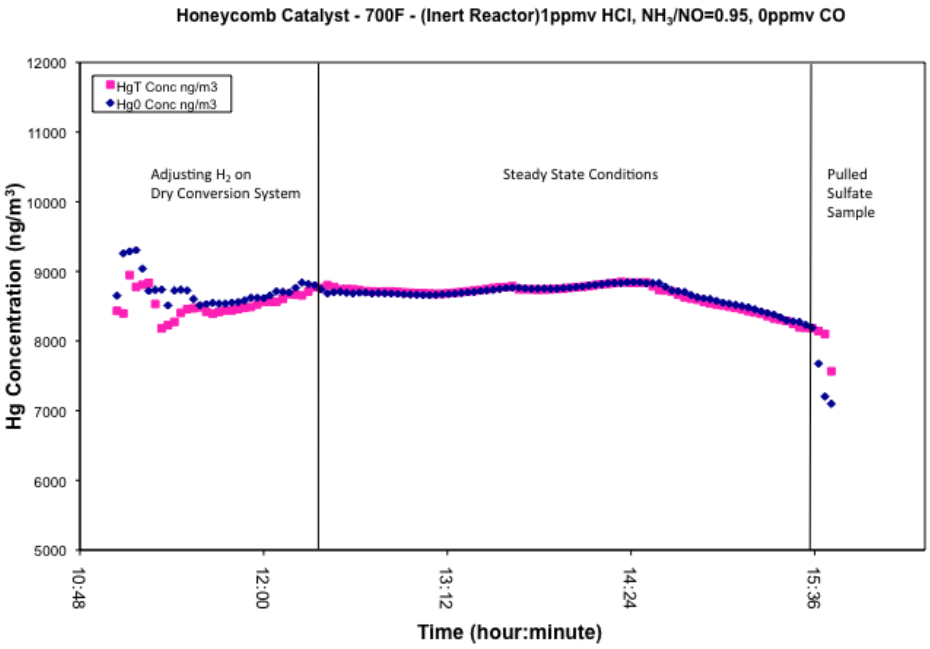

Figure 9. Dependence of mercury oxidation (HgT = Total Hg, Hg0 = Elemental Hg) in the inert reactor in the presence of 1 ppmv HCl, NH_3/NO = 0.95, and absence of CO with other conditions as specified in Table 1.

possible contributions to mercury oxidation from homogeneous reactions, the reactor wall, or relatively inert surface were unable to provide conclusive evidence for the absence of such effects.

The negative extents of mercury oxidation which were occasionally observed, though rarely as high as -12%, may be attributed to absorption of mercury on the surfaces of the mercury reduction system, when the system was not under truly steady state, causing the total mercury measurement to be low.

4.3 Effect of NH_3/NO Feed Ratio on Catalytic NO Reduction

Selective catalytic reduction of NO_x is based on the reaction between nitrogen oxides (typically 95% NO and 5% NO_2), ammonia, and oxygen according to the following reactions, as described by Pritchard et al. (2002):

$$NO + NO_2 + 2NH_3 \rightarrow 2N_2 + 3H_2O \quad \text{(R40)}$$

$$4NO + 4NH_3 + O_2 \rightarrow 4N_2 + 6H_2O \quad \text{(R41)}$$

A series of experiments was conducted to examine the dependence of NO reduction on the NH_3/NO feed ratio over the range from 0 to 1.15. The measurements were made in the presence of 300 ppmv NO, 10 ppmv HCl, in the absence of CO, and with other conditions as specified in Table 1. The experimental data set is summarized in Table 3. The effect of the inlet NH_3/NO feed ratio, for a constant NO concentration and at 378 ^oC (+11, -25 ^oC) is illustrated in Figure 10. Here and in the tables and figures to follow, NO reduction is defined as the difference between the NO mole fractions at the inlet and outlet of the reactor, as a percentage of the NO mole fraction at the inlet:

$$[(\text{NO inlet} - \text{NO outlet}) / \text{NO inlet}] \times 100\%.$$

The data show that the removal of NO is limited by ammonia for NH_3/NO ratios ≤ 0.75, resulting in stoichiometric reduction of NO by NH_3. For NH_3/NO ratios > 1.0, the reduction of NO becomes nearly independent of the reactant ratio, with the highest NO reduction (99.5%) achieved at an NH_3/NO ratio = 1.05. Inlet NH_3/NO_x ratios of 1.1 to 1.2 are typically employed during standard catalytic activity tests over commercial SCR catalysts, to test for NO_x reduction activity and NH_3 slip (Svachula et al., 1993). Machalek et al. (2003) observed a trend very similar to that shown in Figure 10, in their evaluation of slipstream data from subbituminous coal-derived flue gas across a catalytic honeycomb monolith at 371 °C and space velocity of 3000 hr^{-1}.

Many authors, including Tuenter et al. (1986) and Svachula et al. (1993) have investigated the effect of NH_3/NO_x ratio on NO_x reduction by SCR catalysts. Those studies reported that (1) NO reacts with NH_3 in a 1:1 molar ratio in the presence of excess oxygen and (2) the oxidation of ammonia by molecular oxygen is completely retarded in the presence of NO_x. The data presented here, along with much previously published data (e.g. Svachula et al., 1993), indicate that Reactions 40 and 41, account for the overall SCR stoichiometry.

Table 3. Experimental Data Set for the Effect of NH_3/NO Ratio on Catalytic NO Reduction.

HCl (ppmv)	NO Inlet (ppmv)	NH_3 Inlet (ppmv)	NH_3/NO (mol/mol)	NO Outlet (ppmv)	NO Reduction (%)
10	300	0	0.00	300	0.0
10	300	0	0.00	300	0.0
10	300	63	0.21	237	21.0
10	300	92	0.31	208	30.7
10	300	105	0.35	207	31.0
10	300	161	0.54	161	46.3
10	300	195	0.65	105	65.0
10	300	200	0.67	90.5	69.8
10	300	225	0.75	75	75.0
10	300	285	0.95	56	81.3
10	300	315	1.05	1.5	99.5
10	300	345	1.15	1.94	99.35

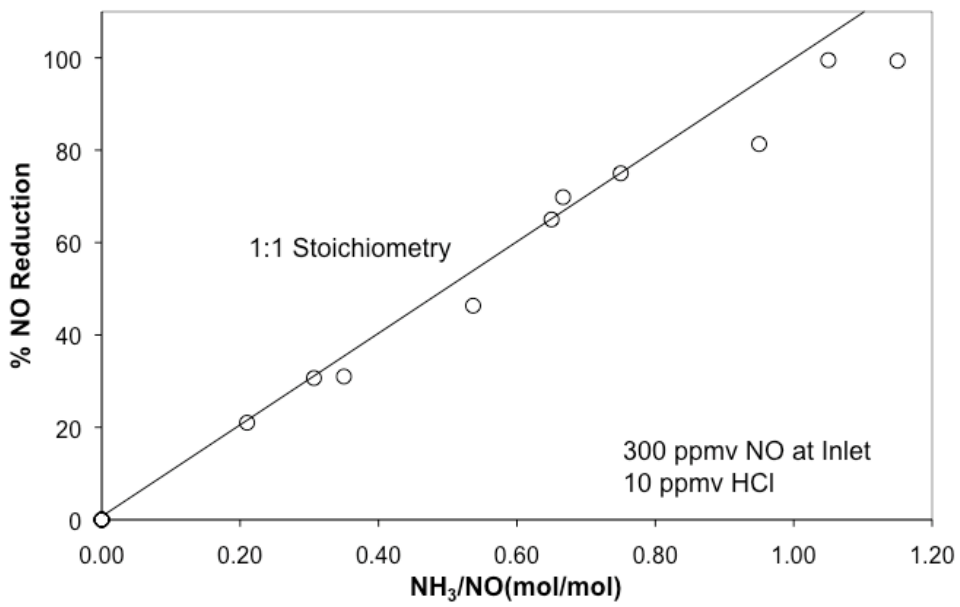

Figure 10. Dependence of NO reduction in the square channel monolithic catalyst on the molar ratio of ammonia to NO in the presence of 10 ppmv HCl and absence of CO, with other conditions as specified in Table 1.

4.4 Effect of HCl on Catalytic NO Reduction

A series of experiments was conducted to examine the dependence of catalytic NO reduction on the volume fraction of HCl over the range from 1 to 75 ppmv, covering the range from low-chlorine Powder River Basin subbituminous coals to moderate-chlorine bituminous coals. The measurements were made in the presence of a substoichiometric NH_3/NO feed ratio of 0.81 and in the absence of CO. The experimental results are summarized in Table 4 and illustrated in Figure 11. As shown by the data, there was a modest increase in catalytic NO reduction from approximately 88 to 98 % across the monolith as the HCl volume fraction increased over the range from 0 to 5 ppmv, followed by a decrease in catalytic NO reduction from 98 to 78 % over the range from 15 to 75 ppmv HCl. Experimental work by Gale et al. (2006) showed that HCl had

little or no effect on catalytic NO reduction over the range of HCl volume fraction from 10 to 100 ppmv.

Table 4. Experimental Data Set for the Effect of HCl on Catalytic NO Reduction.

HCl (ppmv)	NO Inlet (ppmv)	NH_3 Inlet (ppmv)	NH_3/NO (mol/mol)	NO Outlet (ppmv)	NO Reduction (%)	NO Reduction StdDev (%)
0	350	285	0.81	40.8	88.3	3.51
1	350	285	0.81	20	94.3	3.62
1	350	285	0.81	20	94.3	3.62
5	350	285	0.81	8.9	97.5	3.67
7.5	350	285	0.81	10.6	97.0	3.67
10	350	285	0.81	13.4	96.2	3.65
10	350	285	0.81	13.4	96.2	3.65
15	350	285	0.81	16.0	95.4	3.64
20	350	285	0.81	20.6	94.1	3.61
25	350	285	0.81	24.3	93.1	3.60
50	350	285	0.81	35.7	89.8	3.54
75	350	285	0.81	78.5	77.6	3.33
75	350	285	0.81	78.5	77.6	3.33

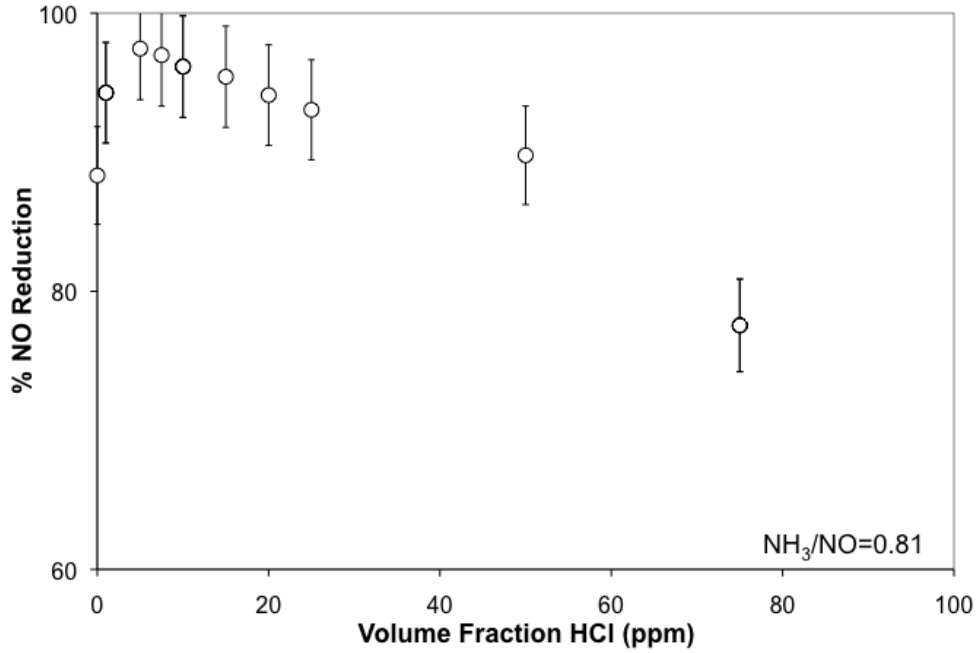

Figure 11. Dependence of NO reduction in the square channel monolithic catalyst on the volume fraction of HCl, in the presence of $NH_3/NO = 0.81$, absence of CO, and other conditions as specified in Table 1.

4.5 Effect of CO on Catalytic NO Reduction

A series of experiments to determine the dependence of the extent of catalytic NO reduction on CO mole fraction, in the presence of approximately 2, 11, and 50 ppmv HCl, 313 and 329 ppmv NO, and $NH_3/NO = 0.91$ to 0.94 was conducted over the range from 0 to approximately 2000 ppmv CO. In addition, an experiment with an inert reactor (no catalyst) in the presence of 2.2 ppmv HCl, 329 ppmv NO, $NH_3/NO = 0.91$, and 102 ppmv CO was conducted to determine the NO reduction due to homogeneous reactions. The experimental results are summarized in Table 5 and illustrated in Figures 12a and 12b.

The presence of CO had little effect on the extent of catalytic NO reduction, as the NO reduction was maintained at 93.2 ± 0.7% over the range of CO volume fraction tested. A slight decrease in the extent of NO reduction from 94.3 ± 0.2% to 93.2 ± 0.1% resulted from an increase in the volume fraction of HCl from 11 to 50 ppmv. But overall, an increase in the volume fraction of HCl from 2 to 50 ppmv had minimal effect on catalytic NO reduction, consistent with the experimental work by Gale et al. (2006). The high NO reduction levels achieved across the SCR in this study were compatible to those observed in the field (86 - 90%) (Srivastava et al., 2003). In the absence of catalyst, the extent of NO reduction was significantly reduced, to 11.1 ± 1.6 %.

Table 5. Experimental Data Set for the Effect of CO on Catalytic NO Reduction.

HCl (ppmv)	NO Inlet (ppmv)	NH_3 (ppmv)	NH_3/NO (mol/mol)	NO Outlet (ppmv)	CO (ppmv)	NO Reduction (%)	NO Reduction StdDev (%)
			Inert Reactor				
2.2	329	300	0.91	292	102	11.1	1.6
			Catalyst-Containing Reactor				
1.93	329	306	0.93	22.16	0	93.3	0.93
1.93	329	306	0.93	22.15	5.03	93.3	0.93
1.92	329	305	0.93	22.59	7.49	93.1	0.93
1.90	329	305	0.93	23.03	10.45	93.0	0.93
2.17	329	302	0.92	26.39	25.16	92.0	0.93
2.13	329	309	0.94	19.12	52.36	94.2	0.93
2.18	329	307	0.93	21.19	101.25	93.6	0.93
10.95	313	285	0.91	18.00	0	94.3	0.93
10.95	313	285	0.91	18.00	0	94.3	0.93
10.95	313	285	0.91	18.00	0	94.3	0.93
10.95	313	285	0.91	18.00	0	94.3	0.93
10.95	313	285	0.91	18.00	0	94.3	0.93
11.47	313	285	0.91	18.07	4	94.2	0.93
11.47	313	285	0.91	18.07	4	94.2	0.93
11.03	313	285	0.91	18.78	19	94.0	0.93
11.03	313	285	0.91	18.78	19	94.0	0.93
12.14	313	285	0.91	18.16	50	94.2	0.92
12.14	313	285	0.91	18.16	50	94.2	0.92
11.52	313	285	0.91	17.76	118	94.3	0.92
11.44	313	285	0.91	16.34	263	94.8	0.97
11.44	313	285	0.91	16.34	263	94.8	0.97
11.71	313	285	0.91	16.86	511	94.6	0.97
11.56	313	285	0.91	17.25	1013	94.5	0.99
11.56	313	285	0.91	17.25	1013	94.5	0.99
11.57	313	285	0.91	18.37	2001	94.1	1.11
11.57	313	285	0.91	18.37	2001	94.1	1.11
50	313	285	0.91	21.5	5	93.1	0.96
50	313	285	0.91	21.82	114	93.0	0.98
50	313	285	0.91	21.23	254	93.2	0.97
50	313	285	0.91	21.1	511	93.3	0.95
50	313	285	0.91	21.56	1043	93.1	0.95
50	313	285	0.91	21.09	2053	93.3	0.94

(a)

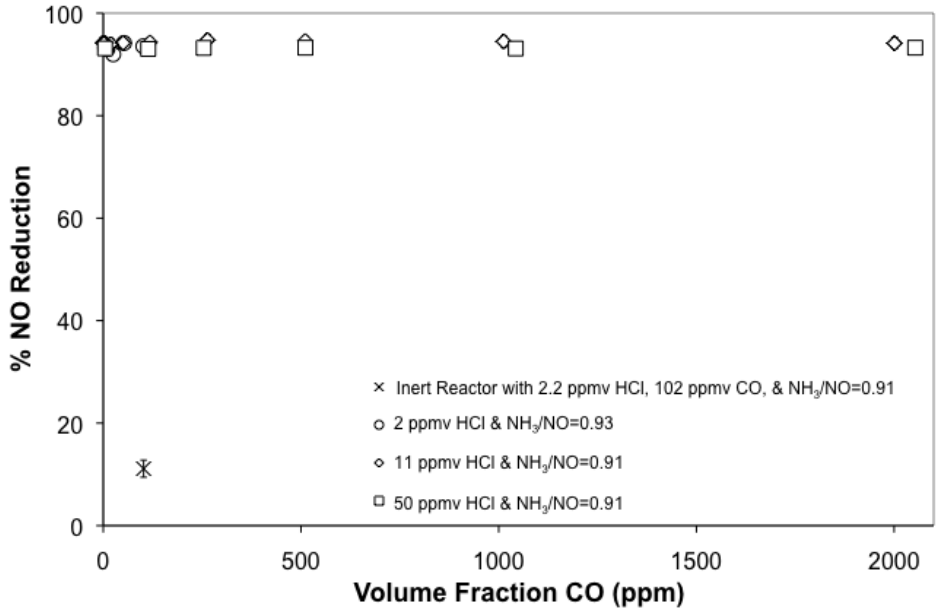

(b)

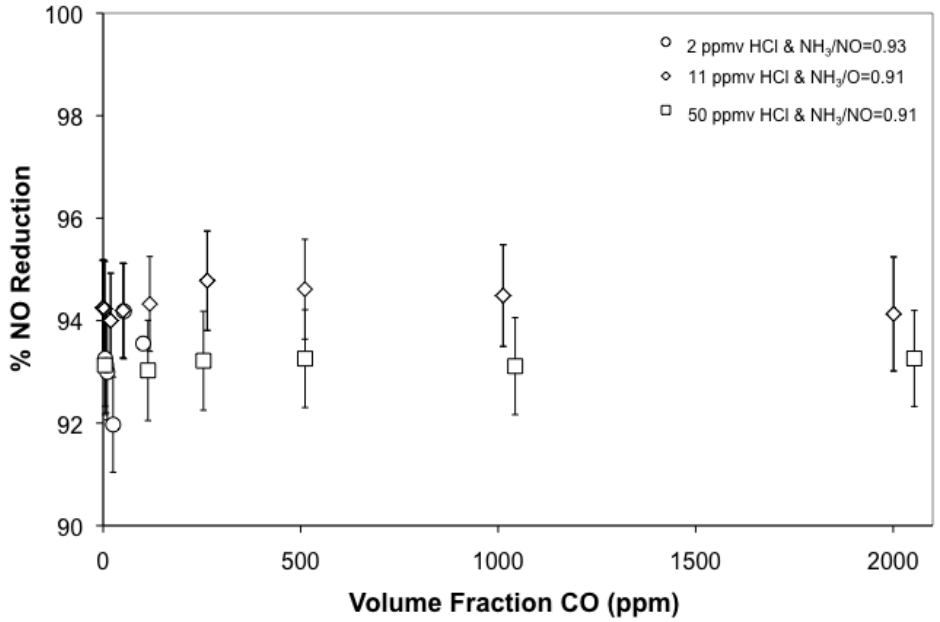

Figure 12. Dependence of NO reduction on the volume fractions of CO and HCl, in the presence of $NH_3/NO = 0.91$ to 0.94: **(a)** in the presence of the square channel monolithic catalyst and with one measurement downstream from the inert reactor **(b)** in the presence of the square channel monolithic catalyst with other conditions as specified in Table 1.

4.6 Effect of NO on Catalytic Mercury Oxidation

A series of experiments was conducted to examine the dependence of mercury oxidation on NO in the simulated flue gas. The measurements were made in the absence and presence of NO (0 and 300 ppmv), in the absence of HCl, NH_3, and CO, with other conditions as specified in Table 1. The experimental results are summarized in Table 6 and illustrated in Figures 13a and 13b.

The complete records of mercury concentration vs. time, from which the average values in Table 6 were derived, are shown in the figures. In the absence of NO, HCl, NH_3, and CO, essentially no catalytic mercury oxidation occurred across the catalyst, as shown in Figure 13a. However, when 300 ppmv NO was added to the system, the extent of catalytic mercury oxidation increased from 0 to approximately 19%, even in the absence of HCl, as illustrated in Figure 13b.

Table 6. Experimental Data Set for the Effect of NO on Catalytic Mercury Oxidation.

HCl (ppmv)	NO (ppmv)	NH_3 (ppmv)	Total Hg (ng/m^3)*	Total Hg StdDev (ng/m^3)*	Hg(0) (ng/m^3)*	Hg(0) StdDev (ng/m^3)*	Hg Oxidation (%)	Hg Oxidation StdDev (%)
0	0	0	9201	326	9210	334	-0.1	5.1
0	300	0	7965	215	6429	204	19.3	3.8

*Mercury concentrations at 20 ^oC, 1 atm pressure, and dry.

(a)

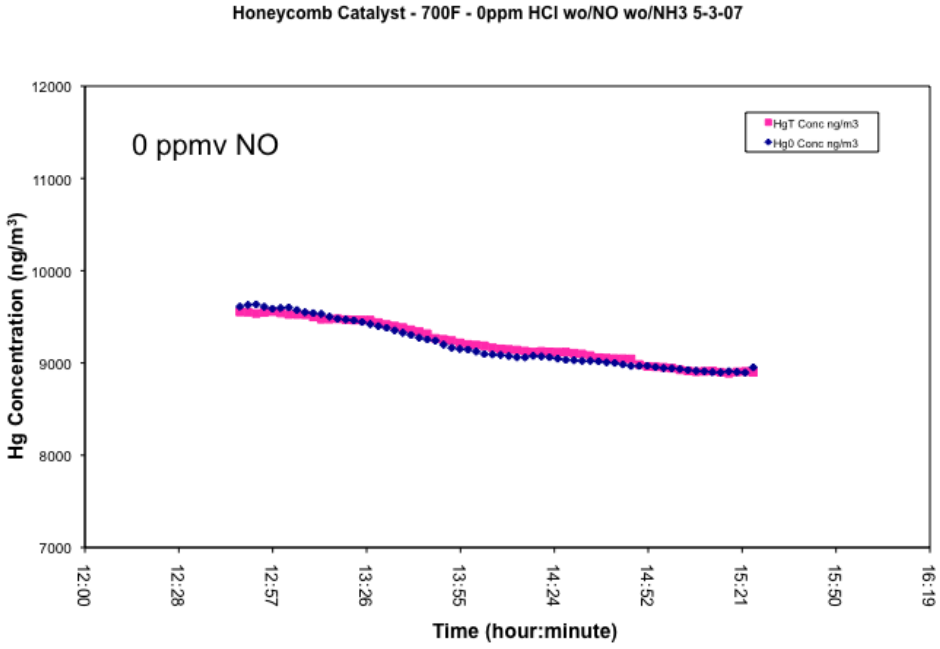

(b)

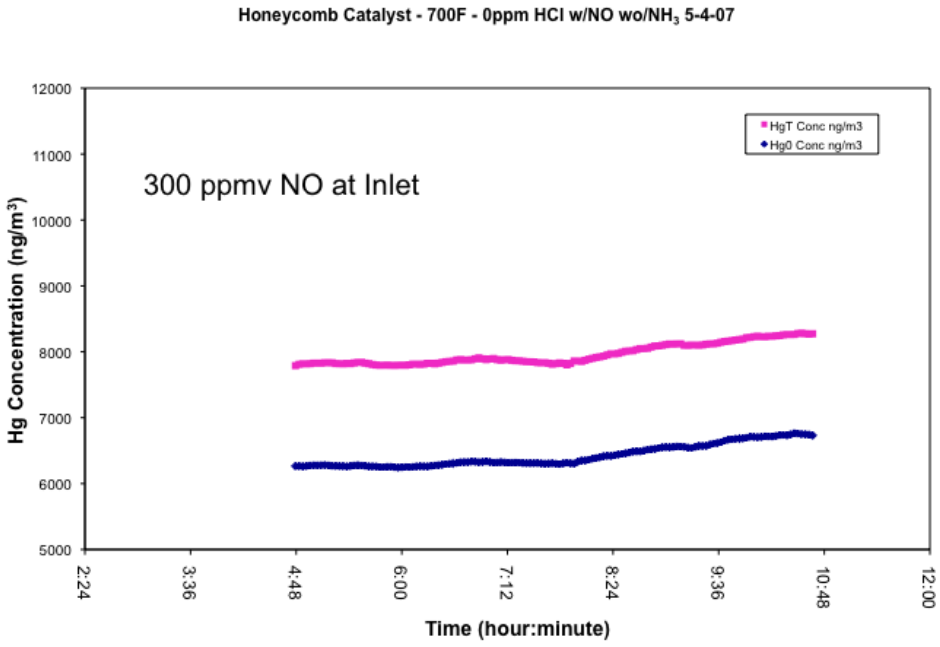

Figure 13. Dependence of mercury oxidation (HgT = Total Hg, Hg0 = Elemental Hg) in the square channel monolithic catalyst on the volume fraction NO: (**a**) 0 ppmv and (**b**) 300 ppmv, in the absence of HCl, NH_3, and CO with other conditions as specified in Table 1.

4.7 Effect of HCl, NO, and NH_3 on Catalytic Mercury Oxidation

Because the expected form of oxidized mercury in flue gas at low temperatures is $HgCl_2$ (Dajnak et al. 2003; Yudovich and Ketris, 2005; Presto and Granite, 2006), one of the most important influences on mercury oxidation is the concentration of HCl. Hall et al. (1991) and Ghorishi (1998) both showed shifts in mercury speciation towards its oxidized form when HCl and NO_x were present in the combustion flue gases. Srivastava et al. (2003) found Hg(0) to be the predominant species at the exit of the SCR catalyst when Powder River Basin coal with no HCl in the combustion flue gas was tested. These observations suggest that a Cl-containing species, such as HCl, is an important source of Cl for mercury oxidation under SCR conditions.

A series of experiments was conducted to examine the dependence of mercury oxidation on the volume fraction of HCl over the range from 0 to 100 ppmv, covering the range from low-chlorine Powder River Basin subbituminous coals to moderate chlorine bituminous coals. The measurements were made in the absence of NO and NH_3, in the presence of NO and absence of NH_3, and in the presence of both NO and NH_3 (NH_3/NO = 0.81 mol/mol). CO was absent under all conditions. The experimental results are summarized in Table 7 and illustrated in Figure 14.

As shown in the figure, there was a steep rise in the fraction of mercury oxidized across the SCR catalyst as the HCl volume fraction increased, over the range from 0 to 10 ppmv, followed by modest increases in mercury oxidation over the range from 10 to 100 ppmv HCl, where the fraction of oxidized mercury approached 100%. The results confirm previously published findings by Eswaran and Stenger (2005), that the extent of

mercury oxidation is highly sensitive to the concentration of HCl at low volume fractions of HCl.

Compared with measurements in the absence of NO and NH_3, the extent of mercury oxidation was moderately suppressed in the presence of NH_3 and NO (NH_3/NO = 0.81 mol/mol). Ammonia competes with at least one or both of the reactants (Hg, HCl) for active surface sites toward the entrance to the monolith, before the NH_3 is consumed by reaction with NO and where it is still present at significant concentration (Niksa and Fujiwara, 2005b).

The steep rise in mercury oxidation at low HCl volume fractions is in contrast to the behavior predicted by Niksa and Fujiwara (2005b) in the presence of both NO and NH_3. In a square honeycomb catalyst at 364 ^oC with an NH_3/NO ratio of 0.9 and space velocity of 3930 h^{-1}, those authors' calculations showed that the fraction of mercury oxidized at the exit from the catalyst increased approximately linearly from 0 % at low HCl volume fractions, to only 14% of mercury oxidized in the presence of 25 ppmv HCl.

Figure 14 also shows that the extent of mercury oxidation was higher in the presence of 300 ppmv NO without NO, than in the absence of both NO and NH_3 for all volume fractions of HCl, consistent with the findings by Hall et al. (1991) and Ghorishi (1998). It appears that NO is able to serve as an oxidizing agent for mercury or, possibly that, when NH_3 is absent, it removes residual strongly-bound NH_3, left on the catalyst from previous tests, freeing active sites on the catalyst for mercury oxidation.

Table 7. Experimental Data Set for the Effect of HCl, NO, and NH_3 on Catalytic Mercury Oxidation, without CO.

HCl (ppmv)	NO (ppmv)	NH_3 (ppmv)	Total Hg (ng/m^3)*	Total Hg StdDev (ng/m^3)*	Hg(0) (ng/m^3)*	Hg(0) StdDev (ng/m^3)*	Hg Oxidation (%)	Hg Oxidation StdDev (%)
0	0	0	9201	326	9210	334	-0.1	5.1
1	0	0	9832	71	9054	87	7.9	1.2
2	0	0	10002	141	8627	122	13.7	1.9
5	0	0	7723	119	2635	109	65.9	2.3
10	0	0	7958	126	1748	164	78.0	2.9
25	0	0	7911	128	1045	164	86.8	3.0
50	0	0	8186	260	778	189	90.5	4.9
100	0	0	8037	233	734	200	90.9	4.6
0	300	0	7965	215	6430	204	19.3	3.8
1	300	0	8926	93	6700	169	24.9	2.2
1	300	0	11133	388	6852	363	38.5	5.0
2	300	0	9321	159	6221	108	33.3	2.1
5	300	0	9726	162	1317	174	86.5	2.8
10	300	0	9593	167	1056	169	89.0	2.9
10	300	0	8319	144	832	159	90.0	3.0
25	300	0	9587	156	858	152	91.1	2.7
50	300	0	9671	178	884	165	90.9	3.0
100	300	0	9489	170	364	136	96.2	2.9
0	350	285	8765	338	9788	321	-11.7	5.3
1	350	285	10560	539	10881	232	-3.0	5.6
1	350	285	10450	123	10439	196	0.1	2.2
2	350	285	10339	235	8303	197	19.7	3.0
3	350	285	11620	326	9756	295	16.1	3.8
4	350	285	10949	187	6977	153	36.3	2.3
5	350	285	9243	157	5158	212	44.2	3.0
7.5	350	285	9693	189	4464	212	54.0	3.1
10	350	285	10106	218	3984	288	60.6	3.8
10	350	285	10706	524	4333	252	59.5	6.2
15	350	285	9561	174	3149	153	67.1	2.7
20	350	285	10004	272	3030	461	69.7	5.7
25	350	285	9027	184	2181	191	75.8	3.3
50	350	285	9320	144	1790	435	80.8	5.1
75	350	285	8813	510	1641	191	81.4	7.8
75	350	285	8561	181	1358	199	84.1	3.6
100	350	285	7546	1114	1183	248	84.3	19.6

*Mercury concentrations at 20 ^oC, 1 atm pressure, and dry.

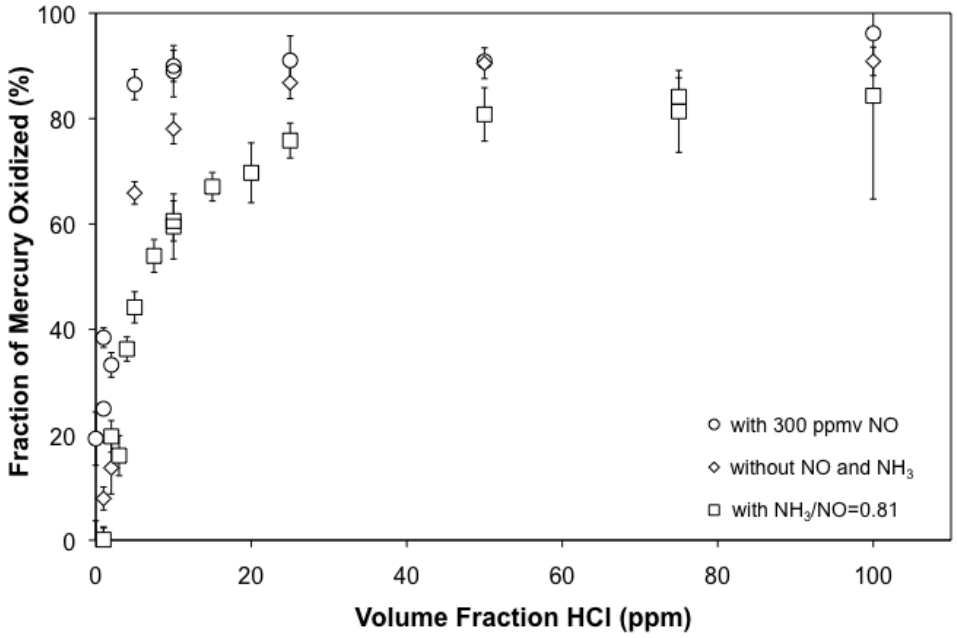

Figure 14. Dependence of mercury oxidation in the square channel monolithic catalyst on the volume fraction of HCl, in the presence and absence of NO and NH_3, and absence of CO, with other conditions as specified in Table 1.

4.8 Effect of NH_3/NO Feed Ratio on Catalytic Mercury Oxidation

Measurements with variation in the volume fraction of NH_3 in the presence of 300 ppmv NO at the catalyst inlet and absence of CO are summarized in Table 8 and illustrated in Figure 15. As shown in the figure, the effect of increasing the NH_3/NO molar ratio, in the presence of 10 ppmv HCl, is small, until the ratio approaches or exceeds stoichiometric, when excess ammonia is present throughout the length of the catalyst and competes with mercury, HCl, or both, for surface sites over the entire length of the catalyst channels (Niksa and Fujiwara, 2005b). In addition, excess NH_3 in the presence of O_2 has been shown to reduce $HgCl_2$ back to Hg(0) by the following homogeneous reaction (Pritchard, 2009):

$$HgCl_2 + NH_3 + 1/4O_2 \rightarrow Hg(0) + 2HCl + 1/2N_2 + 1/2H_2O \quad (R42)$$

In the presence of the lower concentration of HCl, the decline in the extent of mercury oxidation with increasing NH_3/NO molar ratio is more significant, consistent with the predictions of Niksa and Fujiwara (2005b) and Senior (2006). An NH_3/NO molar ratio larger than 0.95 was not examined under the lower HCl condition, but the fraction of mercury oxidized at NH_3/NO = 0.95 mol/mol was less than 20%. Experimental work by Gale et al. (2006) also found that the addition of ammonia hindered mercury oxidation at low HCl concentrations (~2 ppmv), yet had little impact on mercury oxidation at higher HCl concentrations, consistent with the data shown in Figures 14 and 15.

Multiple measurements of the extent of mercury oxidation under identical conditions (1 and 10 ppmv HCl at NH_3/NO = 0 and 1 and 10 ppmv HCl at NH_3/NO = 0.95) were conducted over a time span of eight months. The variation in extent of mercury oxidation over such a long time can be attributed, at least in part, to catalyst aging. The extent of mercury oxidation is most variable in the presence of both NO and NH_3 at NH_3/NO ratios near stoichiometric, when small changes in conditions can cause large changes in unreacted NH_3 toward the exit of the catalyst.

Table 8. Experimental Data Set for the Effect of NH_3/NO Ratio on Catalytic Mercury Oxidation. 300 ppmv NO at catalyst inlet, without CO.

HCl (ppmv)	NH_3/NO (mol/mol)	Total Hg (ng/m^3)*	Total Hg StdDev (ng/m^3)*	Hg(0) (ng/m^3)*	Hg(0) StdDev (ng/m^3)*	Hg Oxidation (%)	Hg Oxidation StdDev (%)
1	0.00	11134	389	6853	363	38.5	5.0
1	0.00	8926	93	6700	169	24.9	2.2
1	0.20	11517	455	7561	314	34.4	5.0
1	0.40	10574	209	7504	184	29.0	2.7
1	0.60	8930	192	6455	190	27.7	3.1
1	0.80	9192	214	7261	120	21.0	2.7
1	0.81	10560	539	10881	232	-3.0	5.6
1	0.81	10450	123	10439	196	0.1	2.2
1	0.95	9813	157	8141	179	17.0	2.4
10	0.00	9593	167	1056	169	89.0	2.9
10	0.00	8320	144	832	159	90.0	3.0
10	0.00	8632	375	1462	142	83.1	5.9
10	0.21	8352	148	813	212	90.3	3.5
10	0.31	8473	162	818	153	90.4	3.2
10	0.35	8529	192	1143	138	86.6	3.4
10	0.54	8023	182	832	144	89.6	3.5
10	0.65	7960	203	882	207	88.9	4.3
10	0.67	8299	176	1206	135	85.5	3.2
10	0.75	8616	386	1468	161	83.0	6.1
10	0.95	8604	392	1468	161	83.0	6.2
10	1.05	8311	157	1989	119	76.1	2.8
10	1.15	7734	401	2379	182	69.2	6.7

*Mercury concentrations at 20 ^oC, 1 atm pressure, and dry.

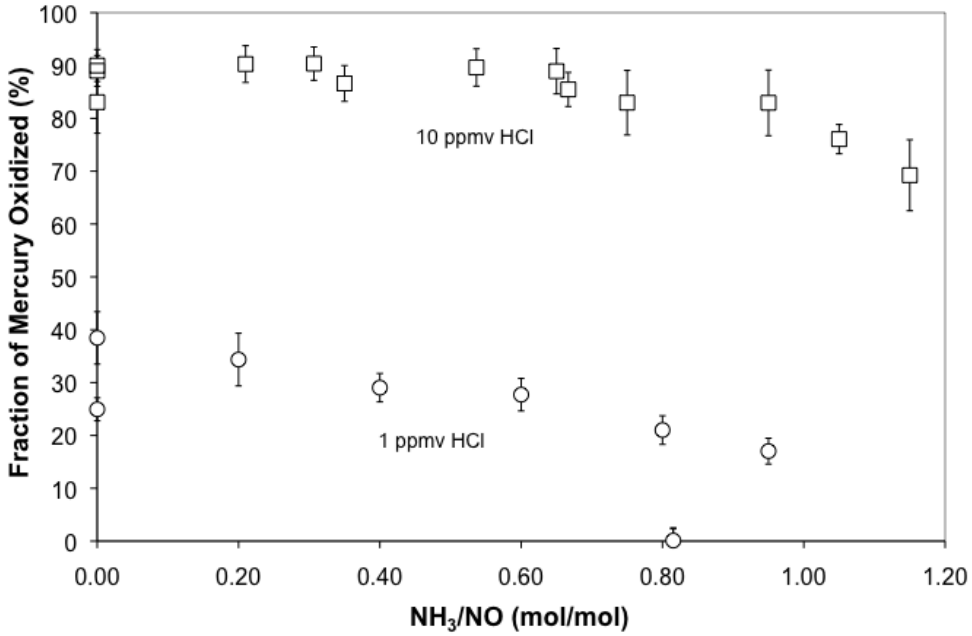

Figure 15. Dependence of mercury oxidation in the square channel monolithic catalyst on NH_3/NO ratio, in the presence of 1 and 10 ppmv HCl, 300 and 350 ppmv NO at the catalyst inlet, absence of CO, and other conditions as specified in Table 1.

4.9 Effect of CO on Catalytic Mercury Oxidation

The possibility that CO in flue gas might interact with Cl adsorbed on SCR catalysts, and the need for examination of the effect of CO on mercury oxidation, were discussed by Presto et al. (2006) and Presto and Granite (2006). Dependence of the extent of mercury oxidation on CO mole fraction, in the presence of 2, 10, and 50 ppmv HCl, 300 ppmv NO, and NH_3/NO = 0.95 was measured over the range from 0 to 2000 ppmv CO, with the results summarized in Table 9 and illustrated in Figure 16. The presence of CO clearly inhibits mercury oxidation at the lower levels of HCl under the conditions investigated. Over the range of CO from 0 to 250 ppmv, in the presence of 10 ppmv HCl, the fraction of mercury oxidized in the catalyst decreased from 71 ± 3% to 43.5 ± 3%.

Even over the range of CO levels that might be encountered under normal operating conditions in coal-fired electric utility boilers, say up to 50 ppmv, the effect on mercury oxidation at 2 and 10 ppmv HCl levels is significant. In the presence of 2 ppmv HCl, a level expected in combustion products from some Power River Basin subbituminous coals, an increase in CO from 0 to 50 ppmv reduced the extent of mercury oxidation from 28% to 6%. A level of 100 ppmv of CO was sufficient to completely suppress mercury oxidation when only 2 ppmv of HCl were present. In contrast, CO has little effect on mercury oxidation in the presence of 50 ppmv HCl. At that HCl level, an increase in CO from 5 to 250 ppmv resulted in no significant decrease in the extent of mercury oxidation, and an increase in CO from 5 to 2053 ppmv was required to reduce the extent of mercury oxidation from 82.9 ± 4.3% to 72.2 ± 5.1%. These findings are consistent with the assumption that CO behaves as a reducing agent, and are in contrast with the predictions by Niksa et al. (2002) that increasing CO promotes mercury oxidation by increasing the Cl atom concentration in the gas phase. Those authors predicted an increase from 28 to 54 % in the extent of mercury oxidation on increasing the CO concentration from 1 to 100 ppmv in the combustion products from lab-scale coal flames, based upon their homogenous and heterogeneous reaction mechanism.

Table 9. Experimental Data Set for the Influence of CO on Catalytic Mercury Oxidation. 300 and 328 ppmv NO at the catalyst inlet.

HCl (ppmv)	NH_3/NO (mol/mol)	CO (ppmv)	Total Hg (ng/m^3)*	Total Hg StdDev (ng/m^3)*	Hg(0) (ng/m^3)*	Hg(0) StdDev (ng/m^3)*	Hg Oxidation (%)	Hg Oxidation StdDev (%)
1.9	0.93	0	10332	289	7457	178	27.8	3.4
1.9	0.93	5	8942	199	6829	123	23.6	2.7
1.9	0.93	8	8660	96	7076	112	18.3	1.7
1.9	0.93	11	8332	60	6907	109	17.1	1.5
2.2	0.92	25	7689	153	6655	118	13.4	2.5
2.1	0.94	52	8294	249	7811	198	5.8	3.8
2.2	0.94	101	8066	146	7976	187	1.1	2.9
11.5	0.95	4	8664	102	3209	219	63.0	2.9
11	0.95	19	8460	84	3627	115	57.1	1.8
11	0.95	19	8349	93	3083	188	63.1	2.6
12	0.95	50	8938	90	3766	108	57.9	1.7
12	0.95	50	8071	122	3571	185	55.8	2.9
11.5	0.95	118	8422	122	4038	183	52.1	2.7
11.4	0.95	263	8223	166	4723	163	42.6	3.0
11.4	0.95	263	8722	113	4844	148	44.5	2.2
11.7	0.95	511	8815	124	5547	152	37.1	2.3
11.6	0.95	1013	8847	72	6579	141	25.6	1.8
11.6	0.95	1013	8869	59	6641	200	25.1	2.4
11.6	0.95	2001	9356	106	8106	159	13.4	2.1
11.6	0.95	2001	9261	79	7918	163	14.5	2.0
50	0.95	5	8333	150	1425	305	82.9	4.3
50	0.95	114	8389	211	1553	286	81.5	4.7
50	0.95	254	8296	191	1571	147	81.1	3.5
50	0.95	511	8503	125	1771	150	79.2	2.6
50	0.95	1043	8441	330	2134	146	74.7	5.2
50	0.95	2053	8603	307	2389	219	72.2	5.1

*Mercury concentrations at 20 ^oC, 1 atm pressure, and dry.

(a)

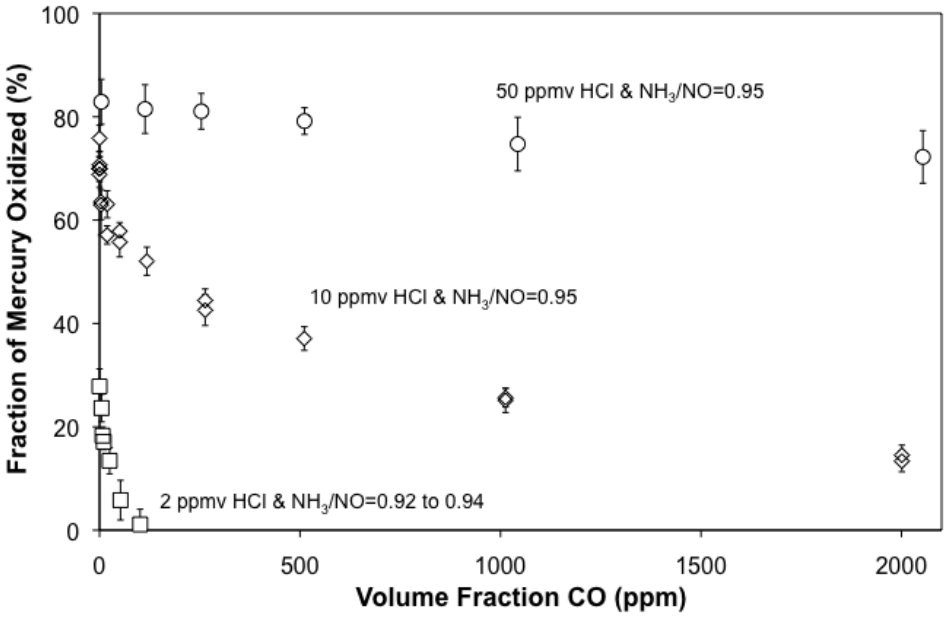

(b)

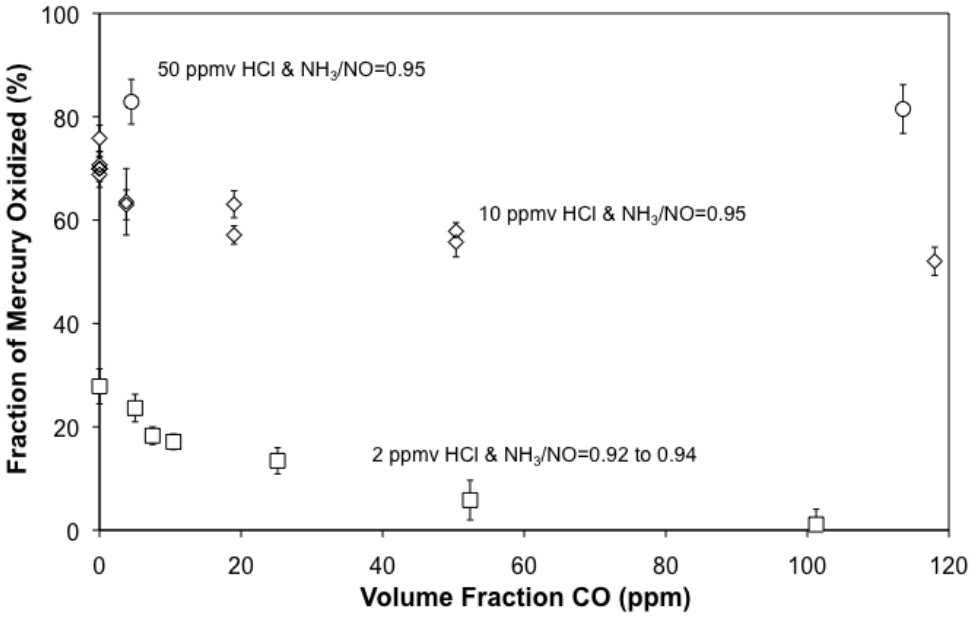

Figure 16. Dependence of mercury oxidation in the square channel monolithic catalyst on the volume fractions of CO and HCl, in the presence of NH_3/NO = 0.95, 300 and 328 ppmv NO at the catalyst inlet, and with other conditions as specified in Table 1. **(a)** over the entire range of CO investigated **(b)** over the practical range of CO in utility boiler flue gas.

Some possible explanations for the inhibition of mercury oxidation by CO are as follows:

1. CO competes with mercury for active sites.

2. CO reduces HgCl (ads) or $HgCl_2$ (ads) while still on the surface of the catalyst, e.g.:

$$Hg(0)\ (g) + S^* = Hg(0)\ (ads) \quad \text{(R43)}$$

$$Hg(0)\ (ads) + HCl\ (g) = HgCl\ (ads) \quad \text{(R44)}$$

$$HgCl\ (ads) + CO\ (g) = Hg(0)\ (ads) + ClCO\ (g) \quad \text{(R45)}$$

$$HgCl\ (ads) = HgCl\ (g) + S^* \quad \text{(R46)}$$

$$HgCl\ (g) + HCl\ (g) = HgCl_2\ (g) + H\ (g) \quad \text{(R47)}$$

(S* - active site on catalyst)

3. CO destroys HgCl (g) or $HgCl_2$ (g) via homogeneous reaction after their desorption from the catalyst surface.

4.10 Catalytic Oxidation of Sulfur Dioxide to Sulfate

Vanadium pentoxide, one of the active ingredients in SCR catalysts, is also the catalyst of choice for oxidation of SO_2 to SO_3 in the manufacture of sulfuric acid, so it is not surprising that vanadium catalysts for NO_x reduction also oxidize SO_2 to SO_3. To be useful in practice, for oxidation of mercury or reduction of NO_x, a catalyst should not promote excessive oxidation of SO_2. Therefore, a comprehensive catalyst evaluation includes measurements of activity for SO_3 formation. Sulfate (SO_3, H_2SO_4, and SO_4^{2-}) was measured by controlled condensation downstream of the reactor under many of the conditions used to investigate mercury oxidation, to determine the fraction of SO_2

oxidized across the catalyst. The sulfuric acid trap used for controlled condensation also collects any NH_4HSO_4 and $(NH_4)_2SO_4$ aerosol formed by reaction of SO_3 with ammonia.

Measurements of the extent of SO_2 oxidation as a function of the NH_3/NO molar ratio, in the absence of CO, with 1 and 10 ppmv HCl, 300 and 345 ppmv NO at the catalyst inlet, 850 ± 50 ppmv SO_2, and other conditions as specified in Table 1, are summarized in Table 10 and illustrated in Figure 17. As seen in the figure, both HCl and NH_3 inhibit oxidation of SO_2 to SO_3. The promotion of SO_2 oxidation in the complete absence of NH_3, and gradual decline in SO_2 oxidation with increasing NH_3/NO ratio, are both consistent with the observations reported by Svachula et al. (1993) and Gale et al. (2006). The sulfate measurements in the presence of 10 ppmv HCl, in the NH_3/NO molar ratio range from 0.95 to 1.15, are close to the detection limit of the controlled condensation protocol, and therefore are not considered to be significantly different from zero. A titrant volume of only 0.3 mL resulted in a calculated SO_3 concentration of 3.1 ppmv. Either a larger gas sample volume (> 14.2 L) or a more dilute (< 0.01 N) barium perchlorate standard solution would help to better differentiate sulfate levels of only several parts per million.

Table 10. Experimental Data Set for the Influence of HCl and NH_3 on SO_2 Oxidation, without CO.

HCl (ppmv)	NO (ppmv)	NH_3 (ppmv)	NH_3/NO (mol/mol)	Inlet SO_2 (ppmv)	Sulfate Formation (mol ppm)	Sulfate Formation StdDev** (%)
1	300	0	0.00	877	10.8	0
1	300	60	0.20	885	8.8	0
1	300	120	0.40	882	8.1	0.4
1	300	180	0.60	871	8.0	0.4
1	300	240	0.80	876	7.2	0.7
1	300	285	0.95	873	6.7	0.7
10	300	0	0.00	*	7.3	0
10	345	0	0.00	*	8.2	0
10	300	63	0.21	*	8.2	0
10	300	92	0.31	*	6.8	0
10	300	105	0.35	*	6.0	0.6
10	300	161	0.54	*	6.2	0.4
10	300	195	0.65	*	5.7	0.3
10	300	200	0.67	*	5.0	0
10	300	225	0.75	*	4.5	0
10	300	285	0.95	*	2.7	0
10	300	315	1.05	*	3.4	0
10	300	345	1.15	*	4.5	0

* Measurements were conducted prior to implementation of FTIR for SO_2 monitoring. An average inlet SO_2 concentration of 838 ± 37 ppmv was estimated from subsequent FTIR measurements under similar conditions.

** Based on titration of two separate controlled condensation samples

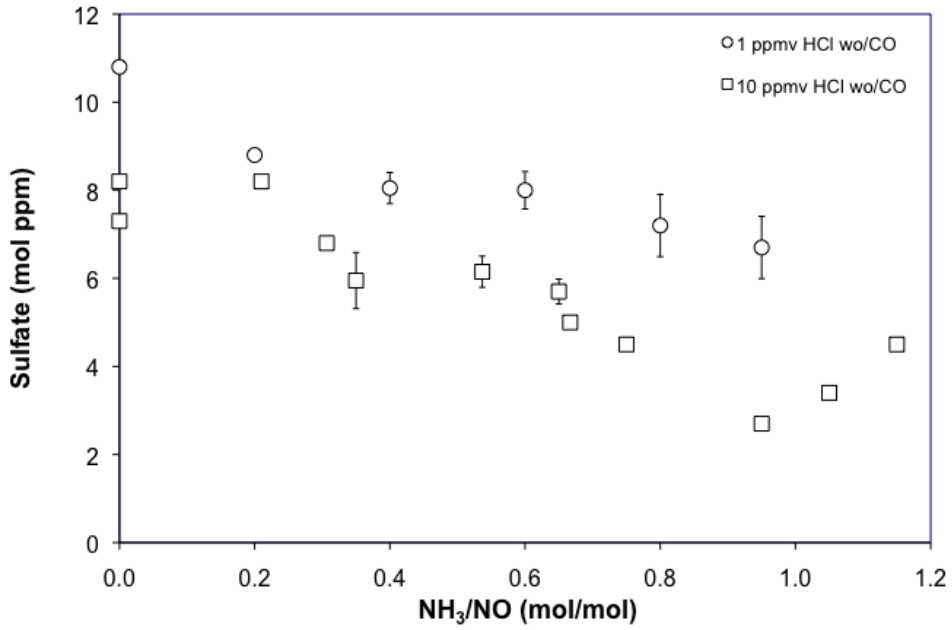

Figure 17. Dependence of sulfate formation in the square channel monolithic catalyst on the NH_3/NO molar ratio in the presence of 300 and 345 ppmv NO, 1 and 10 ppmv HCl, and absence of CO, with other conditions as specified in Table 1.

Dependence of the extent of SO_2 oxidation on CO mole fraction, in the presence of 2, 11, and 50 ppmv HCl, 314 ± 14 ppmv NO, 815 ± 13 ppmv SO_2, NH_3/NO = 0.92 to 0.95, and other conditions as specified in Table 1, was measured over the range from 0 to 2000 ppmv CO, with the results summarized in Table 11 and illustrated in Figure 18. As seen in the figure, there is apparently little influence of CO on sulfate formation, above that observed at the exit from an inert reactor.

The conclusion that may be drawn from the data shown in Figures 17 and 18 are that sulfate formation is slightly inhibited by HCl and by increasing NH_3/NO ratio, is slightly promoted in the presence of CO, and is not formed to significantly greater extent in the SCR catalyst than in the inert reactor containing sand.

Table 11. Experimental Data Set for the Influence of CO on SO_2 Oxidation. 300 and 328 ppmv NO at the catalyst inlet.

HCl (ppmv)	NH_3/NO (mol/mol)	CO (ppmv)	Inlet SO_2 (ppmv)	Sulfate Formation (mol ppm)	Sulfate Formation StdDev* (mol ppm)
		Inert Reactor			
2.2	0.91	102	806	5.9	0
		Catalyst-Containing Reactor			
1.9	0.93	5.0	813	5.7	0.4
1.9	0.93	7.5	807	5.9	0
1.9	0.93	10.5	799	5.9	0
1.9	0.92	25.2	807	6.2	0.4
2.2	0.94	101.3	800	7.0	0.7
11.0	0.95	19	805	5.2	0.4
12.1	0.95	50	838	6.4	0.4
11.6	0.95	1013	824	10.8	0
11.6	0.95	2001	820	9.7	1.5
50	0.95	5	830	6.4	0
50	0.95	254	825	7.0	0
50	0.95	511	820	7.8	0.4
50	0.95	1043	831	7.8	0.4
50	0.95	2053	828	8.0	0

* Based on titration of two separate controlled condensation samples

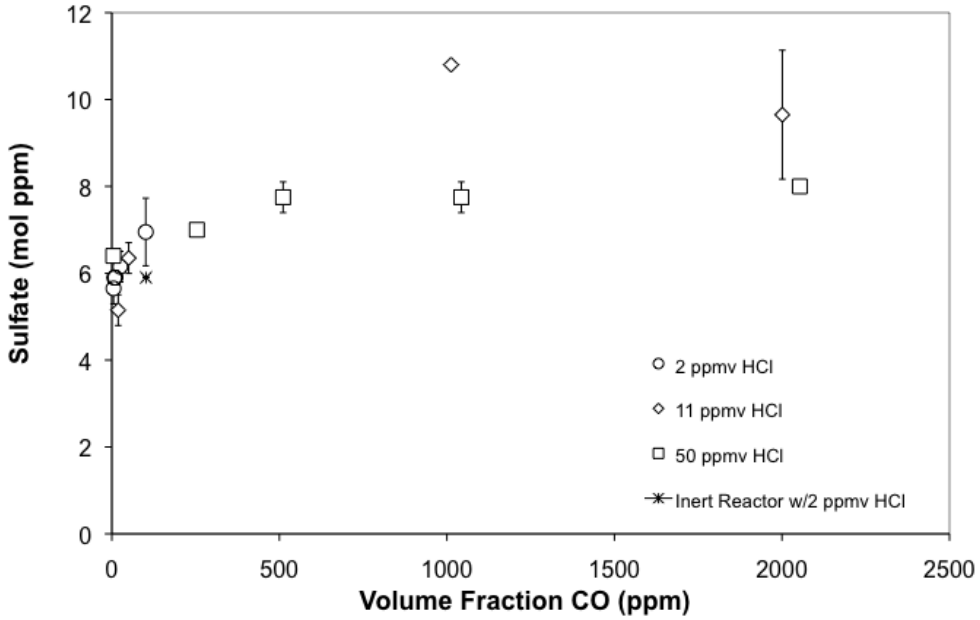

Figure 18. Dependence of SO_2 conversion to sulfate in the square channel monolithic catalyst on the volume fraction of CO in the presence of 2, 11, and 50 ppmv HCl, 314 ± 14 ppmv NO, 815 ± 13 ppmv SO_2, and NH_3/NO = 0.92 to 0.95, with other conditions as specified in Table 1. One measurement also shown downstream from the inert reactor.

4.11 Heterogeneous Chemical Kinetic Model

A model to describe the extent of mercury oxidation by HCl during SCR, in the presence of NO reduction by ammonia, and in the absence of CO, was constructed (Tong et al., 2008), based upon the work of Niksa and Fujiwara (2005b) and Senior (2006). The latter authors compared model calculations to measurements by Machalek et al. (2003) across a monolithic catalyst in a slipstream reactor at 371 ^{o}C and space velocity of 3000 h^{-1} (at standard temperature of 0 ^{o}C). An Eley-Rideal mechanism was adopted in both models. Niksa and Fujiwara assumed that HCl is adsorbed on the catalyst and reacts

with gaseous mercury, while Senior assumed that adsorbed mercury reacts with gaseous HCl. Both assumed that NO_x reacts with adsorbed NH_3.

In the present model, mercury, HCl, and NH_3 are all assumed to be adsorbed on the catalyst surface. Mercury oxidation then occurs by reaction of two adsorbed species. The flow through a catalyst channel is described as laminar and fully developed, with a one-dimensional treatment of diffusion and reaction at the catalyst wall. Although both NH_3 and HCl are adsorbed, they do not compete with each other for the same surface sites, but both compete for sites with elemental mercury. The fraction of surface occupied by mercury is assumed to be small. Pore diffusion in the catalyst wall, considered by Senior (2006), is neglected, and the ratios of effective to geometric surface area are incorporated in the rate coefficients. The pseudo-steady-state rate equation is integrated step-by-step from the entrance to exit of a catalyst channel.

The following transport and reaction steps for NO + NH_3 and Hg(0) + HCl were derived from the mechanisms of Niksa and Fujiwara (2005b) and Senior (2006):

NO Reduction by NH_3:

NH_3 (g) → NH_3 (ads)	diffusion	(R48)
NO (g) + NH_3 (ads) + 1/4 O_2 → N_2 (g) + 3/2 H_2O (g)	reaction	(R49)

Mercury Oxidation by HCl:

Hg(0) (g) → Hg(0) (ads)	diffusion	(R50)
HCl (g) → HCl (ads)	HCl in excess	(R51)
Hg(0) (ads) + HCl (ads) → HgCl (ads or g)	reaction	(R52)
HgCl (ads or g) + HCl (ads or g) → $HgCl_2$ (g)	reaction (fast)	(R53)

There are five adjustable parameters in the model for mercury oxidation: the reaction rate coefficients for NO + NH_3 and Hg(0) + HCl, and the adsorption equilibrium constants for NH_3, Hg(0), and HCl, summarized in Table 12. Ratios of active surface area to geometric surface area incorporated in the rate coefficients. As in the experiments, temperature dependence has not yet been examined. The best fit to the present measurements was obtained with a small value of the HCl adsorption equilibrium constant, suggesting that HCl is only weakly adsorbed. Agreement with the measurements could be improved by introducing different types of surface sites, at the cost of increasing the number of adjustable parameters. The C++ code for the heterogeneous diffusion-reaction model is listed in Appendix A.

A comparison of calculated values with measurements of the fraction of mercury oxidized, as a function of the HCl volume fraction, in the presence and absence of NO and absence of CO and NH_3 is shown in Figure 19.

Table 12. Reaction Rate Coefficients and Adsorption Equilibrium Constants in the Transport and Reaction Model.

Reaction	Reaction Rate Coefficient	Adsorption Equilibrium Constant (m^3/kmol)
NH_3 (g) → NH_3 (ads)	-	3×10^6
Hg(0) (g) → Hg(0) (ads)	-	7.5×10^5
HCl (g) → HCl (ads), competing with Hg(0)	-	7.5
HCl (g) → HCl (ads), competing with SO_2	-	5×10^6
SO_2 (g) → SO_2 (ads)	-	1.5×10^{-7}
SO_3 (g) → SO_3 (ads)	-	5.7×10^6
H_2O (g) → H_2O (ads)	-	0
NO (g) + NH_3 (ads) + 1/4 O_2 (excess) → N_2 (g) + 3/2 H_2O (g)	0.05 m/s	-
Hg(0) (ads) + HCl (ads) → HgCl (ads or g)	0.014 kmol/(m^2·s)	-
HgCl (ads or g) + HCl (ads or g) → $HgCl_2$ (g)	fast	-
$(V_2\text{-}SO_3\text{-}SO_2)_{ox}$ → $(V_2\text{-}SO_3)_{red}$ + SO_3*	$k_{red}C_{tot}$ = 4.2×10^5 kmol/(m^3·s)	-
$(V_2\text{-}SO_3)_{red}$ + 1/2O_2 (g) → $(V_2\text{-}SO_3)_{ox}$*	$k_{ox}C_{tot}$ = 4.2×10^5 $kmol^{1/2}$/($m^{3/2}$·s)	-

* Svachula et al. (1993b)

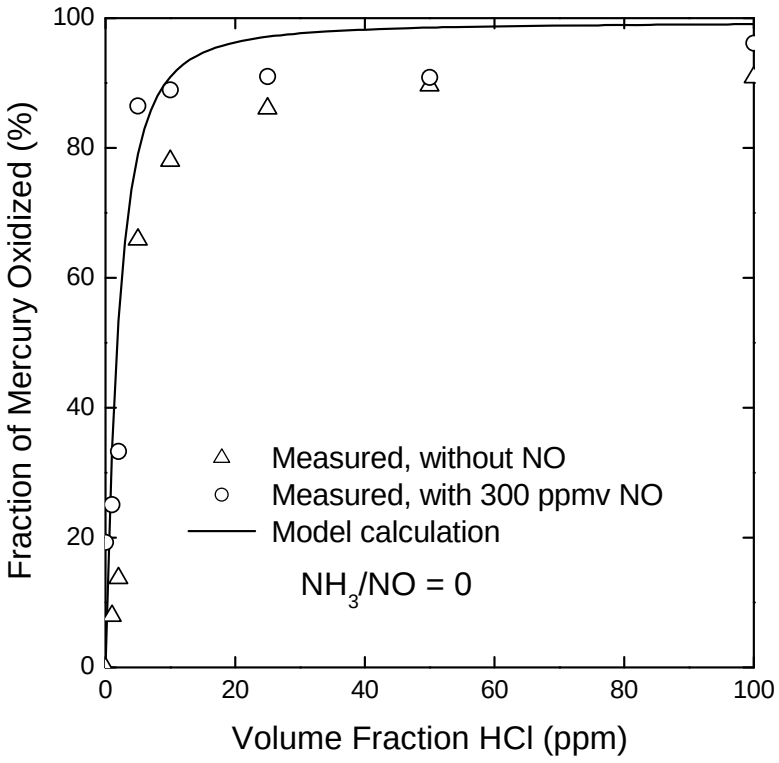

Figure 19. Comparison of calculated extents of catalytic mercury oxidation by HCl with the measurements in the presence and absence of NO, $NH_3/NO = 0$, and CO = 0, with other conditions as specified in Table 1. The model does not account for any influence of NO on Hg(0) oxidation.

A comparison of calculated values with measurements of the fraction of mercury oxidized, as a function of the NH_3/NO ratio, in the presence of 1 and 10 ppmv HCl is shown in Figure 20. The proposed mechanism successfully reproduces qualitative features of both the HCl and NH_3/NO ratio dependences of mercury oxidation. The decline in extent of mercury oxidation as the NH_3/NO ratio approaches and exceeds stoichiometric is captured with accuracy commensurate with the reproducibility of the experimental observations. Some of the scatter in the measurements at NH_3/NO mole

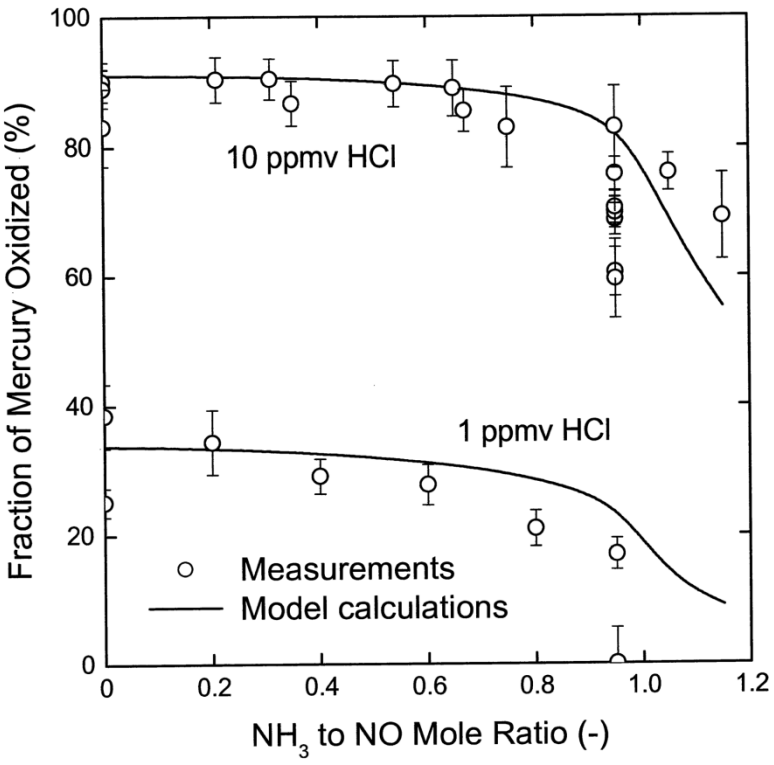

Figure 20. Dependence of mercury oxidation in the monolithic catalyst on the ratio of NH_3 to NO in the presence of 1 and 10 ppmv HCl, and comparison with model calculations. NO = 300 ppmv at the catalyst inlet. CO = 0. Other conditions as specified in Table 1.

ratio of 0.95 is probably due to the sensitivity of unreacted ammonia near the catalyst outlet to the inlet levels of NO and NH_3.

Calculations of the inhibition of mercury oxidation by CO, based on a proposed mechanism (Section 4.9) that CO reacts with, and destroys HgCl(g) or $HgCl_2$(g) after desorption from the catalyst surface, are compared with the measurements in Figure 21. The mechanism is unable to explain why the effect of CO diminishes as the HCl concentration increases. Likewise, simple models based on the other proposed

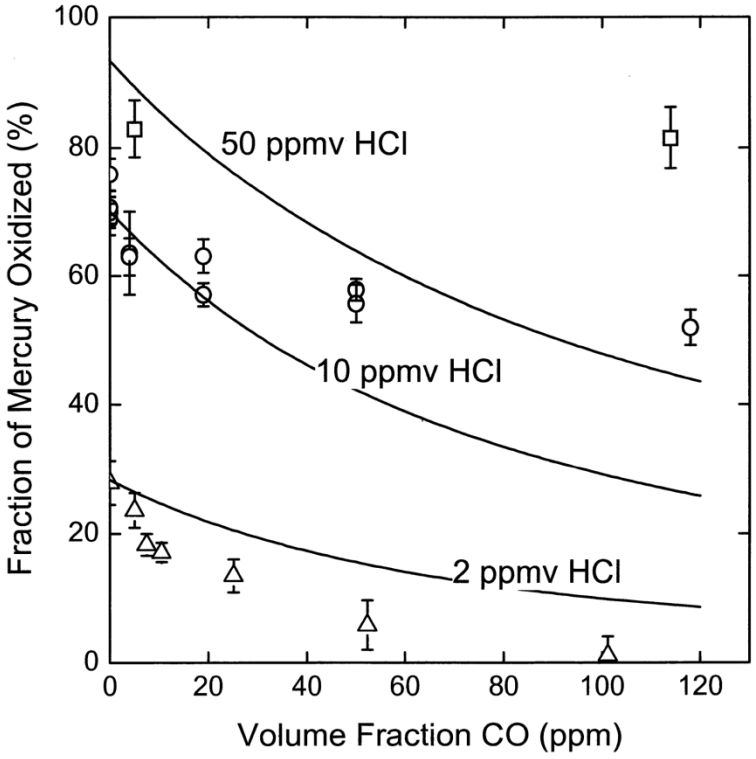

Figure 21. Dependence of mercury oxidation in the monolithic catalyst on the volume fraction of CO over the range from 0 to 120 ppmv CO and comparison with model calculations. Gas composition: 2, 10, and 50 ppmv HCl, 314 ± 14 ppmv NO, and NH_3/NO = 0.92 to 0.95, with other conditions as specified in Table 1.

mechanisms were unable to reproduce this observation. An explanation of the effect of CO on mercury oxidation remains for future work.

SO_3 formation was treated using the rate expression for SO_3 formation in SCR by Svachula et al. (1993b), which describes the dependence of the rate on all of the species, SO_2, O_2, SO_3, H_2O, NO_X, and NH_3. However, the empirical factor introduced by these authors to account for the promotion of SO_2 oxidation by NO_X was not included. The effect of HCl was added to the rate expression of Svachula et al. by assuming that it

competes with SO_2 for active sites. This required a much larger adsorption coefficient than was used to describe the competition of HCl with Hg(0) for sites. Comparisons with measurements are shown by the solid and dashed curves in Figure 22. The dependence of SO_3 formation on NH_3/NO ratio in the presence of 1 ppmv HCl, 300 ppmv NO, ~880 ppmv SO_2, and absence of CO is nicely reproduced, with the exception of the measurement in the absence of NH_3, where the promotion of SO_3 formation by NO is greatest. Agreement of the model calculation with the measurements in the presence of 10 ppmv HCl is less impressive. The measurements hint at an interesting behavior in the presence of excess ammonia, suggesting an interaction of the excess NH_3 with HCl or SO_2. Interpretation of these data is complicated by uncertainty regarding the actual contribution of the SCR catalyst to SO_3 formation (Section 4.10).

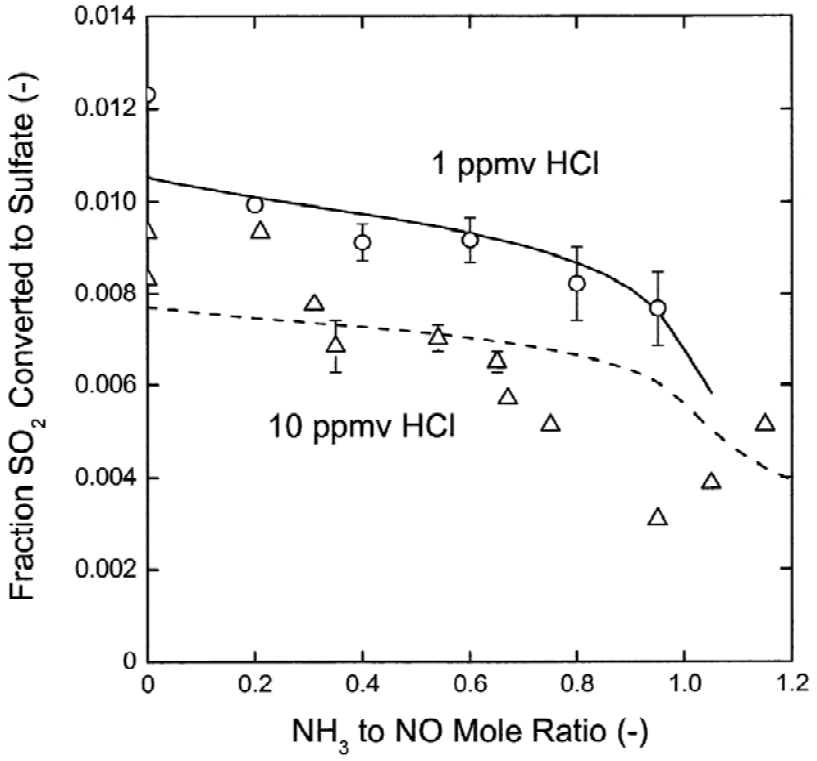

Figure 22. Dependence of SO_2 oxidation to sulfate in the monolithic catalyst on the ratio of NH_3 to NO in the presence of 1 and 10 ppmv HCl, and comparison with model calculations. NO = 300 ppmv at the catalyst inlet. CO = 0. Other conditions as specified in Table 1.

CHAPTER 5

CONCLUSION

Measurements of the performance of a 310-mm-long sample of a widely-used commercial 7 x 7 mm square cell monolithic SCR catalyst, with respect to mercury oxidation, NO reduction, and SO_2 oxidation were performed in the SRI Catalyst Test Facility over a wide range of simulated flue gas composition. The conclusions from the work are:

- The Tennessee Valley Authority's dry, high temperature converter for the reduction of mercury to the elemental state (Van Pelt and Meischen, 1999; Meischen et al., 2004) for analysis by atomic fluorescence is a great improvement over the previously-used wet chemical method for reduction of mercury.
- Mercury oxidation is highly sensitive to HCl at the low levels characteristic of Powder River Basin subbituminous coals (0 to 5 ppmv).
- Mercury oxidation is inhibited by NH_3, as reported by other workers (Machalek et al., 2003; Niksa and Fujiwara, 2005b; Senior, 2006; Gale et al., 2006b), but is promoted by NO in the absence of NH_3, a condition that would be present if flue gas were passed through an SCR catalyst when NH_3 addition is not required for NO_X reduction to meet air quality regulations. However, sulfate formation is also enhanced by NO in the absence of NH_3.

- The inhibitory effect of NH_3 on mercury oxidation increases with decreasing HCl, increases on approach to stoichiometric NH_3/NO, and increases markedly in the presence of excess ammonia, consistent with the predictions of Niksa and Fujiwara (2005b) and Senior (2006).
- Mercury oxidation is inhibited by CO, especially at low levels of HCl (2 and 10 ppmv). This is regarded as one of the most significant findings of the work and has addressed a research need identified by Presto et al. (2006) and Presto and Granite (2006).
- Oxidation of SO_2 to sulfate was slightly inhibited by HCl and by increasing NH_3/NO ratio, but was slightly promoted in the presence of CO. However, sulfate was not formed to significantly greater extent in the SCR catalyst, than in an inert reactor containing sand.
- A simulation of homogeneous gas-phase mercury oxidation reactions in flue gas from combustion of an Ohio bituminous coal (130 ppmv HCl) performed by Balaji Krishnakumar in Joseph J. Helble's research group (Krishnakumar and Helble, Personal communication, 2008), revealed that CO is not expected to have a significant effect on the gas phase chemistry of mercury oxidation over the entire post-combustion temperature range in coal-fired electric utility boilers (1177 to 77 ^{o}C). The effect of CO, in the homogeneous system, is a slight promotion of mercury oxidation, rather than the inhibition of mercury oxidation observed in the present experiments with SCR catalyst.
- The dependence of mercury oxidation on HCl and NH_3/NO ratio was reproduced with accuracy commensurate with the reproducibility of the measurements by a one-

dimensional model for diffusion and reaction in a catalyst channel. The model was based upon the analysis of Niksa and Fujiwara (2005b) and Senior (2006), with reaction occurring between adsorbed mercury and adsorbed HCl or Cl. The adsorption equilibrium constants and rate coefficients, five parameters in all, were adjusted to fit the measurements.

- The best fits of the mercury oxidation model to the measurements were obtained using low values for the HCl adsorption equilibrium constant, suggesting that HCl is weakly adsorbed.
- Models based on assumptions that CO competes with elemental mercury for catalytic surface sites, or reduces oxidized mercury while on the surface or in the gas phase, were not consistent with the CO and HCl dependence of the measurements.
- A model for SO_2 oxidation to SO_3 in a catalyst channel was based upon the mechanism and rate expression of Svachula et al. (1993b). The model was able to reproduce the observed decrease in sulfate formation with increasing NH_3/NO ratio, though the actual contribution of the SCR catalyst to sulfate formation was unclear.

LIST OF REFERENCES

Afonso, R. F.; Senior, C. L. Assessment of Mercury Removal by Existing Air Pollution Control Devices in Full-Scale Power Plants. Proceedings of the Mega Symposium, Chicago, IL, August 20-23, **2001**; Paper No. 237, Air & Waste Management Association, Pittsburgh, PA.

Aposhian, H.V.; Aposhian, M.M. Elemental, Mercuric, and Methylmercury: Biological Interactions and Dilemmas. Proceedings of the Air Quality II: Mercury, Trace Elements, and Particulate Matter Conference, McLean, VA, September 19-21, **2000**, Paper A1-3.

Belkin, H. E.; Finkelman, R. B.; Zheng, B. Mercury in People's Republic of China Coal. *Geol. Soc. Am. Abstr.* **2005**, 37(7), 48.

Beretta, A.; Tronconi, E.; Groppi, G.; Forzatti, P. Selective Catalytic Reduction of NO_x with NH_3 from Stationary Sources. In Structured Catalysts and Reactors; Dekker, New York, **1997**; Chapter 5, pp 121-148.

Breen, B. P.; Gabrielson, J. E. Control of Mercury and Other Elemental Metal Emissions from Combustion Devices by Oxidation. US Pat. Appl. 2003/0147793 A1, **2003**.

Brown, T. D.; Smith, D. N.; Hargis, R. A.; O'Dowd, W. J. Mercury measurements and Its Control: What We Know, Have Learned, and Need to Further Investigate. *J. Air Waste Manage. Assoc.* June **1999**, 1-97.

Bustard, Y.; Durham, M.; Starns, T.; Lindsey, C.; Martin, C.; Schlager, R.; Baldrey, K. Full-Scale Evaluation of Sorbent Injection for Mercury Control on Coal-Fired Power Plants. *Fuel Process. Technol.* **2004**, 85, 549-562.

Butz, J. R.; Turchi, C.; Broderick, T. E.; Albiston, J. Options for Mercury Removal from Coal-Fired Flue Gas Streams: Pilot-Scale Research on Activated Carbon, Alternative and Regenerable Sorbents. Proceedings of 17th Annual Pittsburgh Coal Conference, Pittsburgh, PA, Sept. 11-14, **2000**, Paper 19b-3.

Carey, T. Effect of Mercury Speciation on Removal Across Wet FGD Processes. Proceedings of the Air and Waste Management Association's 92nd Annual Meeting, June, **1999**; Air & Waste Management Association, Pittsburgh, PA.

Chen, Z.; Senior, C. L.; Sarofim, A. F. Modeling of Mercury States in Coal-Fired Utility Boilers. Proceedings of the 27th International Technical Conference on Coal Utilization and Fuel Systems, Clearwater, FL, March 4-7, **2003**.

Chu, P.; Behrens, G.; Laudal, D. Estimating Total and Speciated Mercury Emissions from U.S. Coal-Fired Power Plants. Proceedings of the Mega Symposium, Chicago, IL, August 20-23, 2001; Paper No. 345, Air & Waste Management Association, Pittsburgh, PA.

Cormetech, Inc. SCR Catalysts for Coal-Fired Generators. January **2005**. http://www.cormetech.com/brochures/CormetechCoalBrochure_20050119.pdf (accessed June, 2008).

Cichanowicz, J.E.; L.J. Muzio. Twenty-Five Years of SCR Evolution: Implications for U.S. Application and Operation. Presented at the MEGA Symposium, Chicago, IL, August 20-23, **2001**.

Dajnak, D.; Clark, K. D.; Lockwood, F. C.; Reed, G. The Prediction of Mercury Retention in Ash from Pulverized Combustion of Coal and Sewage Sludge. *Fuel* **2003**, 82, 1901-1909.

Dunham, G. E.; DeWall, R. A.; Senior, C. L. Fixed-Bed Studies of the Interactions Between Mercury and Coal Combustion Fly Ash. *Fuel Process. Technol.* **2003**, 82, 197-213.

Edwards, J. R.; Srivastava, R. K.; Kilgroe, J. D. A Study of Gas-Phase Mercury Speciation Using Detailed Chemical Kinetics. *J. Air Waste Manage. Assoc.* **2001**, 51, 869-877.

Eswaran, S.; Stenger, H. G. Understanding Mercury Conversion in Selective Catalytic Reduction (SCR) Catalysts. *Energy Fuels*, **2005**, *19*, 2328.

Forrest, J.; Garber, R.; Newman, L. Formation of Sulfate, Ammonium, and Nitrate in an Oil-Fired Power Plant Plume. *Atmos. Environ*. **1979**, 13, (9), 1287-1297.

Freme, F. U.S. Coal Supply and Demand 2007 Review. Energy Information Administration. April **2008**. http://www.eia.doe.gov/cneaf/coal/page/special/feature.html (accessed April 2008).

Fry, A. R.; Lighty, J. S.; Silcox, G. D. Fundamental Homogeneous Reactions of Mercury in Coal Fired Utility Boilers. Proceedings of the 30th International Technical Conference on Coal Utilization and Fuel Systems, Clearwater, FL, April 17-21, **2005**.

Fry, A.; Cauch, B.; Lighty, J. S.; Silcox, G. D.; Senior, C. L. Proceedings of the 31st International Symposium on Combustion, Heidelberg, Germany, **2006**.

Fujiwara, N.; Fujita, Y.; Tomura, K.; Moritomi, H.; Tuji, T.; Takasu, S.; Niksa, S. Mercury Transformations in the Exhausts from Lab-Scale Coal Flames. *Fuel* **2002**, 81, (16), 2045-2052.

Galbreath, K. C.; Zygarlicke, C. J. Mercury Speciation in Coal Combustion and Gasification Flue Gases. *Environ. Sci. Technol.* **1996**, 30, 2421-2426.

Galbreath, K. C.; Zygarlicke, C. J. Mercury Transformation in Coal Combustion Flue Gas. *Fuel Process. Technol.* **2000**, 65-66, 289.

Galbreath, K. C., Zygarlicke, C. J., Tibbetts, J. E., Schulz, R. L., Dunham, G. E. Effects of NO_x, α-Fe_2O_3, g-Fe_2O_3, and HCl on Mercury Transformations in a 7-kW Coal Combustion System. *Fuel Process. Technol.* **2004**, 86, 429-448.

Gale, T. K. Mercury Control with Calcium-Based Sorbents and Oxidizing Agents, Topical Report to U.S. DOE/NETL. U.S. Department of Energy Agreement No. DE-FC26-01NT41183. Southern Research Institute, **2002**.

Gale, T. K. Mercury Adsorption and Oxidation Kinetics in Coal-Fired Flue Gas. Proceedings of the 30th International Technical Conference on Coal Utilization and Fuel Systems, Clearwater, FL, April 17-21, **2005**.

Gale, T. K.; Cushing, K. M. Understanding Mercury Chemistry in Coal-Fired Boilers: Biennial Report, December 2001-December 2003. EPRI, Palo Alto, CA: 1008026 (**2003**).

Gale, T. K.; Lani, B. W.; Offen, G. R. Mechanisms Governing the Fate of Mercury in Coal-Fired Power Systems. *Fuel Process. Technol.* **2008**, 89, 139-151.

Gale, T. K.; Blankenship, G. A.; Hinton, W. S.; Cannon, J. W.; Lani, B. W. Mercury Oxidation Compared for Three Different Commercial SCR Catalysts. Proceedings of the EPA-DOE-EPRI-A&WMA Power Plant Air Pollutant Control "Mega" Symposium, Paper No. 55, Baltimore, MD, August 28-31, **2006**.

Ghorishi, S.B. Fundamentals of Mercury Speciation and Control in Coal-Fired Boilers. EPA Report number EPA-600/R-98-014 (NTIS PB98-127095). February **1998**.

Ghorishi, S. B.; Lee, C. W.; Kilgroe, J. D. Mercury Speciation in Combustion Systems: Studies with Simulated Flue Gases and Model Fly Ashes. Proceedings of the Air & Waste Management Association 92nd Annual Meeting & Exhibition, Paper No. 99-651, St. Louis, MO, June 20-24, **1999**.

Ghorishi, S. B.; Lee, C. W.; Jozewicz, W.; Kilgroe, J. D. Effects of Fly Ash Transition Metal Content and Flue Gas HCl/SO_2 Ratio on Mercury Speciation in Waste Combustion. *Environ. Eng. Sci.* **2005**, 22, 221.

Granite, E. J.; Pennline, H. W.; Hargis, R. A. Sorbents for Mercury Removal from Flue Gas. Topical Report DOE/FETC/TR-98-01, National Energy Technology Laboratory: Pittsburgh, PA, January **1998**.

Granite, E. J.; Pennline, H. W.; Hargis, R. A. Novel Sorbents for Mercury Removal from Flue Gas. *Ind. Eng. Chem. Res.* **2000**, 39, 1020.

Hall, B.; Schager, P.; Lindqvist, O. Chemical Reactions of Mercury in Combustion Flue Gases. *Water, Air, Soil Pollut.* **1991**, 56, 3-14.

Hassett, D.; Eylands, K. Mercury Capture on Coal Combustion Fly Ash. *Fuel* **1999**, 78, 243.

Hocquel, M. The Behavior and Fate of Mercury in Coal-Fired Power Plants with Downstream Air Pollution Control Devices. Forschr.-Ber, VDI Verlag, Dusseldorf, Germany, **2004**.

Hocquel, M.; Unterberger, S.; Hein, K. R. G. Influence of HCl, SO_2, CaO and Catalytic Material on the Speciation of Mercury. Proceedings of the Mega Symposium, Chicago, IL, August 20-23, **2001**; Paper No. 348, Air & Waste Management Association, Pittsburgh, PA.

Hranisavljevic, J.; Fontijin, A. Kinetics of Ground-State Cd Reaction with Cl_2, O_2, and HCl Over Wide Temperature Ranges. *J. Phys. Chem.* **1997**, 101, 2323

H. Zinder & Associates. Evaluation of the Cost of Safe Control Strategies in the SIP-Call. Final Report Prepared for the Midwest Ozone Group, October 16, **2000**.

Jensen, R. R.; Karki, S.; Salehfar, H. Artificial Neural Network-Based Estimation of Mercury Speciation in Combustion Flue Gas. *Fuel Process. Technol.* **2004**, 85, 451-462.

Just, J.; Ségala, C.; Sahraoui1, F.; Priol, G.; Grimfeld, A.; Neukirch, F. Short-Term Health Effects of Particulate and Photochemical Air Pollution in Asthmatic Children. *Eur Respir J*. **2002**, 20, 899-906.

Kai, K.; Nagai, Y.; Kato, Y.; Gretta, W.; Kikkawa, H. SCR Catalyst with High Mercury Oxidation and Low SO_2 to SO_3 Conversion. Proceedings of the Combined Power Plant Air Pollution Control Symposium-The Mega Symposium. Baltimore, MD, August 28-31, **2006**.

Kilgore, J. D.; Sedman, C. B.; Srivastava, R. K.; Ryan, J. V.; Lee, C. W.; Thorneloe, S. A. Control of Mercury Emissions from Coal-Fired Electric Utility Boilers: Interim Report. U.S. EPA, **2002**, EPA-600/R-01-109.

Kolker, A.; Senior, C. L.; Quick, J. C. Mercury in Coal and the Impact of Coal Quality on Mercury Emissions from Combustion Systems. *Appl. Geochem.* **2006**, 21, 1821-1836.

Kramlich, J. C.; Castiglone, L. The Forcing of Mercury Oxidation as a Means of Promoting Low-Cost Capture. Final Report for DOE Grant Number DE-FG26-01NT41288. March **2004**.

Krishnakumar, B.; Helble, J. J. Understanding Mercury Transformation in Coal-Fired Power Plants: Evaluation of Homogeneous Hg Oxidation Mechanisms. *Environ. Sci. Technol.* **2007**, 41,7870-7875.

Krishnakumar, B.; Helble, J. J. Thayer School of Engineering, Dartmouth College, Hanover, NH. Personal communication, **2008**.

Laudal, D. L. Field Validation of the Ontario Hydro Mercury Speciation Sampling Method at Site E-29. EERC Final Report for the Federal Energy Technology Center, AAD Document Control, U.S. Department of Energy, July **1999**.

Laudal, D. L. Pilot-Scale Evaluation of the Impact of Selective Catalytic Reduction for NO, on Mercury Speciation. Report for EPRI, U.S. Department of Energy National Energy Technology Laboratory, U.S. Environmental Protection Agency, Ontario Power Generation, EPRI, **2000**.

Laudal, D. L.; Galbreath, K. C.; Heidt, M. K. A State-Of-The-Art Review of Flue Gas Mercury Speciation Methods. Electric Power Research Institute Report No. TR-107080. November **1996**.

Laudal, D. L.; Brown, T. D.; Nott, B. R. Effects of Flue Gas Constituents on Mercury Speciation. *Fuel Process. Technol.* **2000**, 65 - 66, 157 - 165.

Laumb, J.; Benson, S.; Olson, E. S. X-ray Photoelectron Spectroscopy Analysis on Mercury Sorbent Surface Chemistry. *Fuel Process. Technol.* **2004**, 85, 577.

Li, Z.; Hwang, J.-Y. Mercury Distribution in Fly Ash Components. Proceedings of the A&WMA 90th Annual Meeting, Paper WP72B.05. Toronto, Ontario, Canada, June 8-13, **1997**.

Lighty, J.S.; Silcox, G.D.; Fry, A.R.; Senior, C.; Helble, J.; Krishnakumar, B. Fundamentals of Mercury Oxidation in Flue Gas. Technical Annual Report DOE Grant Number DE-FG26-03NT41797. August **2006**.

Lindberg, V. Uncertainties and Error Propagation Part I of a Manual on Uncertainties, Graphing, and the Vernier Caliper. July 1, **2000**. http://www.rit.edu/~uphysics/uncertainties/Uncertaintiespart2.html (accessed June 2007)

Machalek, T.; Ramavajjala, M.; Richardson, M.; Richardson, D. C.; Goeckner, B.; Anderson, H.; Morris, E. Pilot Evaluation of Flue Gas Mercury Reactions Across an SCR Unit. Proceedings of the EPA-DOE-EPRI-A&WMA Power Plant Air Pollutant Control "Mega" Symposium, Paper No. 64, Washington, DC, May 19-22, **2003**.

Mamani-Paco, R. M.; Helble, J. J. Bench-Scale Examination of Mercury Oxidation Under Non-Isothermal Conditions. Proceedings of the Air and Waste Management Association 93rd Annual Meeting, Salt Lake City, UT, **2000**; Paper AE1A 584.

Mars, P. and Maessen, J. G. H. The Mechanism and the Kinetics of Sulfur Dioxide Oxidation on Catalysts Containing Vanadium and Alkali Oxides. *J. Catal.* **1968**, 10, (1) 1-12.

Meij, R.; Vredenbregt, L.; Winkel, H. The Fate of Mercury in Coal-Fired Power Plants. Proceedings of the Mega Symposium, Chicago, IL, August 20-23, **2001**; Paper No. 307, Air & Waste Management Association, Pittsburgh, PA.

Meischen, S. J.; Van Pelt, V. J.; Zarate, E. A.; Stephens, E. A., Jr. Gas-Phase Mercury Reduction to Measure Total Mercury in the Flue Gas of a Coal-Fired Boiler. *J. Air Waste Manage. Assoc*. **2004**, 54, 60-67.

Merritt, R. L.; McCain, J. D.; Cushing, K. M. Evaluation of TVA's Dry Conversion System for Gas Pretreatment Upstream of a Vapor Phase Mercury Monitor. Report to EPRI – EP-P9129/C4597, Feb 1, **2005**.

Miller, S. J.; Dunham, G. E.; Olson, E. S.; Brown, T. D. Flue Gas Effects on a Carbon-Based Mercury Sorbent. *Fuel Process. Technol.* **2003**, 65-66, 343-363.

National Research Council. Toxicological Effects of Methyl Mercury. National Academy Press, Washington D.C. **2000**, August, Library of Congress Card Number 00-108382.

Niksa, S.; Fujiwara, N. Predicting Extents of Mercury Oxidation in Coal-Derived Flue Gases. *J. Air Waste Manage. Assoc*. **2005a**, 55, 930.

Niksa, S.; Fujiwara, N. A Predictive Mechanism for Mercury Oxidation on Selective Catalytic Reduction Catalysts Under Coal-Derived Flue Gas. *J. Air Waste Manage. Assoc*. **2005b**, 55, 1866-1875.

Niksa, S.; Helble, J. J.; Fujiwara, N. Kinetic Modeling of Homogeneous Mercury Oxidation: The Importance of NO and H_2O in Predicting Oxidation in Coal-Derived Systems. *Environ. Sci. Technol*. **2001**, 35, 3701-3706.

Niksa, S.; Fujiwara, N.; Fujita, Y.; Tomura, K.; Moritomi, H.; Tuji, T.; Takasu, S. A Mechanism for Mercury Oxidation in Coal-Derived Exhausts. *J. Air Waste Manage. Assoc*. **2002**, 52, 894-901.

Norton, G. A. Effect of Fly Ash on Mercury Oxidation During Post Combustion Conditions. Annual Report – DE-FG26-98FT40111 for period Sept. 1, 1999 – Aug. 31, **2000**.

Norton, G. A.; Yang, H.; Brown, R. C.; Laudal, D. L.; Dunham, G. E.; Erjavec, J. Heterogeneous Oxidation of Mercury in Simulated Post Combustion Conditions. *Fuel.* **2003**, 82, 107-116.

Olson, E. S.; Sharma, R. K.; Miller, S. J.; Dunham, G. E. Mercury in the Environment: Proceedings of a specialty conference. Air & Waste Management Association, Minneapolis, MN, Sept 15 – 17, **1999,** 121-126.

Pacyna, E. G. and Pacyna, J. M. Global Emission of Mercury from Anthropogenic Sources in 1995. *J. Water Air Soil Pollut.* **2002**, 137, 1-4.

Pacyna, J. and Munthe, J. Presentation at Workshop on Mercury: Brussels, March 29-30, **2004**.

Pan, H.; Minet, R.; Benson, S.; Tsotsis, T. Process for Converting Hydrogen Chloride to Chlorine. *Ind. Eng. Chem. Res.* **1994**, 33, 2996.

Pavlish, J. H. Center for air toxic metals final technical report. Energy and Environmental Research Center, Grand Forks, North Dakota, vol. III, September **2000**.

Pavlish, J. H.; Sondreal, E. A.; Mann, M. D.; Olson, E. S.; Galbreath, K. C.; Laudal, D. L.; Benson, S. A. Status Review of Mercury Control Options for Coal-Fired Power Plants. *Fuel Process. Technol.* **2003**, 82, 89-165.

Pilling, M.; Seakins, P. W. Reaction Kinetics. Oxford Science Publication. New York, **1995**.

Presto, A. A.; Granite, E. J. Survey of Catalysts for Oxidation of Mercury in Flue Gas. *Environ. Sci. Technol.* **2006**, 40, 5601-5609.

Pritchard, S. Catalyst Management: The Key to SCR Effectiveness. *Modern Power Systems*, Progressive Media Markets Ltd. **2009**. http://www.modernpowersystems.com/story.asp?sectionCode=88&storyCode=2050553 (accessed February 2009).

Pritchard, S.; Iskandar, R.; Stevens, F.; Alten, R. V. Cormetech SCR Catalyst Development for Low SO_2 to SO_3 Oxidation. Proceedings of the EPRI SCR Workshop, Atlanta, GA, October 22, **2002**.

Qiu, J.; Helble, J. J.; Sterling, R. Proceedings of the 12th International Conference on Coal Science, Cairns, Australia, **2003**.

Richardson, C.; Machalek, T.; Miller, S.; Dene, C.; Chang, R. Effect of NO_x Control Processes on Mercury Speciation in Utility Flue Gas. Proceedings of the Mega Symposium, Chicago, IL, August 20-23, **2001**; Paper No. 228, Air & Waste Management Association, Pittsburgh, PA.

Schimmoller, B. K. Mercury Rising. *Power Eng.* June, 12, **2001**.

Schofield, K. Mercury Emission Chemistry: The Similarities or Are They Generalities of Mercury and Alkali Combustion Deposition Processes? *Proc. Combust. Inst.* **2005**. 30, 1263.

Senior, C. L. Oxidation of Mercury Across SCR Catalysts in Coal-Fired Power Plants Burning Low Rank Fuels, Final Report to DOE/NETL. U.S. Department of Energy Agreement No. DE-FC26-03NT41728. Reaction Engineering International, **2004**.

Senior, C. L. Oxidation of Mercury Across Selective Catalytic Reduction Catalysts in Coal-Fired Power Plants. *J. Air Waste Manage. Assoc.* **2006**, 56, 23-31.

Senior, C. L.; Helble, J. J.; Sarofim, A. F. Emissions of Mercury, Trace Elements, and Fine Particles from Stationary Combustion Sources. *Fuel Process. Technol.* **2000a**, 65-66, 263-288.

Senior, C. L.; Sarofim, A. F.; Zeng, T.; Helble, J. J.; Mamani-Paco, R. Gas-Phase Transformations of Mercury in Coal-Fired Power Plants. *Fuel Process. Technol.* **2000b**, 63, 197-213.

Sherwell, J. Mercury Speciation Measurements in the Flue Gas and Plume of Two Maryland Combustion Sources: Montgomery County Resource Recovery Facility (RRF) and PEPCO Dickerson Generating Station (DGS). Frontier Geosciences Inc., August **2000**.

Shpirt, M. Y. Transformation of Mercury and its Compounds at the Coal Use. *Solid Fuel Chem.* **2002**, 5, 73-86.

Sjostrom, S.; Ebner, T.; Ley, T.; Slye, R.; Richardson, C.; Machalek, T.; Richardson, M.; Chang, R.; Meserole, F. Assessing Sorbents for Mercury Control in Coal-Combustion Flue Gas. Proceedings of the Mega Symposium, Chicago, IL, August 20-23, **2001**; Paper No. 232, Air & Waste Management Association, Pittsburgh, PA.

Sliger, N. R.; Going, J. D.; Kramlich, J. C. Kinetic Investigation of the High-Temperature Oxidation of Mercury by Chlorine Species. *Combust. Sci. Technol.* **1992**, 85, 1-22.

Sliger, R. N., Kramlich, J. C., Marinov, N. M. Towards the Development of a Chemical Kinetic Model for the Homogeneous Oxidation of Mercury by Chlorine Species. *Fuel Process. Technol.* **2000**, 65-66, 424-438.

Srivastava, R.; Lee, C. W.; Ghorishi, B.; Wojciech, J.; Hasting, T. W.; Hirschi, J. Evaluation of SCR Catalyst for Combined Control of NO_x and Mercury. Final Techincal Report - ICCI 02-1/2.2A-1 for period Sept. 1, 2002 - Aug. 31, **2003**.

Sterling, R. O.; Qiu, J.; Helble, J. J. Proceedings of the 227th ACS Spring National Meeting, Anaheim, CA, 2004; American Chemical Society: Washington, DC, **2004**.

Svachula, J.; Alemany, L.J.; Ferlazzo, N.; Tronconi, E.; Bregani, F. Oxidation of SO_2 to SO_3 Over Honeycomb DeNOxing Catalysts. *Ind. Eng. Chem. Res.* **1993a**, 32, 826-834.

Svachula, J.; Ferlazzo, N.; Forzatti, P; Tronconi, E. Selective Reduction of NO_x by NH_3 Over Honeycomb DeNOxing Catalysts. *Ind. Eng. Chem. Res.* **1993b**, 32, 1053-1060.

Tong, G.; Blankenship, G. A.; O'Neal, J. S.; Gale, T. K.; Ban, H.; Walsh, P. M. Oxidation of Mercury During Selective Catalytic Reduction of Nitric Oxide. Preprints of Papers - American Chemical Society, Division of Fuel Chemistry **2007**, 52(2), 513-514.

Tong, G.; Walsh, P. M.; Blankenship, G. A.; Gale, T. K. Measurements and Modeling of Mercury and Sulfur Dioxide Oxidation During Selective Catalytic Reduction of Nitric Oxide. Preprints of Papers - American Chemical Society, Division of Fuel Chemistry, **2008**, 53 (1), 174-175.

Tuenter, G.; van Leeuwen, W. F.; Snepvangers, L. J. M. Kinetics and Mechanism of the NO_x Reduction with NH_3 on V_2O_5-WO_3-TiO_2 Catalysts. *Ind. Eng. Chem. Prod. Res. Dev.* **1986**, 25, 633.

UK National Air Quality Archive: Air Pollution Glossary. http://www.airquality.co.uk/archive/glossary.php (accessed September 2008).

UNEP Chemicals. Global Mercury Assessment. December **2002**. http://www.eeaa.gov.eg/cmuic/cmuic_pdfs/mercury/final-assessment-report-25nov02.pdf (accessed January 2008).

United Nations Economic and Social Commission for Asia and the Pacific (UNESCAP), **2000**. Asia and the Pacific in Figures – 1998. http://unescap.org/stat/statdata/ apinfig.htm (accessed June 2008).

U.S. Environmental Protection Agency. Hazardous Waste Combustors; Revised standards; Proposed rules. Fed. Regist. **1996**, 61(77), 17357-17536.

U.S. Environmental Protection Agency. Mercury Study Report to Congress. EPA-452/R-97-003, Dec. **1997**

U.S. Environmental Protection Agency. Information Collection Request for Electric Utility Steam Generating Unit Mercury Emission Information Collection Effort. **1998**. http://www.epa.gov/ttn/oarpg/t3/reports/144_ss19.pdf. (accessed July 2007).

U.S. Environmental Protection Agency. Mercury Update: Impact on Fish Advisories. June **2001**. http://www.epa.gov/waterscience/fish/advice/mercupd.pdf (accessed May 2008).

U.S. Environmental Protection Agency. Clean Air Rules of **2004**. http://www.epa.gov/cleanair2004/ (accessed July 2007).

U.S. Environmental Protection Agency. Health Effects of Pollution. November **2007a**. http://www.epa.gov/Region7/programs/artd/air/quality/health.htm (accessed September 2008).

U.S. Environmental Protection Agency. Mercury Health Effects. **2007b**. http://www.epa.gov/mercury/effects.htm (accessed January 2008).

U.S. Environmental Protection Agency. Human-Related Sources and Sinks of Carbon Dioxide. **2008a**. http://www.epa.gov/climatechange/emissions/co2_human.html#fossil (accessed September 2008).

U.S. Environmental Protection Agency. Mercury. **2008b**. http://www.epa.gov/mercury (accessed May 2008).

Van Pelt, V. J.; Meischen, S. J. Determination of Total Mercury in Exhaust Gases. **1999**; U.S. Patent 5,879,948.

Wang, J.; Anthony, E. An analysis of the Reaction rate for Mercury Vapor and Chlorine. *Chem. Eng. Technol.* **2005**, 28, 569.

Wang, J.; Clemens, B.; Zanganeh, K. An Interpretation of Flue-Gas Mercury Speciation Data from a Kinetic Point of View. *Fuel* **2003**, 82, 1009.

Weilert, C. V.; Randall, D. W. Analysis of ICR Data for Mercury Removal from Wet and Dry FGD. Proceedings of the Mega Symposium, Chicago, IL, August 20-23, **2001**; Paper No. 280, Air & Waste Management Association, Pittsburgh, PA.

Widmer, N. C.; West, J.; Cole, J. A. Thermochemical Study of Mercury Oxidation in Utility Boiler Fuel Gases. 93rd Annual Meeting, Air & Waste Management Association, Salt Lake City, UT, June 18-22, **2000**.

Wilcox, J. On the Path to Elucidating the Speciation of Mercury in the Flue Gases of Coal Combustion. PhD Thesis, University of Arizona. 2004.

Wilcox, J.; Blowers, P. Decomposition of Mercuric Chloride and Application to Combustion Flue Gases. *Environ. Chem.* **2004**, *1*, 166-171.

Wilcox, J.; Marsden, C. J.; Blowers, P. Evaluation of Basis Sets and Theoretical Methods for Estimating Rate Constants of Mercury Oxidation Reactions Involving Chlorine. *Fuel Process. Technol.* **2004**, 85(5), 391-400.

Wilcox, J; Robles, J.; Marsden, D; Blowers, P. Theoretically Predicted Rate Constants for Mercury Oxidation by Hydrogen Chloride in Coal Combustion Flue Gases. *Environ. Sci. Technol.* **2003**, *37*, 4199-4204.

Xu, M.; Qiao, Y.; Zheng, C.; Li, L.; Liu, J. Modeling of Homogeneous Mercury Speciation Using Detailed Chemical Kinetics. *Combust. Flame* **2003**, 132, 208-218.

Zhao, Y.; Mann, M.; Pavlish, J.; Mibeck, B.; Dunham, G.; Olson, E. S. Application of Gold Catalyst for Mercury Oxidation by Chlorine. *Environ. Sci. Technol.* **2006**, 40, 1603.

Zhuang Y.; Biswas, M.E.; Quintan, T.G.; Lee, E. Arar, Proceedings of the Air and Waste Management Association 93rd Annual Meeting and Exhibition, **2000,** 331.

Zhuang, Y.; Laumb, J.; Liggett, R.; Holmes, M.; Pavlish, J. Impacts of Acid Gases on Mercury Oxidation Across SCR Catalyst. *Fuel Process. Technol.* **2007**, 88, 929-934.

Zhuang, Y.; Thompson, J. S.; Zygarlicke, C. J.; Pavlish, J. H. Development of a Mercury Transformation Model in Coal Combustion Flue Gas. *Environ. Sci. Technol.* **2004**, 38, 5803-4808.

APPENDIX A

ONE-DIMENSIONAL DIFFUSION AND HETEROGENEOUS REACTION MODEL FOR NO REDUCTION BY NH_3, MERCURY OXIDATION BY HCl, AND SO_2 OXIDATION TO SO_3 IN SCR*

```
// Calculate NO Reduction by NH3, Mercury Oxidation by HCl, and SO2 oxidation to
SO3 in SCR

#include <stdio.h>
#include <math.h>
#include <stdlib.h>

#define  R  8314.47  //universal gas constant, J/(kmol K)
#define  Pref  101325.  //atmospheric pressure, Pa

double  kNO, Sh, T, P, DNO, dh, S, DNH3, Cg, KNH3, dx, x, NH3toNO, XNOo, CNOo,
CNH3o, CNO, a, b, c, CNOs, dCNO, ug;
double  CNH3, kHgs, KHg, KHCl, XHCl, CHCl, kHgbl, kHgeff, DHg, CHgCl, fHgox,
CHg, CHgo, CNH3s, dCHgCl, L, KHClpv;
double  KSO2, KSO3, KH2O, kred, kox, kNOx, CSO2, CO2, CH2O, XSO2, XO2,
XH2O, Ctot, CSO3, CSO3o, XSO3o, XSO2o, CSO2o, dCSO3;

        void main(void)

{

        FILE *outfile;

        outfile = fopen("cout1.dat", "w");


        //Catalyst Geometric and Composition Parameters

        S = 571.;  //surface-to-volume ratio, m2/m3
```

*P. M. Walsh and G. Tong, Unpublished work, 2008

```
L = 0.305;  //length of catalyst, m (ends of some channels damaged)

dh = 0.007;  //hydraulic diameter, m
Sh = 2.98;  //Sherwood No. laminar, fully developed, square channel

Ctot = 42000000.;  //total concentration of active sites, dimensionless

dx = 0.001;  //increment of catalyst length, m


//Catalyst Conditions

T = 700.;  //temperature, deg F

T = (700. + 459.67) * 5. / 9.;  //temperature, K

P = 101325.;  //pressure, Pa

ug = 0.58;  //average gas velocity, m/s

Cg = P / (R * T);  //gas concentration

DNO = 1.13e-9 * pow(T, 1.724) * Pref / P;  //molecular diffusion coefficient, O2-N2, m2/s

DNH3 = DNO * pow(30. / 17., 0.5);  //diffusion coefficient for ammonia, scaled by square root of molecular weight, m2/s

DHg = 0.470e-9 * pow(T, 1.789) * (Pref / P) * pow(131.3 / 200.6, 0.5);  //Xe-N2 (Marrero and Mason, 1972) scaled by atomic weight, m2/s


//Rate Coefficients

kNO = 0.05;  //surface reaction rate coefficient for NO reduction by ammonia, m/s

kHgs = 0.014;  //rate coefficient for reaction between adsorbed Hg and adsorbed Cl or HCl, kmol/(m3s)

kred = 0.01;  //rate coefficient for reduction of active vanadium oxide and oxidation of adsorbed SO2, kmol/(m3s)

kox = 0.01;  //rate coefficient for reoxidation of active vanadium sites, kmol0.5/(m1.5s)
```

kNOx = 0.; //factor accounting for enhancement of SO3 formation rate by NOx ("b" in notation of Svachula et al.), m3/kmol

//Adsorption Equilibrium Constants

KNH3 = 3000000.; //NH3 adsorption equilibrium constant, m3/kmol

KHg = 750000; //Hg adsorption equilibrium constant, m3/kmol

KHCl = 7.5; //HCl (or Cl) adsorption equilibrium constant, competing with Hg, m3/kmol

kHClpv = 5000000; //HCl (or Cl) adsorption equilibrium constant, competing with SO2, m3/kmol

KSO2 = 0.00000015; //SO2 adsorption equilibrium constant, m3/kmol

KSO3 = 5700000.; //SO3 adsorption equilibrium constant, m3/kmol

KH2O = 0.; //H2O adsorption equilibrium constant, m3/kmol

//Gas Composition

XHCl = 1.e-6; //mole fraction HCl

XSO2o = 877.4e-6; //mole fraction SO2

XO2 = 0.05; //mole fraction O2

XH2O = 0.10; //mole fraction water vapor

NH3toNO = 0.0; //ammonia to NO mole ratio

XNOo = 300.e-6; //mole fraction NO at inlet

XSO3o = 1.e-6; //mole fraction SO3 at inlet

CNOo = XNOo * Cg; //inlet NO concentration, kmol/m3

CHgo = 10000.e-12 / 200.6; //inlet elemental mercury concentration (10,000 ng/m3), kmol/m3

CSO3o = Cg * XSO3o; //inlet SO3 concentration

```
CHCl = Cg * XHCl;  //concentration of HCl (constant to good approximation, no
axial or radial gradient), kmol/m3

CSO2o = Cg * XSO2o;  //concentration of SO2

CO2 = Cg * XO2;  //concentration of oxygen

CH2O = Cg * XH2O;  //concentation of water vapor
while (NH3toNO <= 1.20)

{

CNH3o = CNOo * NH3toNO;  //inlet NH3 concentration, kmol/m3

CNO = CNOo;  //initialize NO concentration

CHgCl = 0.;  //initialize HgCl concentration

CHg = CHgo;  //initialize Hg concentration

CSO3 = CSO3o;  //initialize SO3 concentration

CSO2 = CSO2o;  //initialize SO2 concentration

x = 0.;  //initialize position

while (x <= L)

{

        //Calculate CNOs, concentration of NO at catalyst surface

        a = (kNO + (Sh * DNO / dh)) * DNO / DNH3;

        b = kNO * CNH3o - kNO * CNOo + kNO * CNO * (1. - (DNO / DNH3))
        - 2. * (Sh * DNO / dh) * CNO * DNO / DNH3;

        b = b + (1. / KNH3) * (Sh * DNO / dh) + (Sh * DNO / dh) * CNH3o - (Sh
        * DNO / dh) * CNOo + (Sh * DNO / dh) * CNO;

        c = - (Sh * DNO / dh) * CNO * ((1. / KNH3) + CNH3o - CNOo + CNO *
        (1. - (DNO / DNH3)));

        CNOs = (- b + pow((pow(b, 2.) - (4. * a * c)), 0.5)) / (2. * a);
```

```
//Calculate Mercury Oxidation

CNH3 = CNH3o - (CNOo - CNO);

CNH3s = CNH3 - (DNO / DNH3) * (CNO - CNOs);

kHgbl = (kHgs * KHCl * CHCl * KHg) / ((1 + KNH3 * CNH3s + KHCl *
CHCl) * (1 + KHCl * CHCl));

kHgeff = 1. / ((1. / (Sh * DHg / dh)) + (1. / kHgbl));

dCHgCl = (1. / ug) * kHgeff * S * CHg * dx;

CHgCl = CHgCl + dCHgCl;

CHg = CHg - dCHgCl;

fHgox = CHgCl / CHgo;


//Calculate SO3 formation (after Svachula et al., Ind. Eng. Chem. Res.
1993, 32, 826-834)

dCSO3 = (dx / ug) * kred * KSO2 * KSO3 * Ctot * CSO2 * CSO3 * (1 +
kNOx * CNOs)/(1. + KSO3 * CSO3 * (1. + KSO2 * CSO2 * (1. + (kred /
(kox * pow(CO2, 0.5)))) + KH2O * CH2O + KNH3 * CNH3 + KHClpv *
CHCl));

CSO3 = CSO3 + dCSO3;

CSO2 = CSO2 - dCSO3;


//Calculate NO and NH3 Decay

dCNO = (1. / ug) * (Sh * DNO / dh) * S * (CNO - CNOs) * dx;

CNO = CNO - dCNO;

CNH3 = CNH3o - (CNOo - CNO);

x = x + dx;  //increment position

//printf("\n%6.3lf  %6.4lf  %5.2lf  %4.2lf  %6.3lf", x, CNO / CNOo,
CNO * XNOo * 1.e6 / CNOo, CNH3 * 1.e6 / Cg, fHgox);
```

```
            //fprintf(outfile, "\n%10.6lf  %10.6lf  %10.6lf  %10.6lf  %10.5lf"  ,
            x, CNO / CNOo, CNO * XNOo * 1.e6 / CNOo, CNH3 * 1.e6 / Cg,
            fHgox);

        }
            printf("\n%6.3lf  %6.4lf  %5.2lf  %4.2lf  %6.3lf  %6.4lf", NH3toNO,
            CNO / CNOo, CNO * XNOo * 1.e6 / CNOo, CNH3 * 1.e6 / Cg, fHgox,
            CSO3 / CSO2o, KNH3 * CNH3, KHClpv * CHCl);

            fprintf(outfile, "\n%10.6lf  %10.6lf  %10.6lf  %10.6lf  %10.5lf
            %10.5lf"  , NH3toNO, CNO / CNOo, CNO * XNOo * 1.e6 / CNOo,
            CNH3 * 1.e6 / Cg, fHgox, CSO3 / CSO2o);


            NH3toNO = NH3toNO + 0.05;  //increment NH3 to NO ratio

        }

        return;

}
```

APPENDIX B

EXPERIMENTAL DATA SET

HCL (inlet) (ppmv)	NO (inlet) (ppmv)	NH_3 (inlet) (ppmv)	NO (outlet) (ppmv)	CO (inlet) (ppmv)	HgT Avg (ng/m^3)*	HgT StdDev (ng/m^3)*	Hg(0) Avg (ng/m^3)*	Hg(0) StdDev (ng/m^3)*	SO_2 (inlet) (ppmv)	SO_3 (outlet) (ppmv)	H_2SO_4 (outlet) (ppmv)
INERT REACTOR											
2.2	328	300	292	102	6458	155	7459	145	806	5.9	0.7
1	300	285	-	0	8536	76	8894	206	-	-	-
REACTOR with SCR CATALYST											
0	0	0	0	0	9201	326	9210	334	940	-	4.0
1	0	0	0	0	9832	71	9054	87	856	-	0.3
2	0	0	0	0	10001	141	8627	122	851	-	0.2
5	0	0	0	0	7723	119	2635	109	817	-	4.3
10	0	0	0	0	7958	126	1748	164	878	-	3.2
25	0	0	0	0	7910	128	1045	164	867	-	4.3
50	0	0	0	0	8186	260	778	189	860	-	3.9
100	0	0	0	0	8037	233	734	200	861	-	4.0
0	300	0	312	0	7965	215	6429	204	930	-	4.3
1	300	0	314	0	8926	93	6700	169	869	-	2.3
2	300	0	314	0	9321	159	6220	108	853	-	0.5
5	300	0	310	0	9726	162	1317	174	913	-	3.3
10	300	0	311	0	9592	167	1056	169	906	-	3.7
25	300	0	310	0	9587	156	858	152	901	-	2.9
50	300	0	309	0	9671	178	884	165	883	-	3.3
100	300	0	306	0	9489	170	363	136	871	-	3.3
0	350	285	41	0	8765	338	9788	321	-	-	-
1	350	285	20	0	10560	539	10881	232	782	-	0.5
1	350	285	20	0	10450	122	10439	196	782	-	0.5
2	350	285	-	0	10339	235	8303	197	-	10.7	-
3	350	285	-	0	11620	326	9756	295	-	9.9	-
4	350	285	-	0	10949	187	6977	153	-	-	-
5.3	350	285	8.9	0	9243	157	5158	212	827	-	-
8.0	350	285	11	0	9693	189	4464	212	822	-	-
10	350	285	13	0	10106	218	3984	288	815	-	1.1
10	350	285	13	0	10706	524	4333	252	815	-	1.1
15	350	285	16	0	9561	173	3149	153	820	-	-
20	350	285	21	0	10004	272	3030	461	813	-	1.4
24	350	285	24	0	9027	184	2181	191	799	-	9.6
50	350	285	36	0	9320	144	1790	435	811	-	9.7
75	350	285	78	0	8813	510	1641	191	805	-	3.0
75	350	285	78	0	8561	181	1358	199	805	-	3.0
100	350	285	-	0	7546	1114	1182	248	-	-	-
1	300	0	300	0	11134	389	6853	363	877	10.8	2.7
1	300	60	254	0	11517	455	7561	314	885	8.8	2.1
1	300	120	196	0	10574	209	7503	184	882	8.1	2.6
1	300	180	148	0	8930	192	6455	189	871	8.0	2.1
1	300	240	89	0	9192	214	7261	120	876	7.2	1.4
1	300	285	49	0	9813	157	8141	179	873	6.7	1.8

*Mercury concentrations at 20 ^oC, 1 atm pressure, and dry.

HCL (inlet) (ppmv)	NO (inlet) (ppmv)	NH_3 (inlet) (ppmv)	NO (outlet) (ppmv)	CO (inlet) (ppmv)	HgT Avg (ng/m^3)*	HgT StdDev (ng/m^3)*	Hg(0) Avg (ng/m^3)*	Hg(0) StdDev (ng/m^3)*	SO_2 (inlet) (ppmv)	SO_3 (outlet) (ppmv)	H_2SO_4 (outlet) (ppmv)
REACTOR with SCR CATALYST											
10	300	0	0	0	9592	167	1056	169	-	-	-
10	300	0	300	0	8320	144	832	159	-	7.3	-
10	345	0	345	0	8632	375	1462	142	-	8.2	-
10	300	63	237	0	8352	148	813	212	-	8.2	-
10	300	92	208	0	8473	162	818	153	-	6.8	-
10	300	105	207	0	8529	192	1143	138	-	6.0	-
10	300	161	161	0	8023	182	832	144	-	6.2	-
10	300	195	105	0	7960	203	882	207	-	5.7	-
10	300	200	90.5	0	8299	176	1206	135	-	5.0	-
10	300	225	75	0	8616	386	1468	161	-	4.5	-
10	300	285	56	0	8603	392	1468	161	-	2.7	-
10	300	315	1.5	0	8311	157	1989	119	-	3.4	-
10	300	345	1.9	0	7734	401	2379	182	-	4.5	-
1.9	328	306	-	0	10332	289	7457	178	823	-	2.7
1.9	328	306	22.1	5.0	8942	199	6829	123	813	5.7	2.1
1.9	328	305	22.6	7.5	8660	96	7076	111	807	5.9	2.1
1.9	328	305	23.0	10.5	8332	60	6907	109	799	5.9	2.2
2.2	328	302	26.4	25.2	7689	153	6655	118	807	6.2	1.8
2.1	328	309	19.1	52.4	8294	249	7811	198	805	-	1.8
2.2	328	307	21.2	101.3	8066	146	7976	187	800	7.0	1.9
11.0	300	285	18.0	0	8112	111	2529	149	810	-	6.2
11.0	300	285	18.0	0	7986	89	2392	138	810	-	6.2
11.0	300	285	18.0	0	8127	108	2447	147	810	-	6.2
11.0	300	285	18.0	0	8384	106	2459	167	810	-	6.2
11.0	300	285	18.0	0	10442	152	2522	181	810	-	6.2
11.5	300	285	18.1	3.8	8703	308	3173	425	787	-	3.4
11.5	300	285	18.1	3.8	8664	102	3209	219	787	-	3.4
11.0	300	285	18.8	19	8460	84	3627	115	805	5.2	3.1
11.0	300	285	18.8	19	8349	93	3083	188	805	5.2	3.1
12.1	300	285	18.2	50	8938	90	3766	108	838	6.4	3.0
12.1	300	285	18.2	50	8071	122	3571	185	838	6.4	3.0
11.5	300	285	17.8	118	8422	122	4038	183	811	-	4.6
11.4	300	285	16.3	263	8223	166	4723	163	825	-	4.0
11.4	300	285	16.3	263	8722	113	4844	148	825	-	4.0
11.7	300	285	16.9	511	8815	123	5546	152	819	-	3.9
11.6	300	285	17.3	1013	8847	72	6579	141	824	10.8	3.9
11.6	300	285	17.3	1013	8869	59	6641	200	824	10.8	3.9
11.6	300	285	18.4	2001	9356	106	8106	159	820	9.7	3.5
11.6	300	285	18.4	2001	9261	79	7918	163	810	9.7	3.5
50	300	285	21.5	5	8333	150	1425	305	830	6.4	0.7
50	300	285	21.8	114	8389	211	1553	286	832	-	0.6
50	300	285	21.2	254	8296	191	1571	147	825	7.0	0.7
50	300	285	21.1	511	8503	125	1771	150	820	7.8	0.6
49.5	300	285	21.6	1043	8441	330	2134	146	831	7.8	0.2
49.0	300	285	21.1	2053	8603	307	2389	219	828	8.0	1.1

*Mercury concentrations at 20 ^{o}C, 1 atm pressure, and dry.